UNIVERSITY OF CALIFORNIA, SAN DIEGO

Studies of Protein Kinase A N-myristylation and Kinase Reaction Progression

A dissertation submitted in partial satisfaction of the requirements for the degree

Doctor of Philosophy

in

Biomedical Sciences

by

Adam Christopher Bastidas

Committee in charge:

Professor Susan S. Taylor, Chair
Professor Tracy Handel
Professor Elizabeth Komives
Professor Alexandra Newton
Professor JoAnn Trejo

2014

The Dissertation of Adam Christopher Bastidas is approved, and it is acceptable in quality and form for publication on microfilm and electronically:

_____

_____

_____

_____

_____

Chair

University of California, San Diego

2014

DEDICATION

For my parents and my brothers

TABLE OF CONTENTS

LIST OF ABBREVIATIONS

Å. Angstrom

Abl. Abelson

AGC. Group of kinases including PKA, PKG, and PKC

AKAP. A-kinase anchoring protein

AKIP. A-kinase-interacting protein

AMP-PNP. adenosine-5′-(β,γ-imido)triphosphate

ADP. Adenosine diphosphate

ASU. Asymmetric unit

ATP. Adenosine triphosphate

cAMP. Adenosine 3’,5’-cyclic monophosphate

CDK. Cyclin dependent kinase

cGMP. Guanosine 3’,5’-cyclic monophosphate

CNB domain. Cyclic nucleotide binding domain

C-spine. Catalytic spine

C-subunit. The Catalytic Subunit of PKA

C-terminus. Carboxy-terminus

DAG. Diacyl glycerol

D/D domain. Dimerization Docking domain

DTT. Dithiothreitol

E. coli. *Escherichia coli*

FM. Fluorescein maleimide

GPCR. G protein coupled receptor

IP20. Residues 5-24 of PKI

IP3. Inositol 1,4,5-trisphosphate

IS. Inhibitor site

kDa. Kilodaltons

MD. Molecular dynamics

MES. 2-(N-morpholino) ethanesulfonic acid

mg. milligram

µL. Microliter

$MgCl_2$. Magnesium chloride

mM. millimoles/liter

MOPS. 3-(N-morpholino) propanesulfonic acid

MPD. 2-methyl-2,4-pentanediol

NaCl. Sodium chloride

NMT. N-myristyl transferase

N-terminus. Amino-terminus

PAGE. Polyacrylamide gel electrophoresis

PCA. Principal component analysis

PDB. Protein data bank

PDK1. Phosphoinositide-dependent protein kinase

PKA. Protein Kinase A or cyclic-AMP Dependent Protein Kinase

PKC. Protein kinase C

PKI. Protein kinase A inhibitor

RMSF. Root mean squared fluctuation

R-spine. Regulatory spine

R-subunit. The Regulatory Subunit of PKA

SDS. Sodium dodecyl sulfate

TRFA. Time-resolved fluorescence anisotropy

Tris. Tris Hydroxymethylaminoethane

WT. Wild type

LIST OF FIGURES

LIST OF TABLES

ACKNOWLEDGEMENTS

I would like to thank my advisor, Dr. Susan Taylor, for her support and guidance during my time in graduate school. She was always enthusiastic about my work and helped to keep me motivated. She provided insights into my results and helped with designing future experiments. Additionally, I thank Dr. Taylor for encouraging participation in scientific meetings, which allowed me to travel and experience new cities, cultures, and scientific ideas.

I would also like to thank members of my graduate committee for their help with my graduate research. Dr. Elizabeth Komives was very helpful throughout graduate school from rotating in her laboratory as a first year student to our involvement in Academic Connections and with her help during committee meetings. Dr. Komives was always willing and enthusiastic about offering guidance in my research as well as in planning future options in my career. I also thank Dr. JoAnn Trejo who was on my committee and offered important insights during committee meetings and was always a friendly and helpful mentor. I thank Dr. Tracy Handel whose lab I also rotated in and who was very encouraging and supportive. Additionally, Dr. Alexandra Newton on my committee was also an informative and important member of my committee. Each committee member greatly improved my graduate research and experience, and I am very thankful for their support and input.

I would like to thank many members of the Taylor lab who provided support, ideas, and help with the execution and design of experiments. Jie Yang, Jian Wu, and

Jon Steichen were very helpful with crystallography experiments and analysis, and I am extremely thankful for their input and advice. Specifically, I am grateful for Jon Steichen who helped me to analyze my X-ray crystallography data and provided guidance and input for many of my papers. Furthermore, I would like to give special thanks to Mike Deal. Mike provided most of my laboratory training when I joined the Taylor lab and was always helpful with any problems in the lab. Additionally, I am extremely grateful to our collaborator, David Johnson at UC Riverside, who helped to perform time-resolved fluorescence anisotropy experiments. David was always very quick and hard working with experiments, and he provided important insights into the meaning of results. He provided a great deal of support in writing our paper together. I thank Manjula Darshi and Mira Sastri for their help with cell biology experiments. I would like to thank all of the co-authors of my papers including Malik Keshwani, Yurong Guo, Levi Pierce, and Ross Walker who were all important contributors to my research. Finally, I would like to thank everyone in the Taylor lab for their help and friendship including, but not limited to, Ping Zhang, Hiruy Meharena, Jessica Bruystens, Ganapathy Sarma, Sventja von Daake, Eric Smith-Nguyen, Alexandr Kornev, Chris McClendon, Cecilia Cheng, Frank Ma, Issa Moody, CJ Allison, Jeffrey Copps, Chris Eggers, Nina Haste, Phil Chang, and Juniper Pennypacker. Everyone listed provided advice on the design and/or execution of experiments, and I am very grateful.

I would like to thank my friends and members of my BMS class for their friendship and for providing an important and much needed break from lab at times during graduate school. There are too many people to mention, but I want to

specifically thank a few people. I want to thank Spencer Wei who was my roommate and good friend throughout graduate school. I want to thank Isabel Canto, Amanda White, Andrew Borkowski, Jon Steichen, Jon Gonzalez, and Stephanie Dusaban for being such great friends. I want to thank the rest of my BMS class that I did not mention above. I really enjoyed the company of everyone in my class. I would also like to thank Grace Woodruff, my best friend. Grace was always willing to listen and provide input for my practice talks despite how boring they must have been for her after hearing so many of them. Grace and I were always willing to listen to each other complain about lab and provide feedback or just listen and support each other. Grace made graduate school and my life much more enjoyable, and I am very thankful.

Last but definitely not least, I want to thank my family. I thank my mom, Christine, and dad, Julio, for always encouraging and supporting me. I owe all my success to their love and support. I want to thank my brothers Michael, Alex, and Jonathan. I hope that I am providing a good example for them, and I love and think of them all the time. I want to thank my grandparents, Eleanor and Robert Duke, who also always encouraged and supported me and felt like a second set of parents. I owe all my success to my family, and I am extremely grateful for their guidance and love.

Chapter 2, in full, was published as The Role of N-terminal Myristylation in the Structure and Regulation of cAMP-Dependent Protein Kinase. Bastidas AC, Deal MS, Steichen JM, Keshwani MM, Guo Y, Taylor SS. *J. Mol. Biol*. 2012 Sep 14; 422(2):215-229. The dissertation author was the primary investigator and author of this work.

Chapter 3, in full, was published as Influence of N-myristylation and Ligand Binding on the Flexibility of the Catalytic Subunit of Protein Kinase A. Bastidas AC, Pierce LC, Walker RC, Johnson DA, Taylor SS. *Biochemistry* 2013 Sep 17; 52 (37):6368-79. The dissertation author was the primary investigator and author of this work.

Chapter 4, in full, was published as Phosphoryl Transfer by Protein Kinase A is Captured in a Crystal Lattice. Bastidas AC, Deal MS, Steichen JM, Guo Y, Taylor SS. *JACS* 2013 Mar 27; 135(12):4788-4798. The dissertation author was the primary investigator and author of this work.

Chapter 5, in full, will be published in the near future with the tentative title of Apo and ADP Bound Structures of Protein Kinase A Provide Insights into the Mode of Kinase Product Turnover. Bastidas AC, Wu J, Taylor SS. The dissertation author was the primary researcher and author of this work.

VITA

Education

2014 Ph.D., Biomedical Sciences
University of California, San Diego

2008 B.S., Chemistry and Biochemistry & Molecular Biophysics
University of Arizona, Tucson

Publications

Bastidas A. C., Wu J., Taylor S. S. Apo and ADP Bound Structures of Protein Kinase A Provide Insights into the Mode of Kinase Product Turnover. (To be published)

Bastidas, A. C., Pierce, L. C., Walker, R. C., Johnson, D. A. and Taylor, S. S. (2013). Influence of N-myristylation and ligand binding on the flexibility of the catalytic subunit of protein kinase a. *Biochemistry.* **52**, 6368-6379.

Bastidas, A. C., Deal, M. S., Steichen, J. M., Guo, Y., Wu, J. and Taylor, S. S. (2013). Phosphoryl transfer by protein kinase a is captured in a crystal lattice. *J Am Chem Soc.* **135**, 4788-4798.

Bastidas, A. C., Deal, M. S., Steichen, J. M., Keshwani, M. M., Guo, Y. and Taylor, S. S. (2012). Role of N-terminal myristylation in the structure and regulation of cAMP-dependent protein kinase. *J Mol Biol.* **422**, 215-229.

ABSTRACT OF THE DISSERTATION

Studies of Protein Kinase A N-myristylation and Kinase Reaction Progression

by

Adam Christopher Bastidas

Doctor of Philosophy in Biomedical Sciences

University of California, San Diego, 2014

Professor Susan S. Taylor, Chair

The catalytic (C) subunit of cAMP-dependent protein kinase (PKA) can be regulated by co- and post-translational modifications. The C-subunit is co-translationally N-myristylated. N-myristylation is catalyzed by the enzyme N-myristyl transferase (NMT), and it is the incorporation of the 14 carbon, saturated fatty acid, myristic acid, onto the N-terminal glycine residue of a target protein. In PKA, N-myristylation enhances the thermal stability of the protein and increases membrane binding in RII but not RI holoenzyme complexes. In these studies, the myristylated C-subunit was crystallized in different states including bound to a substrate peptide alone as well as to a substrate peptide and an ATP analogue. Furthermore, time-resolved

fluorescence anisotropy and MD simulations were performed to analyze the effects of N-myristylation on C-subunit dynamics. These studies showed that N-myristylation stabilizes the N-terminus and myristate pocket of PKA and exhibits effects on dynamics throughout the enzyme including at the active site. Myristylation may, therefore, provide allosteric regulation of PKA.

The reaction mechanism of PKA is also well-characterized. ADP-release is the rate-limiting step in PKA reaction turnover, and ADP-release is governed by magnesium concentration. PKA binds two magnesium ions termed Mg1 and Mg2 with the numbering based on the order in which the ions were thought to bind. However, recent studies suggest that the magnesium ions may bind in reverse order, and the mode of magnesium and ADP-release following phosphoryl transfer is unresolved. In these studies, the C-subunit was crystallized displaying partial and complete phosphoryl transfer of AMP-PNP onto a substrate peptide. These structures showed that Mg1 is released following complete phosphoryl transfer, and therefore, Mg1 release may be an important step preceding ADP release. Also, the C-subunit of PKA was crystallized in an apo state and bound to ADP. The ADP bound structure showed that ADP binds to the C-subunit with one magnesium ion, and this ion corresponds to Mg2 verifying the results from the partial and complete phosphoryl transfer structures. Furthermore, the ADP bound structure adopts a novel conformation that may represent the possible motions associated with ADP release including opening of the Gly-rich loop and C-tail away from the active site.

Chapter 1

Introduction

Signal transduction regulates nearly every important cellular process including metabolism, cell cycle progression, and apoptosis among many others. Often signal transduction involves relating extracellular signals into intracellular processes through, for instance, binding of hormones or ligands ("first messengers") to cell surface proteins including G-protein coupled receptors (GPCRs) that then initiate intracellular signals. These coupled signaling events often include the production of additional signaling molecules ("second messengers"). Different types of second messengers include cyclic adenosine monophosphate (cAMP), calcium ions (Ca^{+2}), cyclic guanidine monophosphate (cGMP), diacyl glycerol (DAG), and inositol 1,4,5-trisphosphate (IP3) among others. These second messengers then activate downstream signaling proteins that regulate other proteins via post-translational modifications including, but not limited to, phosphorylation, neddylation, ubiquitination, acetylation, and fatty acylation. Of each of these modifications, phosphorylation is one of the most important and well-studied signal transduction events.

1.1 Protein Phosphorylation

Protein phosphorylation is the covalent attachment of a phosphate group onto a protein, which occurs on serine, threonine, and tyrosine residues. Each phosphate group added to a protein creates the addition of negative charges to the modified protein, and the attached phosphate(s) can regulate the modified protein in multiple ways including changing protein activity (active to inactive or vice versa); creating new potential protein interactions; targeting the protein for degradation; or regulating subcellular localization. This post-translational modification was first identified in the

1950's by Fischer and Krebs when phosphorylation was shown to activate glycogen phosphorylase *b* to glycogen phosphorylase *a* (Fischer and Krebs, 1955). Since that initial study, multitudes of signaling processes were also found to be regulated by phosphorylation. In fact, it is estimated that up to 30% of proteins in eukaryotic cells are phosphorylated at any given time (Ptacek et al., 2005). Furthermore, the enzymes that catalyze protein phosphorylation, protein kinases, comprise about 1.7% of the human genome (Manning et al., 2002). Therefore, protein phosphorylation is one of the most abundant and important cellular signaling events. Additionally, phosphorylation of target proteins is typically a reversible event, and the removal of the phosphate group is catalyzed by enzymes known as phosphatases that can reverse the signaling events created by the protein kinases.

1.2 Protein Kinases

Protein kinases are the family of enzymes that catalyze phosphorylation of target proteins by transferring the γ-phosphate of ATP onto the side-chain alcohol group of Ser, Thr, and Tyr residues. Protein kinases are partly categorized by which amino acid residues they phosphorylate, either Ser/Thr residues or Tyr residues. However, there are some kinases known as dual-specific protein kinases because they can phosphorylate the side-chain of all three residues Ser, Thr, and Tyr (Lindberg et al., 1992). Additionally, some kinases are pseudokinases which retain the conserved fold of protein kinases but typically lack crucial amino acid residues found in other protein kinases that often results in a lack of catalytic activity (Boudeau et al., 2006). However, in some cases, proteins initially identified as pseudokinases are actually

active because the function of the important residue that they are lacking can be replaced by a nearby amino acid residue (Min et al., 2004), or catalytic activity of the pseudokinase can proceed in atypical ways (Mayans et al., 1998; Mukherjee et al., 2008). The function of the pseudokinases that are inactive is unclear, but these proteins may serve roles such as adaptor proteins or scaffold proteins in signaling complexes (Fukuda et al., 2009; Zeqiraj et al., 2009). Finally, there are histidine-specific protein kinases that are found in plants, fungi, and prokaryotes, but these enzymes are structurally unrelated to the eukaryotic protein kinases (Li et al., 2010).

There are over 500 protein kinases in the human genome that were categorized into seven different groups based on their evolutionary relationships (**Fig. 1.1**). These different classes include: STE (related to yeast sterile kinases); CK1 (casein kinase 1); AGC (which includes protein kinase A (PKA), protein kinase G (PKG), and protein kinase C (PKC)); CaMK (Ca^{+2}/calmodulin-regulated kinases); CMGC (which includes cyclin-dependent kinases (CDKs), mitogen-activated protein kinases (MAPKs), glycogen synthase kinase (GSK), and CDK-like kinases); TK (tyrosine kinases), and TKL (tyrosine-kinase like) (Manning et al., 2002). There are also atypical protein kinases (aPKs) that do not adopt the typical kinase fold but exhibit phosphoryl transfer activity.

Protein kinases regulate many different cellular events including cell proliferation, cell migration, muscle contraction, memory formation, and apoptosis, and because of the vital role of protein kinases in many different processes, proper regulation of these enzymes is of the upmost importance (Manning et al., 2002). There are several ways that protein kinase activity is regulated including protein

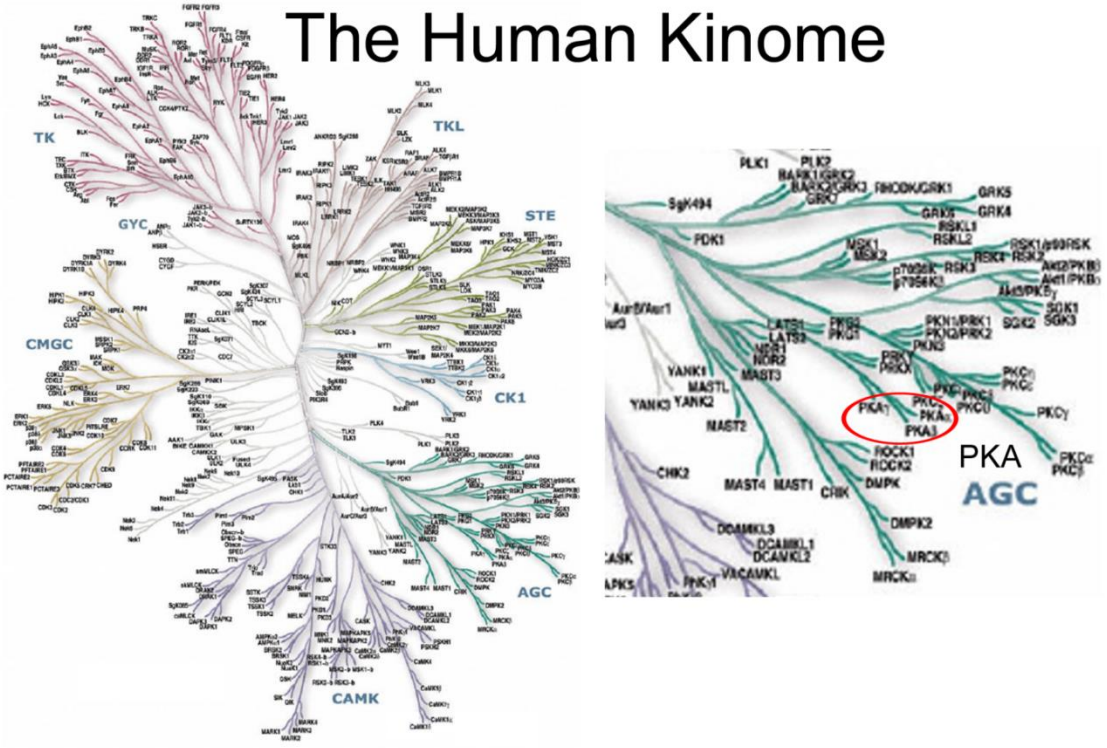

Figure 1.1. The Human Kinome. Human protein kinases were classified into seven groups shown above. Protein kinase A and about 60 other kinases belong to the AGC group of protein kinases. The AGC group and PKA are highlighted on the right. This figure was taken from Manning et al. (2002) *Science* 298:1912.

phosphorylation. Many kinases undergo reversible phosphorylation, which can regulate their activity (Xiao et al., 2011; Yang et al., 2002). Additionally, kinases can be regulated by protein-protein interactions where binding other proteins can either activate or inhibit the protein kinase (Taylor et al., 2012a). Furthermore, some kinases are regulated by localization (Fayard et al., 2010), and others are regulated by dimerization (Huse and Kuriyan, 2002; Lemmon and Schlessinger, 2010). Improper regulation of protein kinases can lead to many diseases including cancer, heart disease, and diabetes (Manning et al., 2002).

Because improper regulation of kinases is associated with diseases, kinases are an important pharmaceutical target and represent the second most important drug targets after GPCRs. Furthermore, there has been success in the treatment of some diseases with kinase inhibitors. For example, the tyrosine kinase, Abelson (Abl), can form a chimeric protein with Bcr (break point cluster) due to a chromosomal translocation. This chimeric protein results in a constitutively active Abl kinase, and this chimeric protein is present in over 90% of people with chronic myelogenous leukemia (CML) (Kurzrock et al., 1987). A small molecule inhibitor, Imatinib (Gleevec), was identified that binds to and inhibits Bcr-Abl and was approved for the treatment of CML (Mauro et al., 2002). Furthermore, a mutation in the Ser/Thr kinase, B-raf, is associated with skin cancer, and recently a small molecule inhibitor, Vemurafenib, was approved for the treatment of melanoma (Vultur et al., 2010). Therefore, protein kinases are important and successful drug targets in the treatment of human disease, and for this reason, structure-function relationship studies of protein kinases are very important. Additionally, protein kinases adopt a conserved fold and

exhibit similar biochemical properties which allow some findings from protein kinases to be generalized to the entire family of kinases.

1.3 cAMP-Dependent Protein Kinase (Protein Kinase A)

cAMP-dependent protein kinase, which is also known as protein kinase A (PKA), is a member of the AGC group of protein kinases. This group contains about 60 Ser/Thr kinases including PKA, PKG, and PKC, which gives the group its name (Pearce et al., 2010). The catalytic regions of these proteins are conserved, but the modes of regulation differ. For instance, the regulatory and catalytic portions of PKG and PKC are fused as one protein, but in PKA, the regulator (R) subunit is a separate protein from the catalytic (C) subunit (Pearce et al., 2010). The C-subunit of PKA is an important model enzyme for the AGC group of protein kinases and all kinases in general because it is more amenable to biochemical and structural studies than other kinases due to the fact that the R- and C-subunits are separate proteins that can be purified in high yields from *E. coli*. In fact, the C-subunit of PKA was the first kinase structure solved (Knighton et al., 1991a).

The way that PKA is regulated is through cAMP concentration. Under non-activating conditions of low concentration of cAMP, PKA exists as a heterotetrameric holoenzyme complex composed of an R-subunit dimer that binds and inhibits two C-subunit monomers (**Fig. 1.2**). The R-subunits bind with high affinity to the C-subunits and keep these proteins in an inactive state by, in part, binding to the active site of the C-subunit with a region of the R-subunit known as the inhibitor site (IS) (Kim et al., 2007). The way PKA is activated is through a hormone binding to a GPCR which then

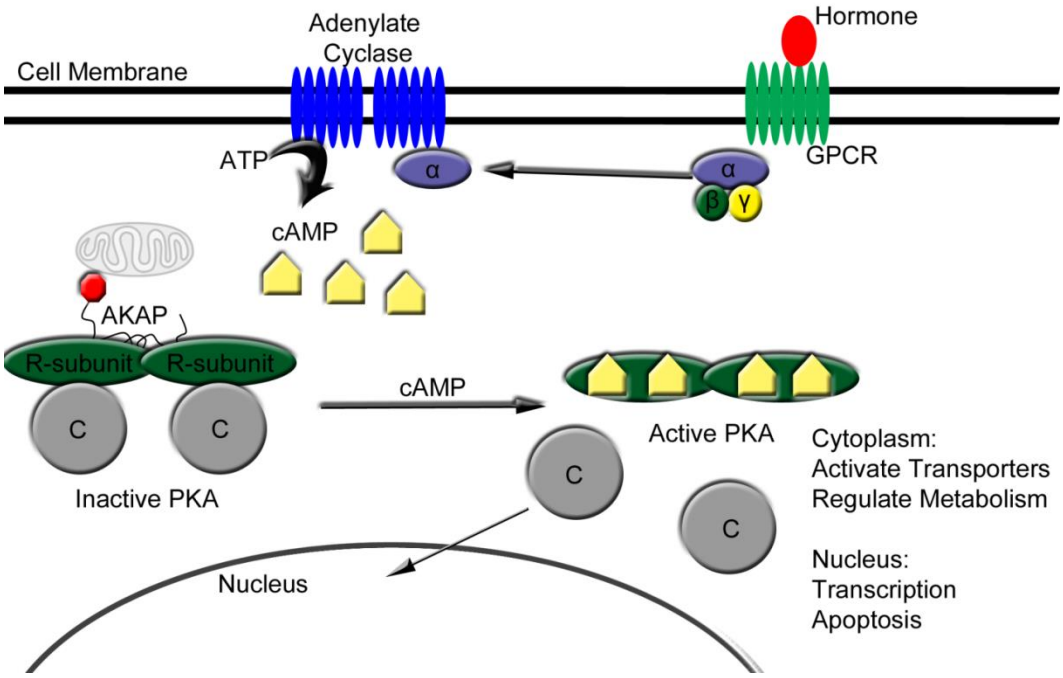

Figure 1.2. PKA Activation and Regulation. Shown is a schematic representation of how PKA is activated and regulated. PKA is activated by cAMP, which binds to the R-subunit proteins with high affinity causing a conformational change that allows for release of the active C-subunit monomers. A-kinase anchoring proteins (AKAPs) regulate PKA by targeting it to specific subcellular locations.

couples to $G_{\alpha s}$. $G_{\alpha s}$, in turn, activates adenylate cyclase which converts ATP into cAMP (Taylor et al., 2008). The R-subunits form dimers due to their dimerization and docking (DD) domain (Sarma et al., 2010), and they act as receptors for cAMP. Each R-subunit protein binds with high affinity to two molecules of cAMP on the cyclic nucleotide binding (CNB) domains within the protein (Su et al., 1995). Once bound to cAMP, the R-subunits undergo a conformational change that lowers their affinity towards the C-subunit, and this then releases their inhibition of the constitutively active C-subunits, which can then phosphorylate target proteins in the cytoplasm and nucleus (Taylor et al., 2008). PKA regulates many different processes including metabolism, memory formation, apoptosis, and transcription.

The complexity of cAMP-dependent protein kinase signaling is also increased by the number of different isoforms of the C-subunit and R-subunit. In humans, there are four functionally non-redundant isoforms of the R-subunit which are RIα, RIIα, RIβ, and RIIβ. The R-subunits exhibit different tissue expression and different phenotypes in mouse knockouts (KOs) (Kirschner et al., 2009). The only R-subunit KO that is embryonically lethal is the KO of RIα. The other R-subunit KO mice have different, less severe phenotypes. Also, in humans there are three isoforms of the C-subunit which are Cα, Cβ, and Cγ. The most abundant C-subunit isoform is Cα, and KO of this protein has the most severe effects in mice resulting in major growth defects. KO of the other isoforms produces mild effects most likely because Cα can compensate for the loss of the other isoforms (Kirschner et al., 2009).

In addition to the R-subunits and C-subunits, there are other proteins that are important for regulating PKA activity. One of these proteins is the protein kinase

inhibitor (PKI). This small, heat-stable protein binds to the C-subunit with high affinity and inactivates the protein. PKI contains a nuclear export signal (NES), and it is thought to regulate PKA by binding to the C-subunit protein in the nucleus and exporting it to the cytoplasm (Fantozzi et al., 1994; Wen et al., 1994). Also, PKI was an important protein for understanding the structure of PKA because the C-subunit is typically crystallized with an inhibitor peptide derived from residues 5-24 of PKI termed IP20 (Knighton et al., 1991a). This peptide greatly improves PKA crystallization and crystal structure resolution. Furthermore, PKA is regulated by another set of proteins called A-kinase anchoring proteins (AKAPs). AKAPs are proteins that bind to the R-subunit D/D domain and act to localize PKA to different subcellular localizations. In this way, AKAPs regulate PKA spatially, and AKAPs poise PKA so that it can act on specific cellular substrates. Additionally, AKAPs are increasingly being appreciated as large signaling complexes that can localize many different proteins including kinases, phosphodiesterases, phosphatases, and membrane proteins (Welch et al., 2010). By localizing all of these proteins, the different proteins and pathways that they control are poised to be activated and then deactivated with high selectivity and sensitivity.

The C-subunit of cAMP-dependent protein kinase was the first kinase structure solved, and this structure identified the conserved kinase fold shared by this entire family of enzymes (Knighton et al., 1991a) (**Fig. 1.3A**). Additionally, the IP20 peptide that was crystallized with the protein helped to identify the mode of substrate binding to kinases. Furthermore, our understanding of PKA structure and signaling was improved by holoenzyme crystal structures. One crystal structure of a truncated form

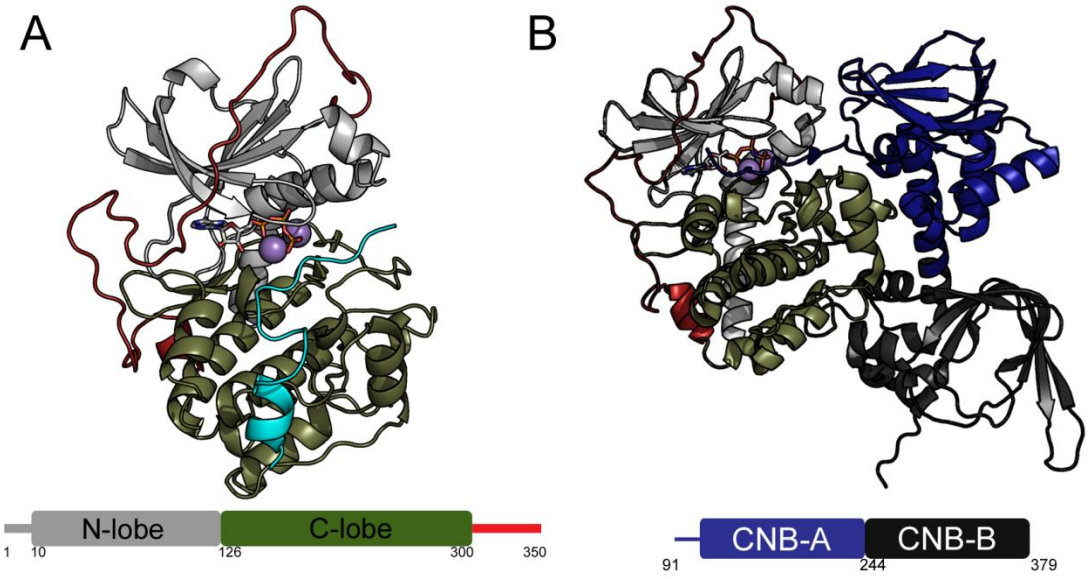

Figure 1.3. PKA Catalytic Subunit and RIα Holoenzyme Structures. A. The overall structure of the C-subunit is shown with the N-lobe colored gray, large lobe colored olive, C-tail colored red, IP20 peptide colored cyan, ATP shown in stick representation and colored by element, and Mg^{+2} ions shown as purple spheres. **B**. The RIα 91-379 holoenzyme crystal structure is shown with the C-subunit colored as in A. The RIα cyclic nucleotide binding domain A (CNB-A) is colored blue and CNB-B is colored black. Depictions of the coloring scheme for the regions of the proteins are displayed for the C-subunit below panel A and for the R-subunit below panel B.

of the RIα isoform (91-379), which forms a heterodimer rather than heterotetramer because it lacks the dimerization and docking domain, identified the mode of cAMP activation (Kim et al., 2007) (**Fig. 1.3B**). Furthermore, there are two recent full length heterotetrameric holoenzyme complexes of RIβ and RIIβ that exhibit much different structures from each other (Ilouz et al., 2012; Zhang et al., 2012), and there is a model of the RIα tetrameric holoenzyme structure that is also unique (Boettcher et al., 2011). These different structures support the idea that the different PKA holoenzyme complexes have distinct structures and functions.

1.4 Protein Kinase Structure and Reaction Mechanism

Protein Kinase Core - Eukaryotic protein kinases contain a conserved core comprised of approximately 250 residues that adopts a bilobal conformation. These two lobes are termed the N-lobe (or small lobe) and the C-lobe (or large lobe) (Knighton et al., 1991a). The N-lobe is comprised largely of β-sheets termed β-strands 1-5 (**Fig. 1.4A-B**). There is one highly conserved residue, Lys72 (with the numbering for this and all subsequent residues corresponding to PKA unless otherwise stated), in β-strand 3. This residue is required for catalytic activity and is often mutated in kinases to make "kinase dead" mutants despite the fact that mutation of Lys72 does not abolish ATP binding (Gibbs and Zoller, 1991; Iyer et al., 2005a; Iyer et al., 2005b; Zoller et al., 1981). This residue is important because it helps to bind and position the phosphate groups in ATP for phosphoryl transfer. Additionally, there is one highly conserved helix in this lobe termed the C-helix, which is an important region of the protein because it contains Glu91 that helps to position Lys72. Also, the orientation of

the C-helix is one method that regulates whether kinases are active or inactive (Xu et al., 1999). Another important region within the N-lobe is the Gly-rich loop. This loop forms part of the active site, and it is important because it helps to bind and position ATP for transfer and excludes water from the active site.

The C-lobe is mostly alpha helical, and it also contains many catalytically essential residues (**Fig. 1.4A, C**). For example, the "catalytic loop" is part of the C-lobe (residues 164-172). This loop is termed the catalytic loop because of the several conserved residues that are important for proper catalytic activity. For instance, Tyr164 is a highly conserved residue that helps to position the "DFG" motif that is important for kinase activity and for forming an active conformation (Schindler et al., 2000; Yang et al., 2002). Additionally, Asp166 is the putative catalytic base, and mutation of this residue causes severe defects in catalytic activity (Gibbs and Zoller, 1991). This residue is thought to correctly position the substrate residue for phosphoryl transfer, and it may accept the hydrogen atom of the substrate residue during the phosphorylation reaction (Cheng et al., 2005). Lys168 is also in this loop. Lys168 forms a hydrogen bond with the γ-phosphate of ATP and is thought to help position it for transfer and may stabilize the phosphate during reaction progression (Cheng et al., 2005). Furthermore, Asn171 helps to position one of the catalytically essential magnesium ions. The "magnesium positioning loop" is also in the C-lobe, which contains the conserved Asp184 that is part of the DFG motif. This aspartate residue helps to coordinate both catalytically essential magnesium ions. Finally, the "activation loop," residues 192-200, contains Thr197 that must be phosphorylated in PKA and most kinases for normal activity (Steichen et al., 2012).

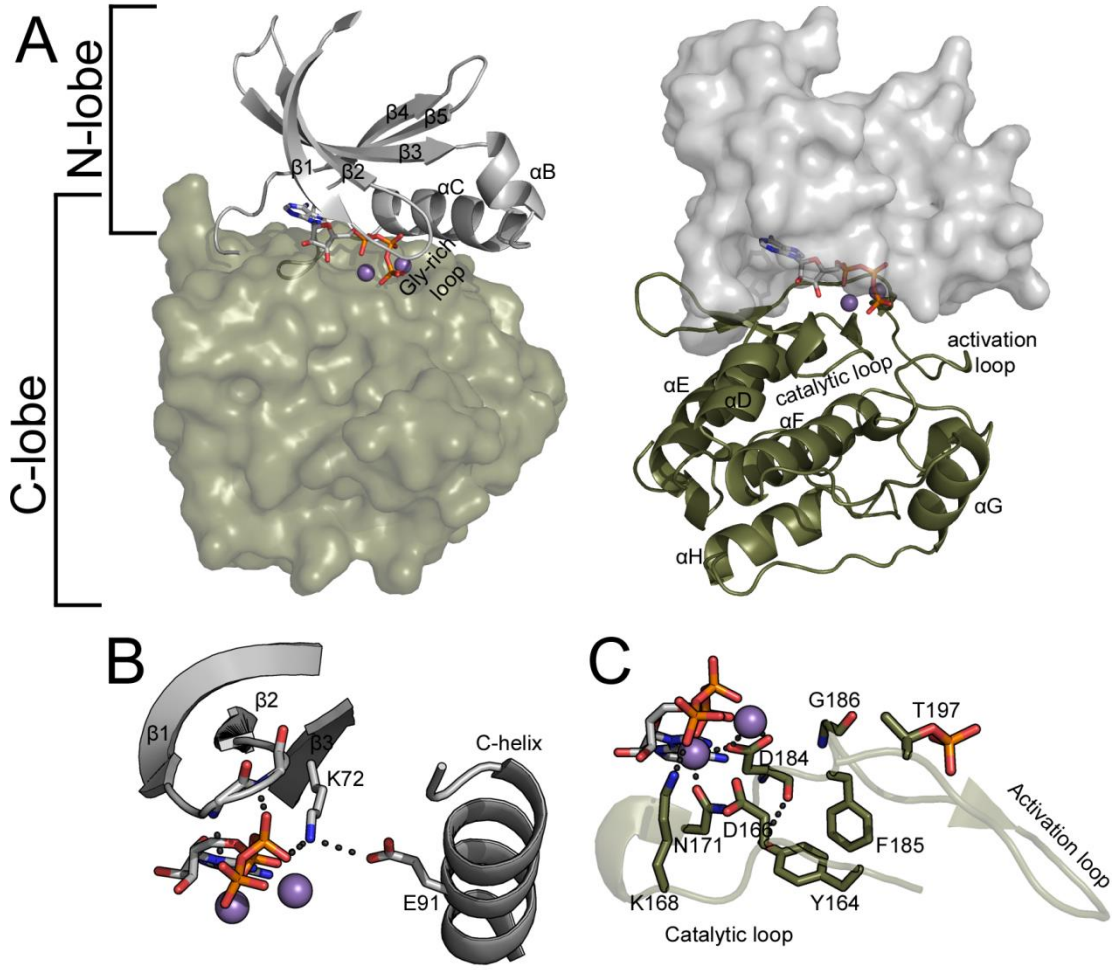

Figure 1.4. Structure of the Kinase Core and Important Catalytic Residues. A. The core of the C-subunit of PKA, 40-300, is displayed. The N-lobe is colored gray, and the C-lobe is colored tan. On the left, the N-lobe is shown in cartoon representation and the C-lobe is shown in surface representation with specific important regions highlighted in the N-lobe, and these representations are reversed on the right. ATP is shown in stick representation and the magnesium ions are shown as purple spheres. **B**. A close up of the Gly-rich loop and C-helix is shown with important residues shown in stick representation. **C**. A close up of the activation loop and catalytic loop and important residues within these regions are displayed in stick representation. This figure was generated from PDB 1ATP.

Hydrophobic Spines – In addition to the residues that make important interactions at the active site, there are also two stacks of hydrophobic residues that are important in the architecture of protein kinases. For instance, there are four hydrophobic residues that are aligned in active kinases and typically not aligned in inactive kinases (Kornev et al., 2006). These residues were termed the "regulatory spine" or "R-spine" because they appear to regulate whether a kinase is active or inactive. In PKA, these residues correspond to Tyr164, Phe185, L95, and L106 (**Fig. 1.5**). PKA, which is constitutively active, has these four residues aligned, but if phosphorylation of T197 is prevented rendering the kinase inactive, then this spine is broken (Steichen et al., 2012). Additionally, there is another parallel spine that forms upon addition of ATP with the adenine ring forming part of the spine, which gave it the name "catalytic spine" or "C-spine," and is comprised of residues Ala70, Val57, Leu173, Ile174, Leu172, Met128, Met231, and Leu227 (Kornev et al., 2008) (**Fig. 1.5**).

Reaction Mechanism – Protein kinases are thought to catalyze phosphoryl transfer using one of two mechanisms termed associative or dissociative mechanisms (Cheng et al., 2005; Szarek et al., 2008; Valiev et al., 2003; Valiev et al., 2007) (**Fig. 1.6**). The main differences between the two proposed mechanisms are the transition states that are adopted during the reaction and what group accepts the hydrogen atom from the substrate residue. The associative mechanism forms a trigonal bipyramidal transition state with a -3 charge where bond formation between the γ-phosphate of ATP and the substrate residue begins before the bond between the β- and γ-phosphates completely breaks. With the associative mechanism, the hydrogen atom on the

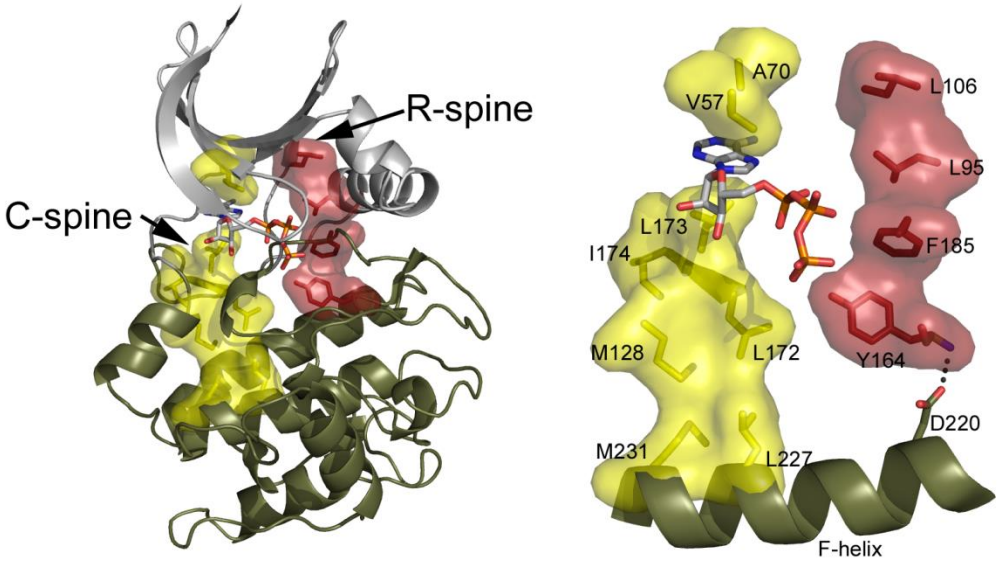

Figure 1.5. Regulatory and Catalytic Spines. On the left, the core of the C-subunit of PKA, residues 40-300, is shown in cartoon representation with the residues that form the C-spine and R-spine shown in stick and transparent surface representation. The C-spine residues are colored yellow and the R-spine residues are colored red. The spines, ATP, and the F-helix are displayed alone on the right. Asp220 connects the F-helix to the R-spine.

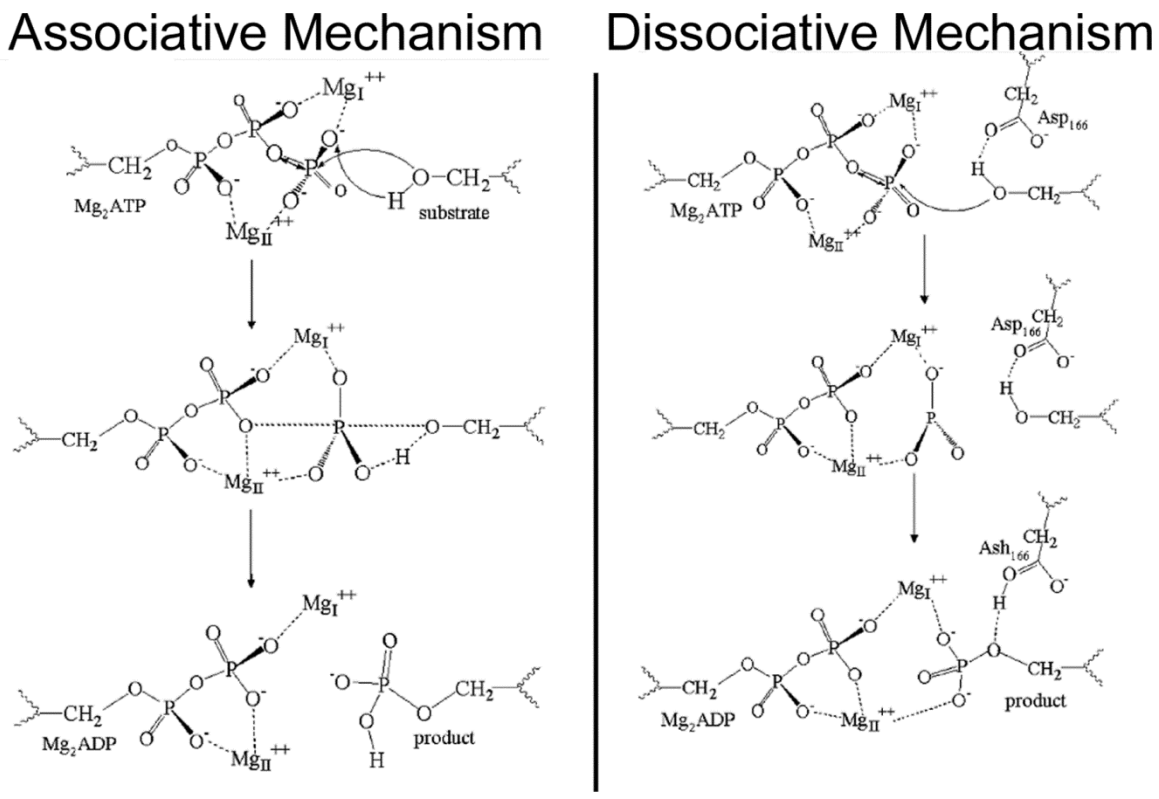

Figure 1.6. Proposed Catalytic Mechanisms for Protein Kinases. A depiction of the associative mechanism for protein kinases is displayed on the left, and the dissociative reaction mechanism is portrayed on the right. This figure was taken from Cheng et al. (2005) *JACS* 127:5.

substrate residue is accepted by the incoming γ-phosphate. The dissociative mechanism involves a complete break in the leaving group producing a metaphosphate with a -1 charge, and the hydrogen atom of the substrate is accepted by the "catalytic base" aspartate residue, Asp166 in PKA (Cheng et al., 2005). There was some debate about the mechanism of phosphoryl transfer, and the mechanism is not resolved. However, the majority of studies now conclude that phosphoryl transfer proceeds through a dissociative mechanism (Cheng et al., 2005; Valiev et al., 2007).

Catalytically Essential Magnesium Ions – In addition to ATP, phosphoryl transfer by most protein kinases is completely reliant on magnesium ions. Magnesium binds to ATP in solution, and it is MgATP that most likely binds together within the active site of most protein kinases. Magnesium ions increase the binding affinity of ATP to kinases (Armstrong et al., 1979) and are required for proper enzyme activity of all kinases except for CASK, which is the only kinase identified thus far that requires no magnesium ions (Mukherjee et al., 2008). Magnesium ions are thought to improve ATP binding and phosphoryl transfer by neutralizing the negative charges of the phosphate groups of ATP as well as the many acidic residues at the kinase active site. Also, the magnesium ions are thought to help stabilize the transition state and to help orient the γ-phosphate for phosphoryl transfer.

Some kinase crystal structures display two magnesium ions at the active site while other kinases crystallize with only one magnesium ion (Bossemeyer et al., 1993; Tereshko et al., 2001; Wu et al., 2008). However, in the structures that display one magnesium ion, the γ-phosphate does not typically appear properly oriented for

phosphoryl transfer (Tereshko et al., 2001; Wu et al., 2008). PKA typically crystallizes with two magnesium ions, and the nomenclature used to describe the two magnesium ions in many protein kinases originates from early structural studies of PKA. In an early crystal structure of PKA at relatively low resolution obtained under low magnesium concentration, there was electron density for mostly one magnesium ion with less density for the other magnesium ion (Zheng et al., 1993a). Therefore, the ion that showed more electron density was thought to bind first in PKA and was thought to be the more important ion for phosphoryl transfer, and as a consequence, this ion was named Mg1 and activating. The other magnesium ion was termed Mg2 and inhibiting. Mg1 is coordinated by Asp184 in a bidentate manner, by the β- and γ-phosphates of ATP, and by two water molecules (**Fig. 1.7**). Mg2 is coordinated by Asn171, one oxygen atom of Asp184, the α- and γ-phosphates of ATP, and one water molecule (**Fig. 1.7**).

The activating/inhibiting nomenclature used to describe the two magnesium ions was given because low concentrations of magnesium (0.5 mM) yield higher k_{cat} values for PKA than high magnesium concentrations (10 mM) (Adams and Taylor, 1993; Cook et al., 1982; Shaffer and Adams, 1999b). Therefore, it was thought that the binding of the second magnesium ion has a negative impact on enzyme activity. However, this terminology is misleading because binding two magnesium ions does not influence the rate of phosphoryl transfer, but instead, it affects the rate of ADP release, which is the rate limiting step at high magnesium ion concentration (Adams and Taylor, 1993; Shaffer and Adams, 1999b).

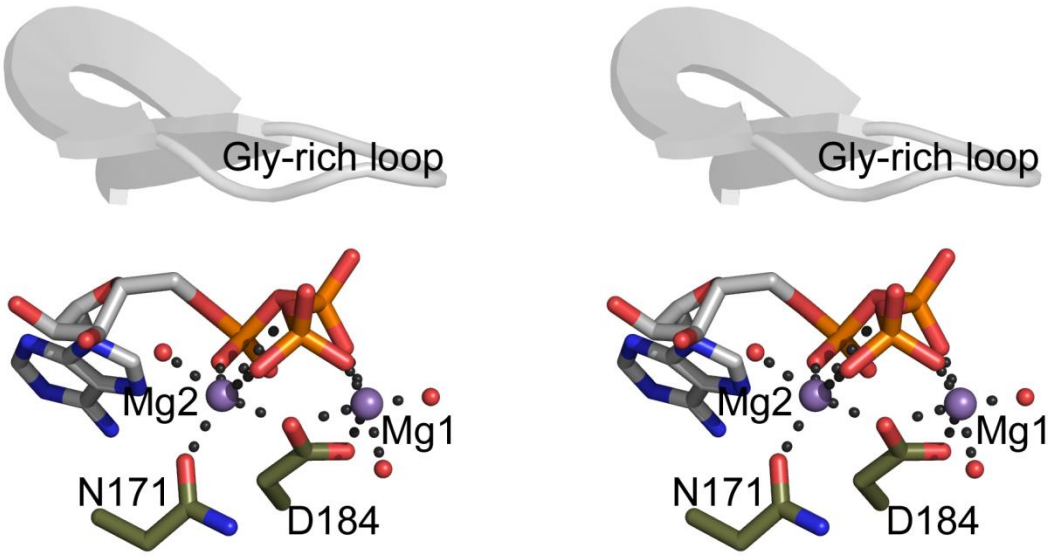

Figure 1.7. Coordination of the Magnesium Ions in PKA. A stereo view of the location and coordination of the two magnesium ions at the PKA active site is shown. The residues that bind magnesium, Asp184 and Asn171, are shown in stick representation. ATP is shown in stick representation. The Gly-rich loop is shown in cartoon representation. Water molecules are shown as red spheres, and the magnesium ions are shown as purple spheres. The coordination of the magnesium ions is shown with dashed lines. This figure was generated from PDB 1ATP.

Despite the fact that the magnesium ions were give the terms Mg1 and Mg2, it is still unclear if this assigned order of binding is correct for PKA and other kinases in general. A recent crystal structure of PKA also obtained under low magnesium concentration showed electron density only for the ion previously termed Mg2 with no density for Mg1 (Kovalevsky et al., 2012). Additionally, in many other kinases that crystallize with only one magnesium ion visible in the electron density, the ion that is visible corresponds to Mg2 (Jacobsen et al., 2012). Therefore, there is still some uncertainty about which magnesium ion binds first and is more important for enzyme turnover in PKA and kinases in general.

In addition to the roles of the magnesium ions in the chemical reaction, the ions are also involved in regulating product release since high magnesium concentrations slow the rate limiting step of ADP-release (Adams and Taylor, 1993; Shaffer and Adams, 1999b). Computational studies directed at understanding how ADP-release may proceed with two magnesium ions bound suggested that release is so energetically unfavorable that it would require local unfolding at the active site or large global conformational changes for release to occur (Khavrutskii et al., 2009). Therefore, it was proposed that one or both magnesium ions may need to be released prior to ADP-release. Consequently, in addition to improving phosphoryl transfer, the magnesium ions regulate the subsequent processes of product release, but this mode of regulation and how the reaction proceeds remains unresolved.

1.5 Protein N-myristylation and N-myristylation of PKA

N-terminal myristylation – N-myristylation is catalyzed by the enzyme N-myristyl transferase (NMT). NMT is an enzyme that is ubiquitously expressed that catalyzes the permanent covalent attachment of the 14 carbon saturated fatty acid, myristic acid, onto the N-terminal glycine residue of target proteins. This modification is typically performed co-translationally where the N-terminal methionine residue is first cleaved by a methionine aminopeptidase, and then NMT covalently attaches myristic acid onto the N-terminal glycine residue (Boutin, 1997; Farazi et al., 2001; Resh, 1999). There are some preferences by NMT for which proteins can be myristylated, but the N-terminal glycine residue at position 1 is the only absolute requirement (Boutin, 1997; Farazi et al., 2001; Resh, 1999). However, not all proteins that contain a glycine residue at the N-terminus are myristylated due to these other preferences.

N-myristylation of proteins is often associated with increased membrane binding, as may be expected. However, myristylation alone is insufficient to retain membrane localization and allows for transient interaction with membranes. Additional factors such as positive charges on the protein; another fatty acylation such as palmitoylation; or protein-protein interactions with membrane bound proteins are required to keep a protein anchored to the membrane (Resh, 1999) (**Fig. 1.8A**). Furthermore, there are mechanisms for reversible membrane binding such as "myristyl ligand switch" and "myristyl electrostatic switch" (Resh, 1999) (**Fig. 1.8B**). With the myristyl ligand switch, binding of a ligand can influence whether the myristic acid group is free to interact with membranes or not, and this type of switch was observed with the protein recoverin with the switch occurring with the binding of Ca^{+2}

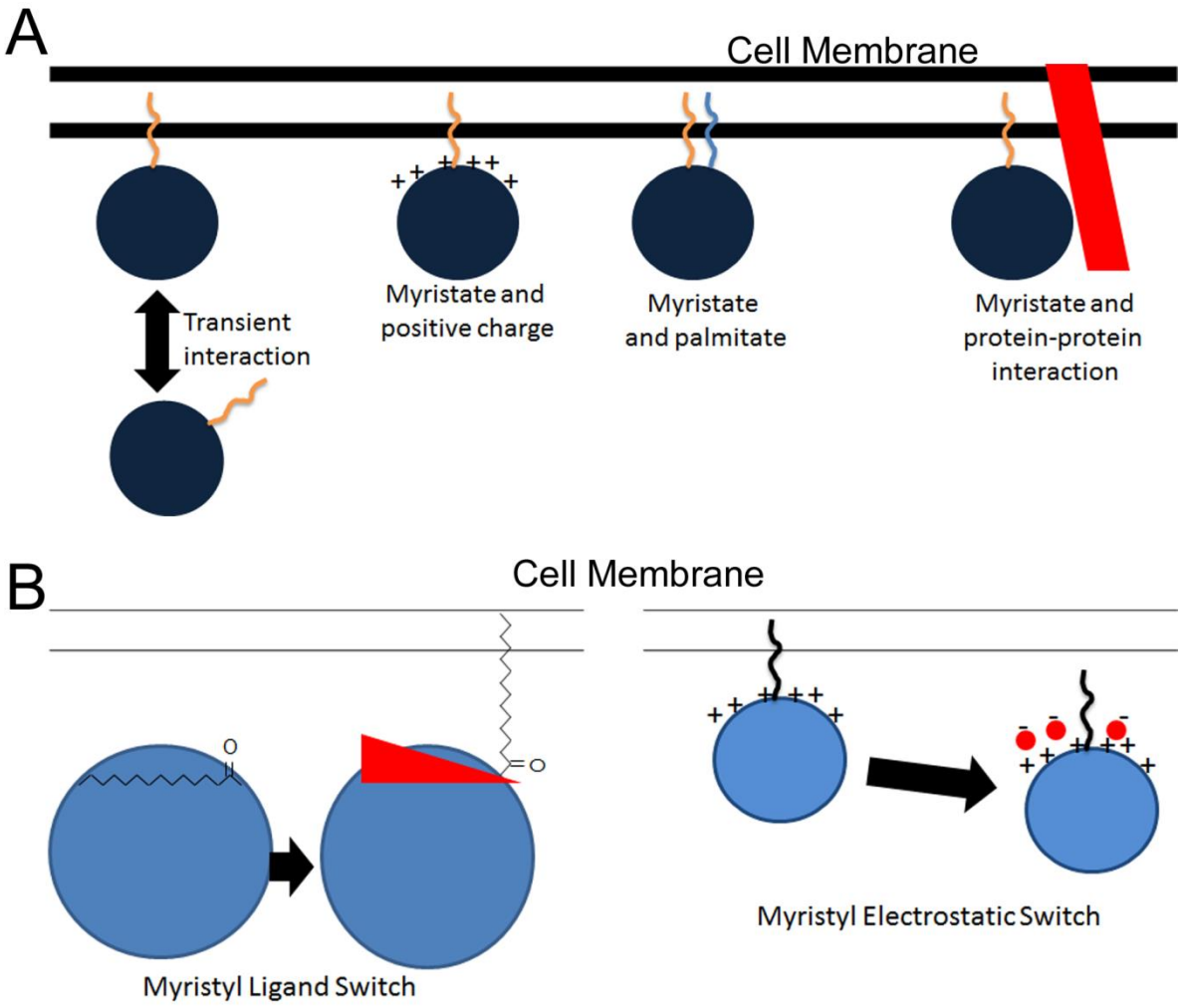

Figure 1.8. Mechanisms for Membrane Binding via N-myristylation. A. N-myristylation alone is insufficient to keep proteins anchored to membranes. Additional factors are required to maintain membrane binding as illustrated here. **B**. Mechanisms for reversible membrane binding with N-myristylation are illustrated including myristyl ligand switch (ligand is depicted as red triangle) or myristyl electrostatic switch (added negative charges depicted with red spheres). This figure was adapted from Resh (1999) *Biochim. Biophys. Acta* 1451:1.

(Ames et al., 1995; Tanaka et al., 1995; Weiergraber et al., 2003). For the myristyl electrostatic switch, proteins that are bound to membranes via positive charges can be released from the membrane due to phosphorylation reversing the favorable electrostatic interactions with the membrane, and this type of switch regulates the protein myristylated alanine-rich C-kinase substrate (MARCKS) (Thelen et al., 1991). In addition to membrane binding, N-myristylation is also involved in several other functions of proteins. For example, N-myristylation is involved in enzyme activity for proteins such as Abelson (Abl) (Hantschel et al., 2003; Nagar et al., 2003) and Src (Patwardhan and Resh, 2010). Myristylation can also regulate substrate binding, enzyme stability, and protein folding (Chida et al., 2013; Schroder et al., 2011; Shental-Bechor et al., 2012; Stephen et al., 2007).

N-terminus and N-myristylation of PKA – The core of the catalytic subunit of PKA (residues 40-300) is conserved among all protein kinases. The C-tail, residues 301-350, is unique to the AGC group of protein kinases, and the N-terminus, residues 1-39, is unique to PKA. The C-tail of PKA is important for enzyme activity, and it contains a phosphorylation site that is important in PKA processing and activity (Batkin et al., 2000). The N-terminus is unique to PKA. This region is comprised largely of one helix termed the A-helix. The N-terminus is required for proper stability of the enzyme, and it is the N-terminus that exhibits the largest differences between C-subunit isoforms (Herberg et al., 1997). Furthermore, the N-terminus is a dynamic region of the protein because of the many co- and post-translational modifications that it undergoes as well as protein-protein interactions.

The N-terminus can be phosphorylated on Ser10, deamidated at Asn2, and myristylated at Gly1 (Tholey et al., 2001) (**Fig. 1.9**). The Ser10 residue is a site that can undergo autophosphorylation when the C-subunit is expressed in *E. coli*, but it is unclear whether or not this phosphorylation also occurs in mammalian cells (Yonemoto et al., 1993a). Deamidation is the conversion of an asparagine residue to an aspartate residue, which occurs when the side-chain of the asparagine residue cyclizes with the backbone of the protein, and it is then deamidated forming either aspartate or *iso*-aspartate (Shimizu et al., 2005). This modification is generally a non-enzymatic process that is thought to be part of protein aging, but with PKA, this modification showed effects on C-subunit localization suggesting that it may be functionally significant in PKA and possibly other proteins (Pepperkok et al., 2000). Finally, N-myristylation of the N-terminal glycine residue is a modification that happens co-translationally on the C-subunit of PKA. This modification was first identified with PKA when an attempt to identify the amino acid residues of the protein via Edman degradation was prevented due to something blocking the N-terminus (Carr et al., 1982). This entity blocking the process was covalently attached myristic acid. In addition to these modifications, the N-terminus binds A-kinase interacting protein (AKIP) between residues 15-30 and regulates C-subunit localization (Sastri et al., 2005) (**Fig. 1.9**).

The N-myristylation of PKA is a difficult modification to study because the recombinant protein purified from *E. coli* is not myristylated due to lack of NMT in *E. coli,* but myristylated PKA can be generated by co-expression of NMT with the C-subunit (Duronio et al., 1990). Additionally, there are some early structural studies of

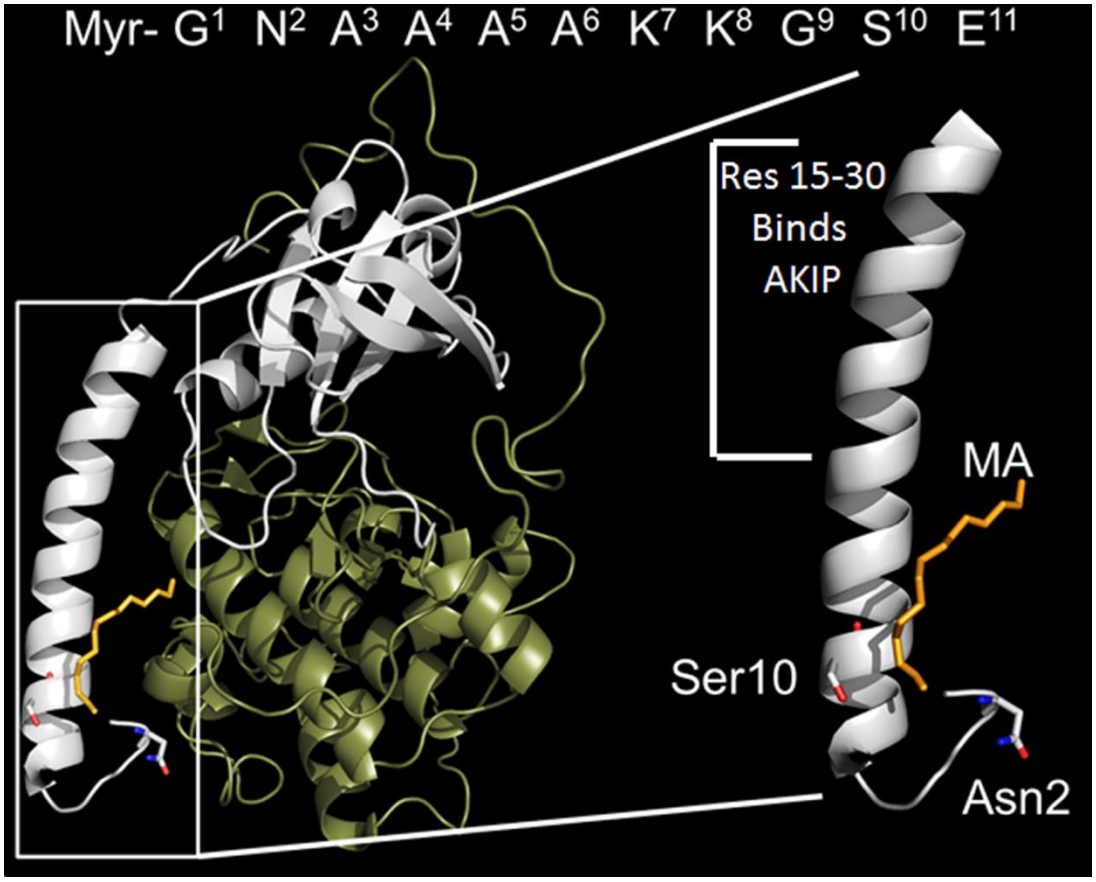

Figure 1.9. The N-terminus of PKA. The C-subunit of PKA is depicted with the N-lobe (residues 1-126) colored gray and the large lobe (residues 127-350) colored tan. This structure is of the N-myristylated protein, and the myristic acid group is colored orange and shown in stick representation. The N-terminus is highlighted in the figure. The N-terminus is comprised largely of one helix termed the A-helix. The N-terminus can be phosphorylated at Ser10, deamidated at Asn2, and myristylated at Gly1. These residues are shown in stick representation on the right. Also, the A-helix is a binding site for the protein A-kinase interacting protein (AKIP) between residues 15-30. The first 11 residues are listed above the structure for reference. This figure was generated from PDB 1CMK.

the N-myristylated C-subunit from when the protein was purified from source tissues (Bossemeyer et al., 1993; Zheng et al., 1993b). For PKA, N-myristylation increases the thermostability of the enzyme suggesting that the modification stabilizes the core of the protein (Yonemoto et al., 1993b). Also, N-myristylation increases membrane binding of the C-subunit alone and in RII but not RI holoenzyme complexes (Gangal et al., 1999). There are structures of the N-myristylated C-subunit. However, in one of these structures, most of the N-terminus and myristic acid group are not visible in the electron density (Bossemeyer et al., 1993). In another crystal structure, the entire N-terminus and myristic acid group are modeled in the structure. However, at 2.9 Å resolution, this region is not well-resolved in this structure and represents a possible conformation (Zheng et al., 1993b) (**Fig. 1.9**). Therefore, how N-myristylation may regulate the structure of the N-terminus of PKA is still unclear. Furthermore, N-myristylation does not alter C-subunit activity or signal transduction (Clegg et al., 1989), and therefore, it is still unclear what roles this modification may have on C-subunit activity or regulation.

1.6 Questions and Goals of the Thesis

There are several unresolved questions regarding the role of N-myristylation of the C-subunit of PKA. How does N-myristylation influence the structure of the N-terminus of the C-subunit? What role does myristylation have on C-subunit dynamics? Can myristylation influence the C-subunit active site or enzyme activity? The goal of this thesis was to answer these and other questions that may arise. One of these additional questions arose out of an unexpected finding that the generally non-

hydrolyzable analog of ATP, AMP-PNP, can slowly hydrolyze in protein crystals. This finding allowed for a characterization of reaction progression in PKA and lead to a new set of questions. How does PKA reaction progression proceed? Which of the two magnesium ions is more important for enzyme activity, and how do the magnesium ions regulate and allow for ADP-release?

There were several major goals of this thesis, and one of these goals was to obtain new crystal structures of the N-myristylated C-subunit. We hypothesized that N-myristylation alters the structure of the C-subunit, and we believed that there is a novel conformation or conformations of the C-subunit yet to be identified that arise because of this modification. However, before the goal of new crystal structures could be achieved, new methods to purify large quantities of the myristylated protein from *E. coli* had to be developed because previous protocols resulted in extremely low yields. These low yields are a major reason for the lack of structural studies of this modification. After increasing these yields, then the goal was to crystallize the myristylated C-subunit.

Another major goal was to elucidate how N-myristylation influences C-subunit dynamics using time-resolved fluorescence anisotropy and molecular dynamics (MD) simulations. The fact that N-myristylation increases the structural stability of the enzyme suggests that it stabilizes the core of the protein, and it suggests that the modification likely decreases motions at the N-terminus and myristate pocket. Our goal was to test this hypothesis and to determine whether decreased motion at the myristate pocket causes long-range effects on the motion of the entire protein.

Finally, a goal was to determine the mode of PKA reaction progression and product release. These studies arose out of the serendipitous finding that AMP-PNP can undergo slow phosphoryl transfer in protein crystals. It was still unclear which of the two magnesium ions binds first within the PKA active site and how these magnesium ions regulate ADP-release. Also, because kinases are highly conserved, the findings from PKA could likely be generalized to many, if not all, protein kinases.

Chapter 2

Role of N-terminal Myristylation in the Structure and Regulation of cAMP-Dependent Protein Kinase

2.1 Introduction

cAMP-dependent protein kinase [protein kinase A (PKA)] is a Ser/Thr phosphoryl transferase that consists of two catalytic (C) subunit monomers which phosphorylate target substrates as well as a regulatory (R) subunit dimer that binds to and inactivates the C-subunit (Taylor et al., 2008). PKA is regulated by the second messenger, cAMP, which binds to the R-subunit dimer causing a conformational change that allows for the release of the active C-subunit monomers (Taylor et al., 2008). There are four isoforms of the regulatory subunit which are RIα, RIβ, RIIα, and RIIβ. These R subunit isoforms serve non-redundant functions, and RIα/RIIα are ubiquitously expressed while RIβ/RIIβ exhibit tissue specific expression (Kirschner et al., 2009; Mucignat-Caretta and Caretta, 2002). The RI subunits are thought to typically be cytosolic while RII subunits are generally localized to specific regions within the cell via A-kinase anchoring proteins (AKAPs). However, RI subunits can also be localized by AKAPs (Kirschner et al., 2009; Mucignat-Caretta and Caretta, 2002). Therefore, there are specific mechanisms to localize and regulate PKA activity.

The catalytic subunit of PKA performs the phosphoryl transfer reaction, and it is well characterized structurally and biochemically (Francis and Corbin, 1994; Johnson et al., 2001; Shabb, 2001; Tasken et al., 1997). The C-subunit of PKA was the first protein kinase structure solved (Knighton et al., 1991b), and there are many structures of the enzyme in multiple states including apo (Akamine et al., 2003; Wu et al., 2005); bound to a peptide (binary complex) (Knighton et al., 1993; Knighton et al., 1991b; Madhusudan et al., 1994; Zheng et al., 1993b); and bound to a peptide and ATP (ternary complex) (Bossemeyer et al., 1993; Yang et al., 2004; Yang et al.,

2012). The C-subunit of PKA serves as an important model for the kinase family because the core of the C-subunit (residues 40-300) is conserved throughout the protein kinase superfamily, whereas the C-terminus (residues 301-350) is a distinguishing feature of the AGC group of protein kinases. In contrast, the N-terminus of the C-subunit (residues 1-39) is not found in other kinases and is variable even within different PKA isoforms. The N-terminus of PKA is largely comprised of one helix termed the A-helix which is a site for protein interactions. A-kinase-interacting protein (AKIP) binds to the N-terminus between residues 15-30 and acts to localize PKA to the nucleus (Sastri et al., 2005). Additionally, the N-terminus is a site of many potential modes of co- and posttranslational regulation via different modifications including myristylation of the N-terminal glycine, deamidation of Asn2, and phosphorylation of Ser10, any or all of which may influence PKA interactions, activity, or localization (Tholey et al., 2001).

Myristylation is the irreversible, covalent attachment of the 14 carbon saturated fatty acid, myristic acid, onto the N-terminal glycine of target proteins which typically occurs co-translationally via N-myristyl transferase (NMT) (Farazi et al., 2001). Many signaling and viral proteins are myristylated, and myristylation is important for membrane binding and proper localization of many proteins (Li et al., 2007; Song et al., 1997). However, myristylation has many other roles beyond membrane binding. For example, myristylation is important for the autoinhibition of c-Abelson (c-Abl) tyrosine kinase by stabilizing the autoinhibited state of the protein (Hantschel et al., 2003; Nagar et al., 2003). Additionally, myristylation enhances c-Src kinase activity and may be involved in proper ubiquitination and degradation of the protein

(Patwardhan and Resh, 2010). Also, proteins such as recoverin undergo myristyl-switch mechanisms where binding to Ca^{2+} influences the location and effect of myristylation on the protein (Ames et al., 1995; Tanaka et al., 1995; Weiergraber et al., 2003). With respect to PKA, N-myristylation enhances the thermal stability of the enzyme (Gaffarogullari et al., 2011; Yonemoto et al., 1993b) and the myristylated C-subunit has a higher affinity for membranes alone, however, association with membranes is further enhanced in RII but not RI holoenzyme complexes (Gangal et al., 1999).

In addition to N-myristylation, the C-subunit of PKA may be regulated by irreversible deamidation of Asn2. Deamidation is a process that is thought to occur non enzymatically where asparagine or aspartate residues can cyclize with the backbone amide forming a succinimide intermediate and can then be deamidated to form aspartate or iso-aspartate (Shimizu et al., 2005). Although this modification is generally thought to occur non enzymatically, there are some virulence factors that catalyze deamidation of proteins to evade immune response (Buetow and Ghosh, 2003; Cui et al., 2010). The deamidation of residues to iso-aspartate can be reversed by the enzyme L-isoaspartyl methyltransferase (PIMT), which converts the residue back to aspartate (Shimizu et al., 2005). However, if the residue was originally asparagine, then it is permanently changed to aspartate. Additionally, proteins that contain aspartate at residue 2 are not typically myristylated and, indeed, PKA cannot be myristylated if Asn2 is mutated to Asp (Jedrzejewski et al., 1998). Therefore, deamidation is a mechanism where aspartate can be present at residue 2 within a myristylated protein. With PKA that is purified from tissues, irreversible deamidation

of Asn2 to Asp or *iso*Asp occurs in about 1/3 of the total C-subunit protein. Also, the deamidated form of the protein has a higher cytosolic to nuclear ratio than the non-deamidated protein (Pepperkok et al., 2000). Thus, deamidation may influence protein localization, and this influence could be attributed to effects from myristylation. For instance, it is possible that the added negative charge at the N-terminus in the deamidated protein may remove myristic acid from its binding pocket allowing the myristate group to interact with membranes or other binding partners and retain cytosolic localization.

The N-terminus of the C-subunit may also be regulated by phosphorylation of Ser10. Phosphorylation of Ser10 has not been observed from PKA purified from tissues (Pepperkok et al., 2000), which suggests that it may be a transient phosphorylation event. However, when the C-subunit is expressed in *E. coli*, most of the protein is autophosphorylated on Ser10 (Yonemoto et al., 1993a). Furthermore, PKA purified from tissues can autophosphorylate at Ser10 but only if the protein is deamidated at Asn2 (Toner-Webb et al., 1992). This fact suggests the possibility of Ser10 phosphorylation and Asn2 deamidation acting synergistically to add negative charges at the N-terminus which may prevent membrane binding. Furthermore, NMR studies were recently performed on the myristylated C-subunit which suggested that Ser10 phosphorylation destabilizes the N-terminus of PKA and causes the myristyl moiety to be removed from its hydrophobic pocket (Gaffarogullari et al., 2011). The authors argue that removal of the myristic acid group following Ser10 phosphorylation may improve the capacity for PKA to bind to membranes. Additionally, removing

myristic acid from the hydrophobic pocket may also improve the ability for PKA to bind protein partners such as AKIP via the A-helix.

In addition to the potential role of N-myristylation and other N-terminal modifications regulating C-subunit localization and interactions, it is also possible that myristylation can influence the active site of the enzyme. Although C-subunit activity is not altered by myristylation, there is some evidence of a potential influence of myristylation on the active site of the enzyme. First of all, recent NMR studies of the myristylated protein identified chemical shifts near the active site of the enzyme with the myristylated protein (Gaffarogullari et al., 2011). Additionally, NMR studies performed in the presence and absence of nucleotide and peptide provide further evidence of a potential cross talk between the myristic acid binding pocket and the active site of the enzyme. These studies identified Trp302, which is in the myristate pocket, as a sensor for binding of both nucleotide and peptide. It exhibits a large chemical shift upon binding to AMP-PNP and PKI (Masterson et al., 2011). This finding provides further evidence that the myristate pocket and the active site could influence each other. Trp302 is especially significant because it lies at the junction of the C-lobe in the kinase core and the beginning of the C-terminal tail. The position of this C-terminal tail is highly conserved in all AGC kinases as is Trp302. Therefore, myristylation of the C-subunit may regulate PKA activity or substrate binding in addition to potential roles in localization.

In this study, we were interested in further elucidating the role of N-myristylation on the structure and regulation of the C-subunit. Structural information about myristylation of PKA is lacking because currently reported structures of the

myristylated C-subunit display only part of the N-terminus and the myristic acid group (Bossemeyer et al., 1993; Karlsson et al., 1993) or are at relatively low resolution with poor density at the N-terminus (Zheng et al., 1993b). Using X-ray crystallography and kinetics, we investigated the role of N-myristylation on the structure and function of the C-subunit. We obtained crystal structures of binary and ternary complexes of the WT enzyme and a K7C mutant that exhibited altered kinetics in a myristylated state. We identified a novel conformation of PKA and suggest that the myristic acid binding pocket may be an allosteric regulator of PKA.

2.2 Experimental Procedures

Purification of the myristylated C-subunit proteins. The non-myristylated WT and K7C C-subunits were expressed and purified as described previously (Herberg et al., 1993). The myristylated C-subunit was prepared by co-expression with yeast NMT as described previously (Duronio et al., 1990) and purified following a method described previously (Hemmer et al., 1997). Cultures of NMT/PKA were grown at 37 °C to an OD_{600} of ~0.6 and induced with 1.0 mM isopropyl β-D-thiogalactopyranoside (IPTG) and 0.26 mM sodium myristate. The cultures were grown for 18-24 hours at 24 °C before being harvested. The PKA/NMT pellet and a H_6-tagged RIIα(R213K) pellet corresponding to at least a third of the culture volume of the PKA/NMT pellet (i.e. 12 L PKA/NMT: 4 L H_6-RIIα(R213K)) was re-suspended in lysis buffer (50 mM KH_2PO_4, 20 mM imidazole, 150 mM KCl, 200 µM ATP, 2 mM $MgCl_2$, 5 mM β-mercaptoethanol, pH 6.5). The re-suspended pellets were then lysed using a microfluidizer (microfluidics) at 18,000 p.s.i. The cells were clarified by

centrifugation at 15,000 rpm at 4°C for 60 min in a Beckman JA20 rotor, and the supernatant was incubated with ProBond Resin (Invitrogen) for 24 hour at 4°C. The resin was loaded onto a column and washed twice with the lysis buffer. Three 10 mL elutions were then collected using 1 mM cAMP dissolved in lysis buffer. The elutions were combined and dialyzed overnight into 20 mM KH_2PO_4, 25 mM KCl, and 5 mM DTT, pH 6.5 and then loaded onto a pre-packed Mono-S 10/100 (GE health) cation exchange column equilibrated in the same buffer. The protein was eluted from the column with a KCl gradient ranging from 0 to 1 M. The myristylation state of the protein was confirmed using mass spectrometry. The myristylated protein eluted from the MonoS at a higher KCl concentration than the non-myristylated protein allowing for effective separation of non-myristylated from myristylated protein. Also, the majority of the protein was myristylated (around 75% for WT and ~100% for K7C).

Crystallization. Myristylated WT and myristylated K7C ternary (AMP-PNP, Mg^{2+}, SP20) and binary (SP20) complexes were crystallized under very similar conditions utilized for previous C-subunit structures (Wu et al., 2005; Yang et al., 2004). In each case, the protein being crystallized was dialyzed overnight into 50 mM bicine, 150 mM ammonium acetate, 10 mM DTT, pH 8.0. Then the protein was concentrated to 8-10 mg/mL. The proteins were setup for crystallization using the hanging drop vapor diffusion method at 4 °C. Immediately preceding the crystal tray preparation, the protein was combined in 1:10:20:5 molar ratio of protein:AMP-PNP:Mg^{2+}:SP20 for the ternary complex or 1:5 protein:SP20 for the binary complex. These complexes were screened under different MPD concentrations ranging from 2-18% and with

different buffer conditions in the well solution including no buffer or buffers ranging from pH 5.35 to pH 8.5. The drop contained 1:1 volume of protein solution to well solution, and 9-13% methanol was added to the well solution before sealing the well. For the ternary complexes, crystals were typically seen after 1-2 weeks and generally appeared to reach maximum size by 4-6 weeks, and with the binary complexes, crystals appeared after 4-6 weeks and reached maximum size by 8-10 weeks. The myristylated WT C-subunit ternary structure was obtained from a crystal grown with a well solution containing 10% MPD and 9% MeOH added to the well. The myristylated K7C ternary structure was obtained from a crystal grown with a well containing 12% MPD, 100 mM Bis-Tris pH 6.5, and 9% MeOH added to the well. The myristylated WT and K7C binary structures were obtained from crystals grown with wells containing 6% MPD and 9% MeOH added to the well solution. The WT and K7C binary complexes were crystallized from protein samples with two phosphates on Thr197 and Ser338. The WT and K7C ternary complexes were crystallized from a protein mixture containing two or three phosphates with phosphates being on Thr197 and Ser338 for all proteins and some proteins with phosphate on Ser139. The WT and K7C ternary structures were both modeled with 40% phosphorylation of Ser139.

Data collection and refinement. The crystals were flash cooled in liquid nitrogen with cryoprotectant solution (16% MPD and 15% glycerol). Data was collected on the synchrotron beamline 8.2.1 of the Advanced Light Source, Lawrence Berkeley National Labs (Berkeley, California). For each crystal structure, the data was

integrated using iMOSFLM (Battye et al., 2011). All protein variants and complexes crystallized in the $P2_12_12_1$ space group similar to the wild type structure. Molecular replacement was carried out using Phaser (McCoy et al., 2007) with a previously solved C-subunit structure PDB ID: 3FJQ(Thompson et al., 2009) as a search model. The refinement was performed using refmac5(1994) and model building was done in Coot (Emsley and Cowtan, 2004). With the binary complexes and ternary K7C complex, positive density was readily apparent at the N-terminus of the protein. The myristylated ternary K7C structure had the clearest density at the N-terminus due to its high resolution, and the N-terminus and myristic acid were modeled into this density. Then, the conformation seen with the K7C ternary complex was modeled into the binary complexes and also fit the density for these proteins very well with only slight changes necessary. The myristylated WT ternary structure, myristylated K7C ternary structure, myristylated WT binary structure, and myristylated K7C binary structure were refined to R_{work}/R_{free} of 19.4%/22.7%, 15.5%/17.9%, 19.2%/21.1%, and 20.5%/23.4% respectively. The data collection and refinement statistics are shown in **Table 2.1**.

Steady state kinetics. The kinetics were performed as described previously (Cook et al., 1982; Steichen et al., 2010). Reactions were performed in 100 mM MOPS (pH 7.0) and 10 mM $MgCl_2$. To measure the K_m for ATP, the concentration of kemptide (LRRASLG) was fixed at 250 μM and ATP was varied from 10 – 500 μM. To

Table 2.1. Crystallography data collection and refinement statistics of myristylated proteins. All data collection was performed at ALS laboratory in Berkeley, CA on beamline 8.2.1.
[a]Values in parenthesis correspond to the highest resolution shell. [b]5% of the data was excluded from the refinement to calculate the R_{free}. [c]Ramachandran plot quality as defined in MolProbity (Davis et al., 2007).

	Myr-WT Ternary	**Myr-WT Binary**	**Myr-K7C Ternary**	**Myr-K7C Binary**
PDB ID	4DG0	4DG2	4DFX	4DFZ
Data Collection				
Space group	$P2_12_12_1$	$P2_12_12_1$	$P2_12_12_1$	$P2_12_12_1$
Cell dimensions				
a (Å)	57.80	48.48	48.10	48.46
b (Å)	78.73	79.63	79.70	79.63
c (Å)	99.00	117.89	117.23	118.06
Unique reflections	31,277 (4,494)	25,942 (3,628)	95,939 (13,243)	30,558 (4,292)
Multiplicity	6.5 (6.5)	6.2 (6.4)	5.3 (5.7)	5.0 (5.2)
Resolution range (Å)	39.37-2.0 (2.11-2.00)[a]	39.30-2.00 (2.11-2.00)[a]	25.03-1.35 (1.42-1.35)[a]	37.46-2.00 (2.11-2.00)[a]
R_{sym} (%)	11.4 (38.7)	7.2 (26.8)	4.8 (35.9)	11.7 (54.5)
$I/\sigma I$	9.5 (4.2)	16.3 (5.9)	15.8 (3.9)	9.3 (2.9)
Completeness (%)	100 (100)	82.6 (80.5)	96.5 (92.5)	96.8 (94.7)
Refinement				
R_{work}/R_{free} (%)[b]	19.4/22.7 (22.4/24.6)	19.2/21.1 (21.4/25.1)	15.5/17.9 (22.4/25.5)	20.5/23.4 (26.1/27.3)
Ramachandran angles (%)[c]				
Favored regions	98.31	98.07	98.07	98.07
Allowed regions	100	100	100	100
r.m.s. deviations				
Bond lengths (Å)	0.006	0.006	0.009	0.006
Bond angles (°)	0.952	0.866	1.34	0.887

measure the K_m for kemptide, the concentration of ATP was fixed at 1 mM and kemptide was varied from 10 – 300 μM. The final concentration of enzyme was ~0.003 $mgmL^{-1}$. Three separate protein preparations of each C-subunit isoform were measured. All measurements were done in triplicate. Data were fit using GraphPad Prism.

Mass spectrometry analysis of myristylated proteins. Proteins (5μg each) were dissolved in 14% acetonitrile, 0.1% TFA and separated using Magic 2002 HPLC system (Michrom BioResources, Inc.) and eluted into an LTQ-Orbitrap XL mass spectrometer (Thermo Fisher Scientific, San Jose, CA) using electrospray ionization. The HPLC gradient was 14-100% Buffer B in 10min (Buffer A: 2% acetonitrile, 0.05% TFA; Buffer B: 90% acetonitrile, 0.04% TFA). The flow rate was 10μL/min. The LTQ-Orbitrap was set to scan from 400-2000 (MS only) with a resolution of 100,000 in positive, profile mode. The raw data was deconvoluted using Xtract to get the intact protein molecular weight.

Rapid Quench Flow Experiments. Pre-steady state kinetic measurements of the myr-K7C versus non myristylated WT protein were performed using rapid quench flow apparatus (Model RGF-3) from KinTek Corp, following previously described procedures (Adams et al., 1995; Steichen et al., 2012). Experiments were performed with 200 μM ATP and 2 mM kemptide. The activity of γ-32P-ATP was (5000-15000 cpm/pmol). The reaction was carried in 100 mM MOPS (pH 7.4), 10mM Mg^{2+}, 5mg/ml BSA. The reaction was quenched using 30% acetic acid.

PDB coordinates: The coordinates for the structures reported here are deposited in the Protein Data Bank. K7C ternary (PDB ID: 4DFX); K7C binary (PDB ID: 4DFZ); WT ternary (PDB ID: 4DG0); WT binary (PDB ID: 4DG2).

2.3 Results

Purification and kinetic characterization of the myristylated C-subunit.

One of the difficulties of studying the myristylated C-subunit *in vitro* is that bacterial expression of the acylated C-subunit yields a heterogeneous mixture of phosphorylation/myristylation states. One mutation, K7C, initially generated for fluorescent labeling studies, provided several advantages for studying the effects of N-terminal myristylation. This mutation eliminates the PKA recognition sequence at Ser10 and therefore blocks autophosphorylation of Ser10, which minimizes the total number of phosphorylation isoforms of the C-subunit. More importantly, eliminating Ser10 phosphorylation increased the total yield of myristylated protein (**Fig. 2.1**) because we found that myristylation and Ser10 phosphorylation typically do not occur together in our bacterial co-expression system, which was also observed previously with the recombinant myristylated protein (Yonemoto et al., 1993a).

Additionally, we measured the steady-state kinetics of the WT and K7C proteins in myristylated and non-myristylated states. Myristylation of the WT protein does not alter the kinetics. However, the K7C mutant exhibited modest changes in kinetics including increased k_{cat} and K_m values compared to the WT C-subunit when myristylated (**Table 2.2**). Increased activity of the myr-K7C protein was also verified using rapid quench pre-steady state kinase assay (Adams et al., 1995) with

radiolabeled [γ-32P]-ATP experiments, which yielded a similar 55% increase in steady state rate with no effect on phosphoryl transfer rate (**Fig. 2.2**). The increased k_{cat} also appears specific to the cysteine mutation as several other mutations of this residue including K7A and K7S did not yield this increase (data not shown).

Myristylated WT ternary structure (AMP-PNP, Mg^{2+}, and SP20).

We were interested in obtaining crystal structures of the ternary myristylated WT and K7C C-subunits in hopes of further elucidating how myristylation affects the structure and activity of the C-subunit. To further understand substrate binding rather than inhibitor binding, we utilized the peptide, SP20, which corresponds to the minimal 20 residues in PKI (5-24) that are necessary for inhibition of the C-subunit with two mutations (N20A, A21S) that convert this peptide from an inhibitor to a substrate (Madhusudan et al., 1994). We solved the crystal structure of the myristylated WT ternary complex to 2.0 Å resolution, but we obtained very little novel information compared to the older ternary structure obtained by Bossemeyer et al. (Bossemeyer et al., 1993). Like the previous structure, only part of the N-terminus and myristic acid are visible in the electron density. The density for the N-terminus begins at Ser10, and although the entire myristic acid group was included in the structure, the electron density is strong for only part of the myristic acid group (**Fig. 2.3**).

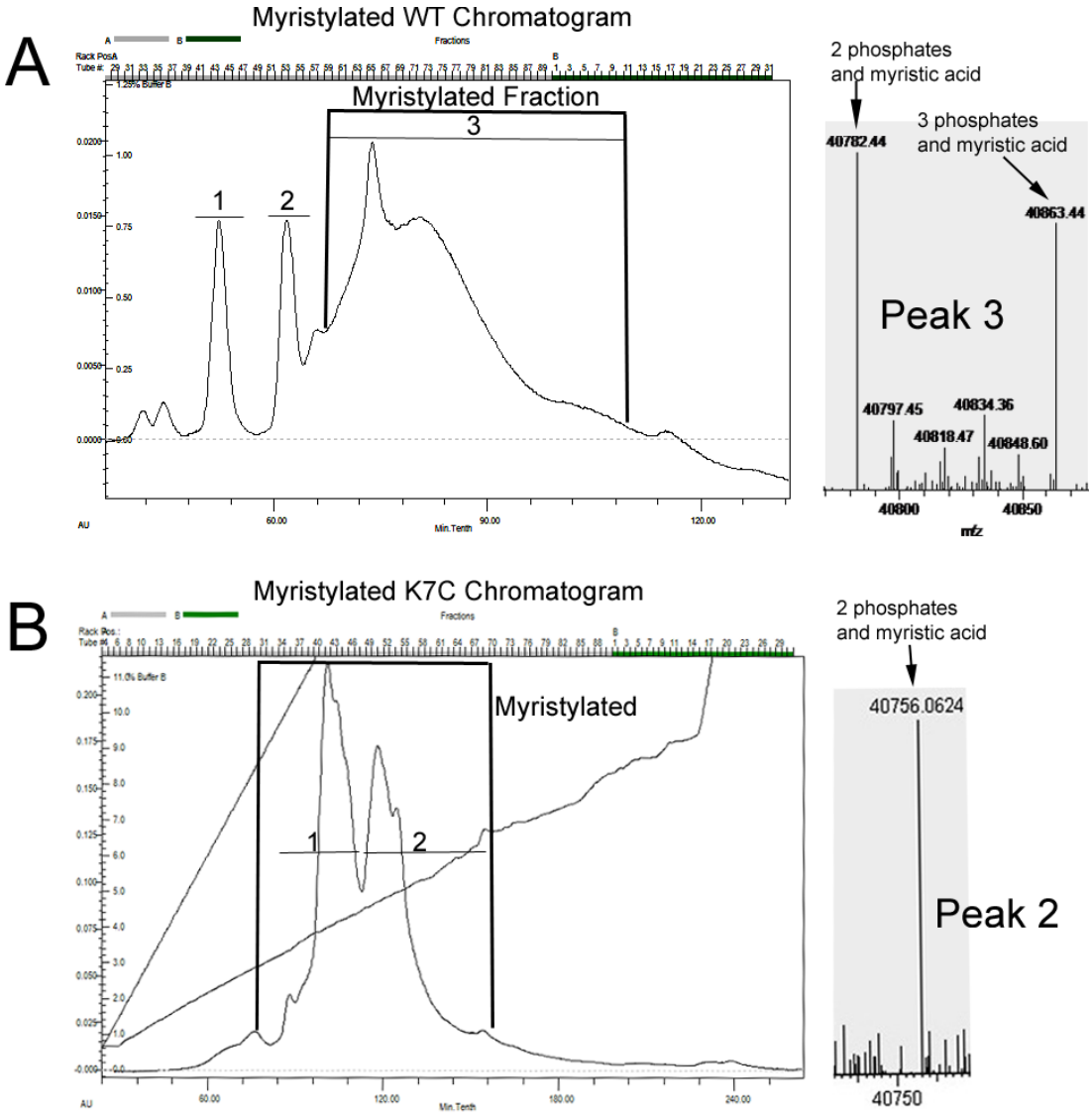

Figure 2.1. The myristylated C-subunit purification on MonoS column and myristylation verification by mass spectrometry. Typical MonoS chromatograms for myr-WT (**A**) and myr-K7C (**B**) proteins are shown along with mass spectrometry results of myristylated fractions within each chromatogram. The fractions within the chromatograms corresponding to myristylated protein are boxed.

Table 2.2. Kinetic parameters of myristylated and non-myristylated WT and K7C proteins. Values represent mean ± SD from three separate protein preparations that were each measured in triplicate.

	K_M (μM) Kemptide	K_M (μM) ATP	k_{cat} (s^{-1})
WT	29 ± 5	19 ± 3	19 ± 2
Myr-WT	23 ± 2	23 ± 2	18 ± 3
K7C	27 ± 2	23 ± 7	18 ± 3
Myr-K7C	43 ± 9	32 ± 7	29 ± 2

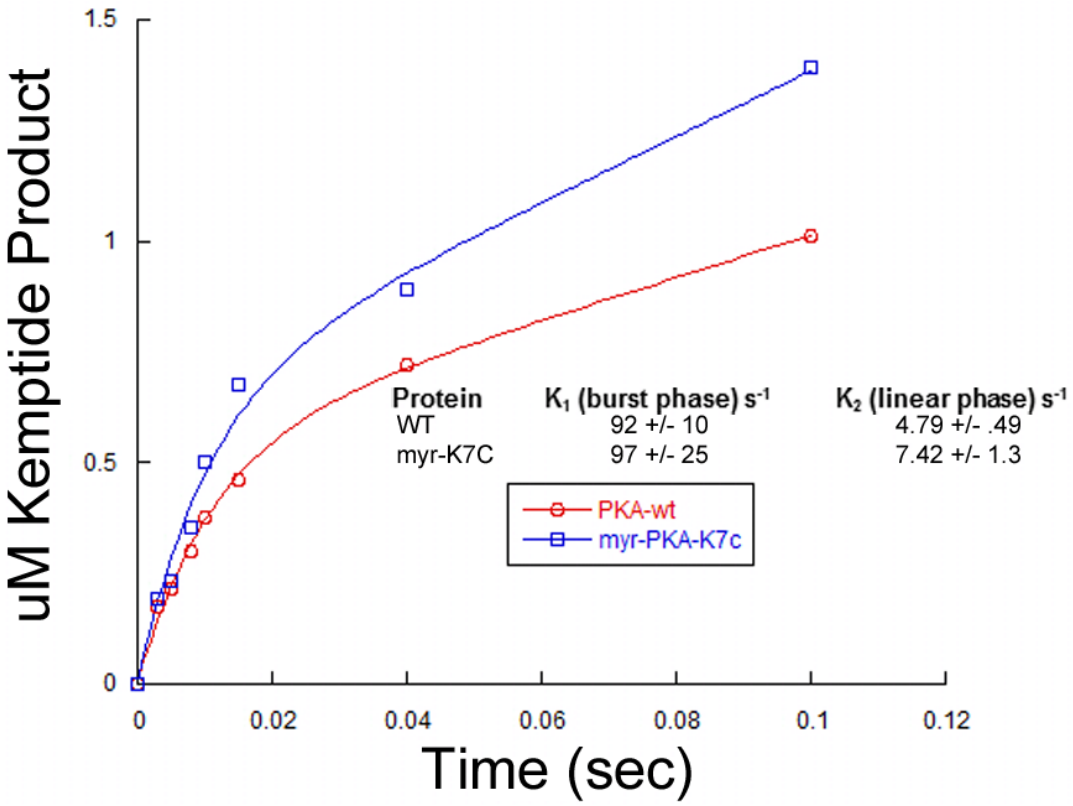

Figure 2.2. Pre-steady state kinetics of myr-K7C and non-myristylated WT PKA. The increased activity of myr-K7C was also confirmed by *in vitro* kinase assay with radiolabeled [γ-32P]-ATP phospho-incorporation of kemptide substrate. This experiment yielded a 55% increase in turnover rate (linear phase) which is consistent with the increased k_{cat} values obtained with the spectrophotometric assay. Also, there is no change in phosphoryl transfer rate (burst rate) for myr-K7C compared to the WT protein.

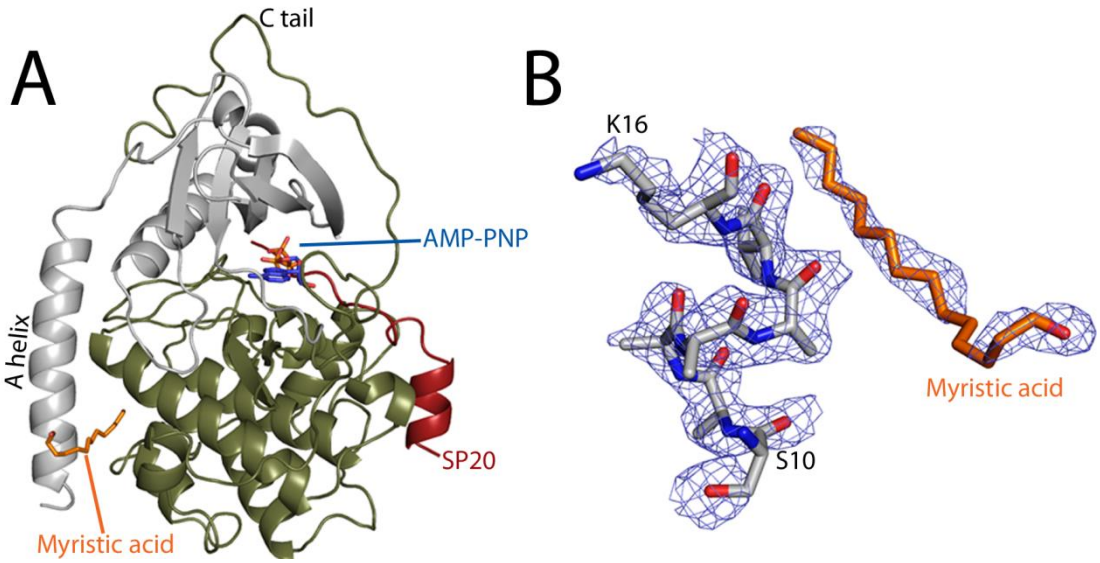

Figure 2.3. The structure of the myristylated WT ternary complex. A. The overall structure of the myristylated WT ternary C-subunit complex is displayed in cartoon representation with the myristic acid group shown in orange; the small lobe colored gray; the large lobe colored olive; the SP20 peptide colored red; and ANP-PNP shown in blue. **B**. The $2F_o$-F_c map at 1σ is shown in blue for residues 10-16 and myristic acid.

Myristylated K7C ternary structure.

In contrast to the structure of the myr-WT C-subunit, the ternary complex of myr-K7C displays a well ordered N-terminus. The structure of the ternary myristylated K7C complex was solved to 1.35 Å resolution, which is one of the highest resolution PKA structures reported. This structure reveals a novel conformation (**Fig. 2.4A-B**) with the entire N-terminus and myristic acid visible in the electron density (**Fig. 2.5**). The myristyl moiety binds within its previously defined hydrophobic pocket but for the first time there is strong electron density for each atom of the myristic acid (**Fig. 2.6 A**). The N-terminus adopts a new conformation in which the A-helix ends at Ser10 and is preceded by a small loop from Ser10 to Cys7. A new helix is formed from Cys7 through the myristic acid group, which is also part of the helix with its carbonyl oxygen hydrogen bonding with the backbone amide of Ala4 (**Fig. 2.6 B**). Specifically, the carbonyl oxygen is capping the N-terminus of the helix. To our knowledge, this is the first instance of myristic acid being part of a protein's secondary structure.

Structures of myristylated WT and K7C proteins in binary complex with SP20.

Binary complexes were also crystallized in hopes that they might yield further insights into the role of myristylation in the catalytic cycle of PKA. Both myristylated WT and K7C proteins bound to the SP20 peptide were crystallized and the structures refined to 2.0 Å resolution. Both binary structures, like the K7C ternary structure, have completely resolved N-termini. The entire N-terminus and myristic acid are visible in the electron density (**Fig. 2.5**) and display the same conformation that was seen with

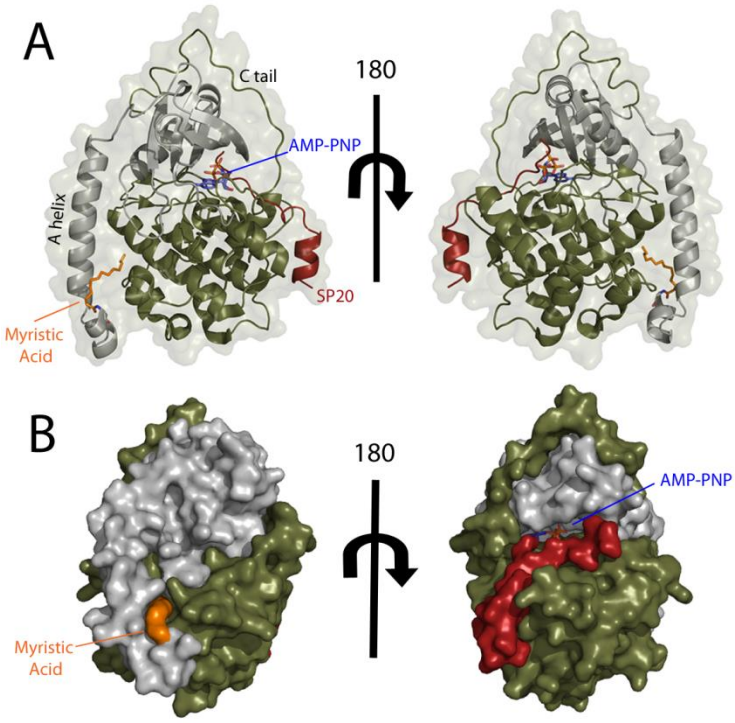

Figure 2.4. The overall myristylated K7C ternary structure which displays the entire N-terminus in a novel conformation. A. The overall structure of the myristylated K7C ternary complex is shown in cartoon representation with the small lobe colored gray, large lobe colored olive, SP20 colored red, AMP-PNP colored blue, and myristic acid colored orange. The protein surface is shown in transparent representation. This is the first time that the entire N-terminus and myristic acid are visible in a ternary complex and displays a novel alpha helix from residues 1-7, unlike the WT ternary complex. **B**. The K7C ternary complex is shown as a surface representation with same color scheme as in (A). The surface representation highlights the myristic acid binding pocket as well as the platform created by the novel N-terminal helix.

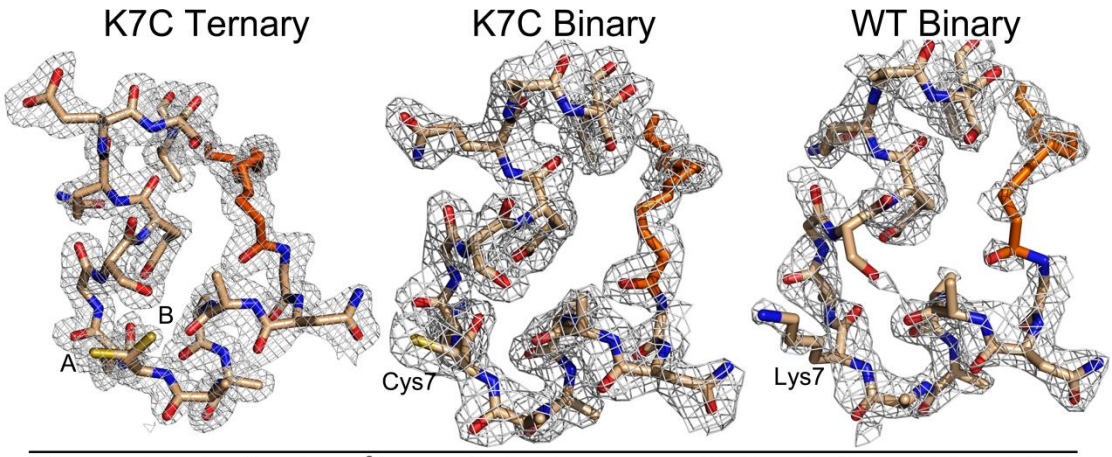

Average B Factor (Angstroms^2):	All Residues	Residues1-15	Ratio 1-15/All
K7C Ternary	16.38	30.24	1.85
K7C Binary	21.17	39.77	1.88
WT Binary	22.31	56.19	2.52

Figure 2.5. Electron density of the N-termini for the structures displaying the entire N-terminus and myristic acid. The $2F_o$-F_c electron density maps contoured to 1σ are shown for the first 15 residues and myristic acid for the myristylated K7C ternary, K7C binary, and WT binary structures. Residue 7 is annotated in each structure, and the K7C ternary structure adopts two conformations, A (65%) and B (35%). There is strong electron density for each structure at the N-terminus. However, the electron density for the WT binary structure is not as good with density lacking at some regions including part of the myristic acid and the Ser10 side-chain. This is also reflected by the average B factors for all residues compared to residues 1-15 for each structure which are listed in the figure.

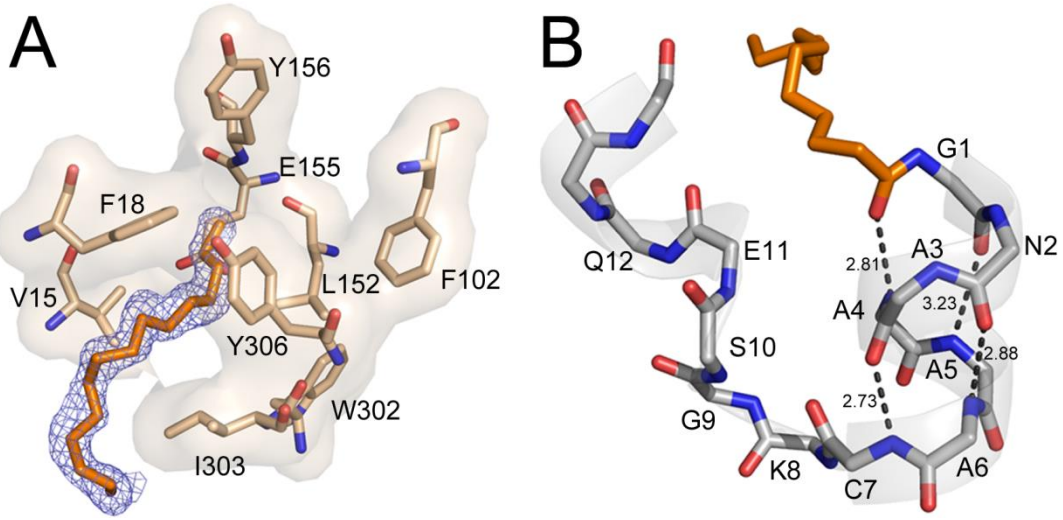

Figure 2.6. The myristic acid binding pocket and N-terminal helix. (A) The location of the myristic acid and interacting residues within its binding pocket are shown in stick representation with the $2F_o$-F_c electron density map at 1σ displayed for myristic acid in blue. (B) The myristic acid and main chain atoms of the novel helix are shown in stick representation with H-bonding distances shown to highlight the properties of the helix.

the K7C ternary structure. Again, the A-helix ends at Ser10 and both binary structures display the novel helix from residues 1-7.

The fact that the myr-WT protein displays this conformation suggests that the conformation is not an artifact of the mutation, and it allows us to make conclusions about why the myr-K7C protein retains this conformation in a ternary complex. Alignment of the myr-K7C and myr-WT binary structures reveals one possible explanation for stabilization of this conformation with the K7C protein. The distance between the Ser10 side-chain and backbone carbonyl of residue 7 is around 2.7 Å in the K7C structure compared to around 3.1 Å in the WT structure (**Fig. 2.7A**). Therefore, the mutation possibly stabilizes this hydrogen bond which may help to order the N-terminus. Further evidence that the N-terminus is more stable in the myr-K7C protein than the WT protein is evident from the electron density and B factors of the binary structures. Although the binary K7C and WT structures were refined to the same resolution, the electron density is better at the N-terminus for the K7C structure than the WT structure (**Fig. 2.5**). Also, the B-factors at the N-terminus are greater for the WT structure (56 $Å^2$) than the K7C structure (40 $Å^2$) despite similar overall B-values (~20 $Å^2$) for both enzymes which further suggests that the N-terminus is more stable in the mutant (**Fig. 2.5**).

Crystal contacts in structures with an ordered versus disordered N-terminus.

Another difference between the complexes with ordered N-termini (WT binary, K7C binary, and K7C ternary structures) versus the WT ternary complex that

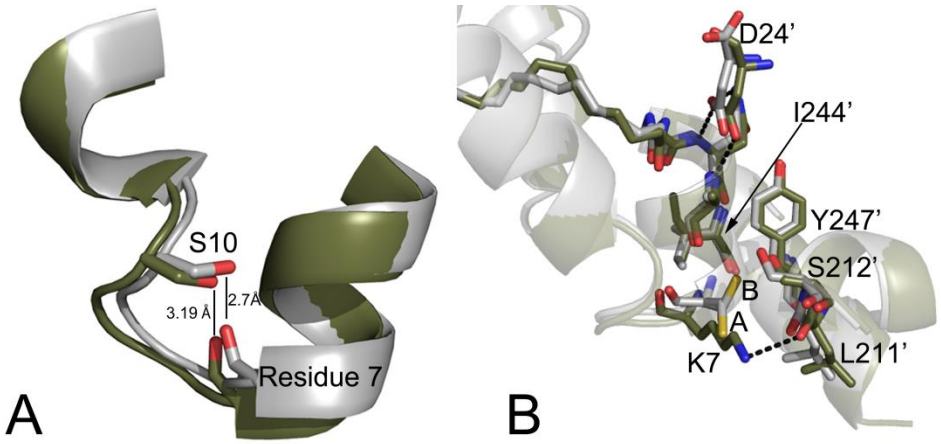

Figure 2.7. Potential roles of the K7C mutation in the stabilization of the N-terminus. A. The K7C (gray) and WT (olive) binary structures are aligned with the backbone atoms of residue 7 and side-chain of Ser10 shown in stick representation. The distance between the Ser10 side-chain and backbone carbonyl of residue 7 are displayed showing that the atoms are in H-bonding distance in the K7C mutant but not the WT structure. It is possible that this hydrogen bond could stabilize the N-terminus. (**B**) K7C ternary and WT binary structures are aligned and colored as in (A), and shown here are the crystal packing interactions with symmetry related molecules at the N-terminus. The K7C and WT structures adopt similar crystal packing with Ile210, Leu211, and Ser212 which are near the APE motif; Ile244 and Tyr247 from the G-Helix; and Asp24 from the SP20 peptide. However, residue 7 and Leu211 from the symmetry related molecule are slightly shifted in the WT structure possibly to facilitate packing and possibly to form a hydrogen bond between Lys7 and the backbone carbonyl of Leu211. Also, the K7C ternary structure adopts two conformations, A (65%) and B (35%), but the K7C binary structure only has density for conformation A. This B conformation would destabilize this crystal packing with the WT lysine residue.

exhibits a disordered N-terminus is changes in unit cell dimensions. Both conformations crystallized in the same space group.

However, the WT ternary complex crystallized with unit cell dimensions of a = 57.80 Å, b = 78.73 Å, c = 99.00 Å, and the complexes with resolved N-termini crystallized with unit cell dimensions of a = 48 Å, b = 80 Å, c = 118 Å (**Table 2.1**). The WT ternary complex unit cell dimensions are a fairly common crystal form for PKA (Thompson et al., 2009; Yang et al., 2009; Yang et al., 2004; Yang et al., 2012). In contrast, the a = 48 Å, b = 80 Å, c = 118 Å unit cell dimensions were observed only once previously in 1SMH (Breitenlechner et al., 2004). This previous structure also exhibits a completely resolved N-terminus except that the N-terminus adopts a single alpha helix from residues 1-31.

The ordered N-terminus in the myristylated structures forms crystal contacts with Ile210, Leu211, and Ser212 which are near the APE motif and Ile244 and Tyr247 from the G-Helix. Additionally, Asp24 from the SP20 peptide may make hydrogen bonds with the Asn2 side-chain and with the backbone nitrogen atoms from Asn2 and Ala3 and could help to stabilize this N-terminal helix (**Fig. 2.7B**). 1SMH forms similar crystal contacts except that it does not interact with the PKI peptide and instead forms additional contacts with Glu248 and Val251 with the extended A-helix (**Fig. 2.8A**). Additionally, one other PKA structure, 3QAM (Yang et al., 2012), exhibits similar crystal packing at the N-terminus as 1SMH and these myristylated structures. Although this structure is a different space group, $P2_1$, it has similar a and b cell dimensions (a = 48 Å, b = 80 Å, c = 61 Å) and exhibits similar crystal packing with

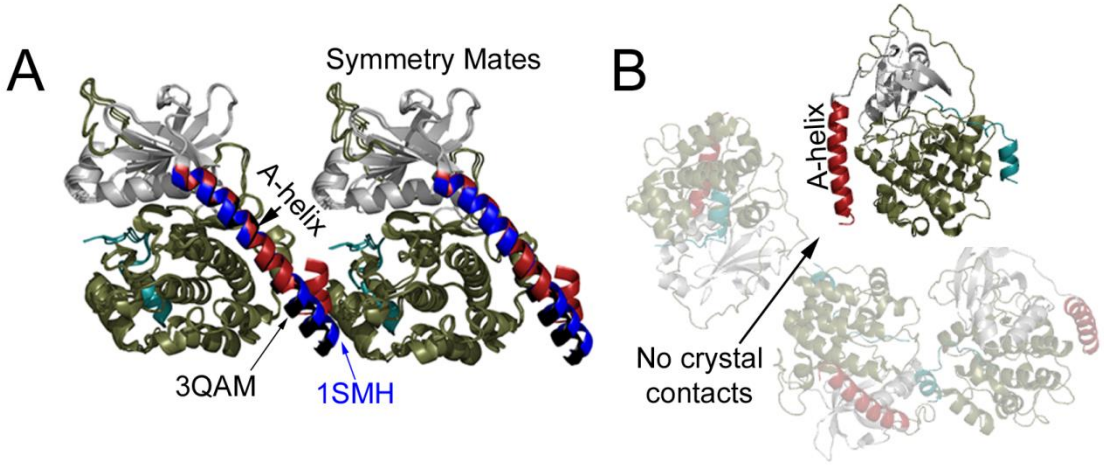

Figure 2.8. Crystal contact differences between structures with a disordered or ordered N-terminus. A. The myristylated structures with ordered N-termini crystallized with unit cell dimensions of a = 48, b = 80, c = 118. The crystal packing at the N-terminus is shown for these structures. The small lobe is colored gray, large lobe is colored olive, SP20 is colored teal, and the A-helix from these myristylated structures is colored red. Also aligned is 1SMH that crystallized in the same unit cell as these structures. The A-helix of 1SMH is shown in blue. One other structure, 3QAM that crystallized in a different space group and with a different unit cell but adopts similar crystal packing at the N-terminus as these structures, is aligned. The A-helix from 3QAM is colored black. These myristylated structures adopt close packing at their N-terminus with residues Ile210, Leu211, and Ser212 which are near the APE motif; Ile244 and Tyr247 from the G-Helix; and Asp24 from the SP20 peptide. **B**. The WT ternary complex crystallized with unit cell dimensions of a = 57.8, b= 78.73, c= 99 and displayed here are the symmetry mates near the N-terminus in transparent representation. The A-helix is colored red, SP20 is colored teal, small lobe is colored gray, and large lobe is colored olive for both the structure and symmetry mates. The N-terminus makes no crystal contacts and, in fact, there is an open space near the N-terminus that could allow for flexibility of this region within the crystals.

a symmetry related molecule at the N-terminus. This structure shows similar interactions as 1SMH and also forms an extended A-helix (**Fig. 2.8A**). In contrast to these ordered structures, the WT ternary structure does not make crystal contacts at the N-terminus, which supports the possibility of high flexibility of this region within protein crystals. There is a large space near the N-terminus that may allow for flexibility of the region without interfering with crystal packing (**Fig. 2.8B**).

Additionally, another aspect to consider is how the K7C mutation may have influenced the crystal packing in these structures. This possibility is especially important because previous reports suggest that mutation of lysine residues to small hydrophobic residues may improve crystallization by decreasing conformational entropy and improving crystal packing (Derewenda and Vekilov, 2006). Alignment of the K7C structures with the WT binary structures illustrates very similar packing. However, there is one change which a difference in the positioning of Lys7 and Leu211, from the symmetry related molecule, in the WT binary structure compared to Cys7 and Leu211 in the K7C structures. In the WT binary structure, Lys7 is moved down relative to the Cys7 structures by about 1.7 Å which may be necessary to facilitate packing and possibly to optimize the formation of a hydrogen bond between Lys7 and the backbone carbonyl of Leu211 (**Fig. 2.7B**). Furthermore, in the K7C ternary structure, Cys7 adopts two conformations, A modeled with 65% occupancy and B modeled with 35% occupancy, and one of these conformations, termed conformation B, is facing the symmetry related molecule (**Fig. 2.7B**). The K7C binary structure only shows density for conformation A. This B conformation and the potential for increased flexibility of the N-terminus in a ternary structure may partially

explain why the WT protein does not adopt this conformation in a ternary complex. If a lysine is present at residue 7, then the B conformation observed in the K7C ternary structure would interfere with this crystal packing.

Comparison of myristylated binary and ternary structures.

All structures reported here crystallized in a closed conformation except for a slightly raised glycine rich loop which was seen in all structures (**Fig. 2.9A**). There were not many major differences between the binary and ternary structures suggesting that the active site and active state of the enzyme can be formed by substrate binding alone. This result was not surprising since other binary structures also crystallized in a closed conformation (Madhusudan et al., 1994). The majority of residues involved in ATP binding are essentially pre-formed in the binary complex. One exception is repositioning of the P-site Ser after AMP-PNP binding, and the P-3 Arg repositions from binding Asp328 in the C-tail in a binary complex to coordinate AMP-PNP by potentially hydrogen bonding with the hydroxyl group from the 3' carbon on the ribose and/or via a water molecule in a ternary complex (**Fig. 2.9B**). The binary complexes were modeled with one conformation, facing the C-tail, but display some positive density for the P-3 Arg facing the active site and may exhibit some exchange between the two conformations. However, the ternary complex only shows density for the conformation with the P-3 Arg facing the active site. At least one other binary structure, 1APM (Knighton et al., 1993), displays both conformations of the P-3 Arg facing the active site and C-tail.

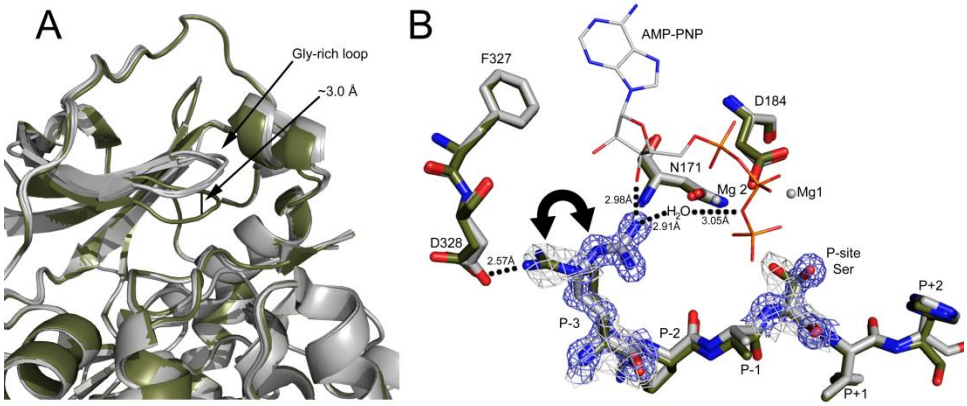

Figure 2.9. Changes at the active site in the myristylated structures. A. The four myristylated structures presented here are colored gray and aligned. Also aligned and displayed is another PKA structure, 1RDQ (Yang et al., 2004), in olive. The myristylated structures adopt a slightly raised glycine-rich loop, about 3Å, compared to most closed PKA structures. **B**. The active site residues of the myr-K7C binary complex (olive) and myr-K7C ternary complex (gray) are shown. Also displayed is the location of the magnesium ions (gray spheres) and AMP-PNP (stick representation) from the ternary complex. The $2F_o$-F_c electron density maps at 1σ are shown in gray for the binary complex and in blue for the ternary complex for the P-site Ser and P-3 Arg highlighting the shifts in these residues upon formation of a ternary complex. The P-3 Arg was modeled facing the C-tail in the binary complexes but there is some positive density for the P-3 Arg facing the active site, and it may exert some exchange between the two conformations. However, the residue only faces the active site in a ternary complex.

Furthermore, although the myristylated K7C mutant retains an ordered N-terminus in both a binary and ternary complex, the myr-WT protein apparently undergoes a disordering of its N-terminus upon formation of a ternary complex (**Fig. 2.10**). This result suggests that the formation of a ternary complex and catalysis by PKA may cause long-range dynamic effects throughout the enzyme which causes the N-terminus to become disordered. Also, with no other major differences between the myr-WT and myr-K7C proteins, it is possible that the altered kinetics observed with myr-K7C may be due to its ability to retain an ordered N-terminus with myristic acid bound within its hydrophobic pocket in a ternary complex.

2.4 Discussion

Acylation adds potential modes of protein regulation and in the case of myristylation, the acyl moiety is added co-translationally, and thus the modification is carried throughout the lifetime of the protein. Having established previously that the N-terminal myristylation site in the PKA C-subunit serves as a "switch" that can be mobilized in type II holoenzymes to associate with membranes (Gangal et al., 1999), here we show how the N-myristylated N-terminus can be docked to the kinase core where it may influence the active site of the enzyme. We identify a new conformation of the N-terminus that is present in the WT binary complex and appears to be stabilized by a K7C mutation that allows the protein to retain this conformation in a ternary complex. Since this conformation was seen in the wild type protein when a high affinity peptide was bound, we believe that this reflects a true physiological state of the protein.

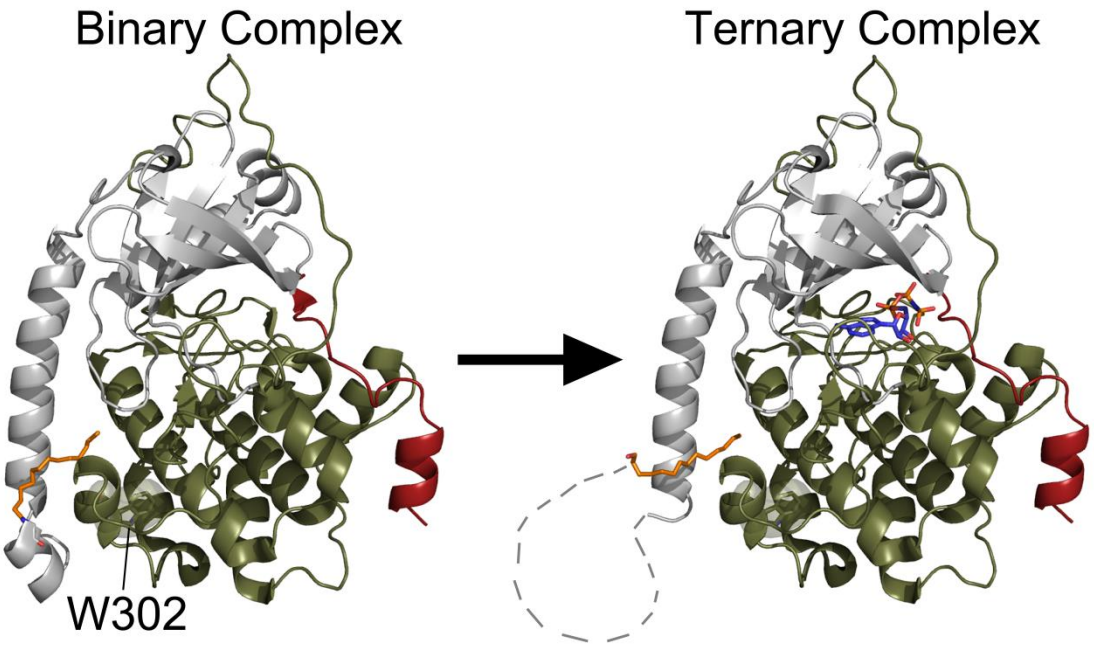

Figure 2.10. The formation of a ternary complex produces dynamic movements within the C-subunit that causes a disordering of the N-terminus. The C-subunit of PKA is shown in cartoon representation with the small lobe colored gray, large lobe colored olive, SP20 colored red, myristic acid colored orange, and AMP-PNP colored blue. The WT binary complex has a completely ordered N-terminus which is displayed on the left, but upon formation of a ternary complex, the N-terminus of the WT C-subunit becomes disordered as illustrated on the right. The disordered regions of the N-terminus are displayed as connecting lines. Also, highlighted is Trp302 which is thought to be a sensor of active site occupancy (Masterson et al., 2011) and may support the link between nucleotide binding and the conformation of the N-terminus.

Myristylation of the C-subunit is important for the structural stability of the enzyme as evident by an increase in thermostability with myristylated compared to non-myristylated PKA (Gaffarogullari et al., 2011; Yonemoto et al., 1993b), and structural stabilization with myristylation may be a general trend for many proteins (Stephen et al., 2007). The results presented here provide a structural basis for the stabilizing effect of myristylation on PKA. Myristylation results in a completely ordered N-terminus in the binary complexes of both the mutant and WT C-subunit structures and in the K7C ternary structure, which is not typically observed in PKA structures. Also, binding of myristic acid to the hydrophobic pocket may stabilize the A-helix which spans both lobes of the kinase (**Fig. 2.4A**) and could therefore stabilize the entire protein. Additionally, the myristic acid group interacts directly with the core of the protein, which may provide structural stability.

Although myristic acid is present within its hydrophobic pocket in all four structures, the WT C-subunit shows density for only part of the N-terminus and myristic acid in the ternary complex (**Fig. 2.3**), but the K7C mutant C-subunit retains an ordered N-terminus in a ternary complex. The stabilization of this conformation in the K7C protein may be attributed to a hydrogen bond between the side-chain of Ser10 and backbone carbonyl oxygen of Cys7 which are in hydrogen bonding distance in the K7C structures but not in the WT structure (**Fig. 2.7A**). It also may be due to enhanced crystal packing with the K7C mutant that may allow this conformation to exist in a crystal lattice even with a more flexible N-terminus which cannot occur with the WT lysine at residue 7 (**Fig. 2.7B**). Because both WT and K7C C-subunits form a stable helix at the N-terminus in a binary complex, this conformation is relevant to the WT

enzyme and provides several possibilities with regard to other N-terminal modifications.

First of all, the structures with the ordered N-termini suggest functional roles for the other N-terminal modifications including Ser10 phosphorylation and Asn^2 deamidation. In the structures with ordered N-termini, the Ser10 side-chain hydroxyl group is around 4.0 Å or less distance away from the backbone carbonyl of Lys7, the backbone carbonyl of Ala3, the Cα carbon of Ala3, and the Cα carbon of Ala4. Therefore, phosphorylation of Ser10 would almost certainly destabilize this conformation. Based on NMR studies, Gaffarogullari et al. suggested that Ser10 phosphorylation may remove myristic acid from the myristate pocket, which could increase membrane binding of the enzyme (Gaffarogullari et al., 2011). Phosphorylation of Ser10 may also make the A-helix more mobile which may enhance protein-protein interactions via the A-helix with other proteins such as AKIP (Sastri et al., 2005). Furthermore, Asn2 deamidation may exhibit a similar destabilizing effect on the N-terminus because of the added negative charge near the myristic acid group. Also, because the deamidated form of PKA can autophosphorylate on Ser10 (Toner-Webb et al., 1992), these two modifications may act synergistically to prevent membrane binding of the enzyme by adding negative charges at the N-terminus. These structures suggest interplay between N-myristylation and other N-terminal modifications which are likely to have biological significance.

In addition, these structures reveal a role of ATP binding on the structure of the N-terminus. With the WT protein, the ordered N-terminus in the binary complex (bound only to SP20) becomes disordered in the ternary complex with the addition of

AMP-PNP binding (**Fig. 2.10**). This crosstalk is interesting considering that the N-terminus or myristic acid and the ATP binding site are 20-30 Å apart which suggest allosteric networks throughout the enzyme. This possibility is further exemplified by c-Abl which is affected by small molecules binding within its myristic acid binding pocket. Abl can be either inhibited (Choi et al., 2009; Fabbro et al., 2010) or activated (Yang et al., 2011) in response to small molecule binding within its myristate pocket. The location of the myristate pockets in c-Abl versus PKA differ. The myristic acid group in c-Abl binds in the hydrophobic core of the large lobe between the E and F-helices. In PKA, the myristate pocket is formed between the A, J, and E-helices near the surface of the protein. Despite different locations of the myristate pockets, the findings presented here offer evidence that the myristic acid binding site may influence the active site or enzyme activity of PKA. This idea is further supported by the increased k_{cat} and K_m values exhibited by the myristylated K7C protein which only differed in structure from the WT protein with its ordered N-terminus, suggesting that myristylation has the potential to influence catalytic activity.

An examination of interactions of the A-helix and the myristic acid binding pocket with the enzyme provides possible reasons why myristylation may influence the active site of the enzyme. First of all, one of the most important features for an active kinase is an interaction between Glu91 from the C-helix and Lys72 from the β3 strand (Kornev et al., 2006). Lys72 binds to the α and β phosphate of ATP and is positioned by Glu91. The A-helix may influence the C-helix, and therefore Glu91, because Trp30 from the A-helix is packed against Arg93 from the C-helix, and if myristylation influences A-helix dynamics or interactions, it could influence the

important K72-E91 interaction and possibly influence ATP binding (**Fig. 2.11 A, C**). Furthermore, the same Trp30 interacts with the activation loop which is a critical component for PKA activity (Steichen et al., 2012). Trp30 is near Arg190 from the activation loop and may also impact this region of the protein when myristylated. Therefore, these A-helix interactions may be altered by myristylation which, in turn, may influence the active site.

Additionally, it is possible that the myristic acid group may influence the active site or enzyme activity via interactions that are known to be important for activity of PKA and all kinases. Comparison of many eukaryotic and prokaryotic kinases identified a hydrophobic "spine" that is thought to be important for kinase activity and is comprised of Leu95, Leu106, Tyr164, and Phe185, with numbering based on PKA (Kornev et al., 2006). Although the myristic acid group and residues within its hydrophobic pocket do not directly interact with the regulatory spine, it is possible that it can influence these elements via residues surrounding the myristic acid pocket. For example, Phe154, which is directly opposite of the myristate pocket in the E-helix (**Fig. 2.11 B-C**), interacts with Tyr164 that is part of the hydrophobic spine, and if myristylation influences Phe154 and the spine, then it could influence magnesium binding, ATP binding, or the active site and enzyme activity in general. Additionally, Trp302 is part of the myristic acid binding pocket (**Fig. 2.6A, Fig. 2.11B)**, and although very distant from the active site, it exhibits very large chemical shifts following peptide and AMP-PNP binding based on NMR studies (Masterson et al., 2011). Therefore, this residue provides further evidence of cross-talk between the active site and myristate pocket.

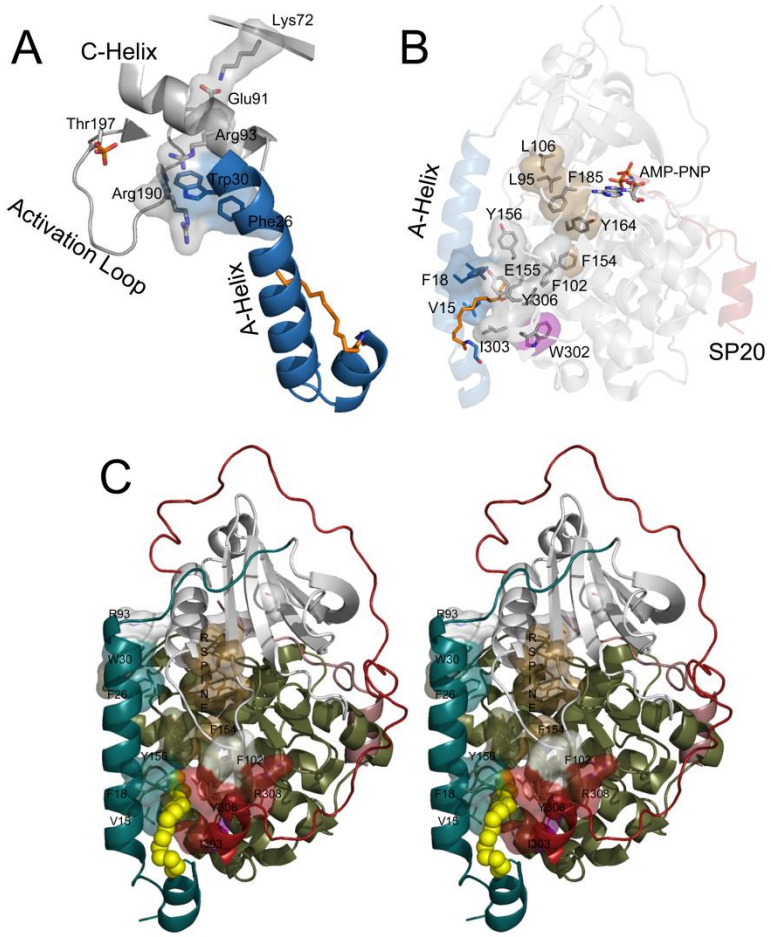

Figure 2.11. Interactions of the myristic acid group and the A-helix within the C-subunit could influence the active site. A. The A-helix is colored blue, myristic acid is colored orange, and other elements are colored gray. The A-helix residues Trp30 and Phe26 may interact with Arg93 and Arg190 which may influence the C-helix and the important Lys72-Glu91 interaction or the activation loop, respectively. **B**. The A-helix is colored blue, myristic acid colored orange, small lobe colored gray, large lobe colored olive, and SP20 colored red. The protein is shown in transparent cartoon representation with specific residues highlighted in stick and surface representation. Residues in or near the myristate pocket may influence the active site such as Phe154 that is directly opposite of the myristate pocket and may influence the spine, residues Y164, F185, L95, and L106 which are colored brown, and active site of the enzyme. Also, W302, highlighted in purple, is known to be a sensor of active site occupancy (Masterson et al., 2011) and suggests potential cross-talk between the myristate pocket and active site. **C**. A stereo view of the myristic acid pocket and interacting residues is displayed. In this depiction, the myristylated K7C binary structure is shown in cartoon representation with the N-terminus (residues 1-40) colored teal, the small lobe (residues 41-126) colored gray, the large lobe (residues 127-300) colored olive, the C-tail (residues 301-350) colored red, the myristic acid colored yellow and depicted in sphere representation, and the R-spine residues colored brown.

Occupation of the myristate pocket may increase the dynamics at the active site. This possibility could explain why the myr-K7C protein had increased k_{cat} but also increased K_m values. The enzyme efficiency (k_{cat}/K_m) is essentially unchanged with the myr-K7C protein, and this may be due to a faster ADP off-rate, the rate limiting step for activity (Adams and Taylor, 1993), but also lower affinity for substrates. This possibility may suggest increased dynamics at the active site and may explain the slightly raised Gly-rich loop observed in these myristylated structures (**Fig. 2.9A**). Therefore, although the kinetics of the WT protein is not influenced by myristylation, it is possible that different binding partners or ligands may influence the active site or enzyme activity by binding to the N-terminus. For instance, AKIP or other N-terminal binding partners may keep myristic acid within its binding pocket to influence PKA activity. Additionally, other lipids or ligands may alter the activity of PKA by utilizing this allosteric site. Like c-Abl, the myristate pocket of PKA may be a potential site for small molecule activators or inhibitors. Indeed, a recent study of Cα2, which is not myristylated but retains the hydrophobic myristate pocket, exhibited small but not significant increases in enzyme activity in the presence of excess fatty acid (Hereng et al., 2012). Perhaps specific lipids, ligands, or protein interactions can enhance this effect on PKA activity. In general, these structures suggest that, in addition to potential roles in localization, myristylation may serve additional regulatory roles on active site dynamics, substrate binding, or enzyme activity when bound into the hydrophobic pocket.

Chapter 2, in full, was published as The Role of N-terminal Myristylation in

the Structure and Regulation of cAMP-Dependent Protein Kinase. Bastidas AC, Deal MS, Steichen JM, Keshwani MM, Guo Y, Taylor SS. *J. Mol. Biol*. 2012 Sep 14; 422(2):215-229. The dissertation author was the primary investigator and author of this work.

Chapter 3

Influence of N-Myristylation and Ligand Binding on the Flexibility of the Catalytic Subunit of Protein Kinase A

3.1 Introduction

The catalytic (C) subunit of cAMP-dependent protein kinase (PKA) is a Ser/Thr kinase that mediates many cAMP signaling functions (Taylor et al., 2012b). At low concentrations of cAMP, PKA exists as a heterotetrameric holoenzyme composed of an R-subunit homodimer that binds and inactivates two C-subunit monomers (Kim et al., 2007). At high concentrations, cAMP binds to the R-subunit dimer to induce a conformational change that reduces the affinity of the R-subunit toward the C-subunit and leads to C-subunit activation (Taylor et al., 2008). The C-subunit has served as an important model for the protein kinase family not only because it was the first kinase whose structure was solved (Knighton et al., 1991b) but also because its regulatory component is separate from its catalytic component, and therefore, it can be studied independently.

Protein kinase structures include a bilobal structure comprised of the N-lobe (or small lobe) and C-lobe (or large lobe) (Knighton et al., 1991b). ATP binds in the cleft formed between these lobes, thereby coupling them (Masterson et al., 2008; Zheng et al., 1993a). Crystal structures of the C-subunit of PKA reveal multiple conformations of the enzyme termed “open”, “closed”, and “intermediate” on the basis of the relative orientations of the small and large lobes with respect to each other (Johnson et al., 2001). The open conformation is typically observed with the apo C-subunit (Akamine et al., 2003; Wu et al., 2005). The closed conformation is typically observed when nucleotide and IP20 are crystallized with the protein (Bossemeyer et al., 1993; Zheng et al., 1993a), and the intermediate conformation is observed when the C-subunit is crystallized with adenosine alone (Narayana et al., 1997). The C-

subunit is regulated by noncovalent ligand and protein binding as well as covalent co- and post-translational modifications. For example, the N-terminus undergoes cotranslational N-myristylation of Gly1, phosphorylation of Ser10, and deamidation of Asn2 (Tholey et al., 2001), which may regulate C-subunit interaction with membranes or subcellular sites (Gangal et al., 1999; Pepperkok et al., 2000; Tholey et al., 2001). Additionally, N-myristylation increases the structural stability globally (Yonemoto et al., 1993b) and locally near the myristylation site (Bastidas et al., 2012; Cembran et al., 2012; Gaffarogullari et al., 2011).

To further assess how myristylation and ligand binding influence C-subunit dynamics, a combination of time-resolved fluorescence anisotropy and molecular dynamics (MD) simulations was utilized. Specifically, five single-site cysteine substitution C-subunit mutants were engineered and conjugated with fluorescein maleimide (FM). The cysteine mutations were placed along the A-helix at the N-terminus of the protein (K7C and K16C) near the myristate pocket (N99C), and at the C-tail (S325C and native C343) (**Fig. 3.1A−C**). Additionally, the mutants were prepared in both myristylated and nonmyristylated configurations, and the time-resolved fluorescence anisotropy measurements were performed in the absence of ligands (apo/open state) and in the presence of ATP plus IP20 (ternary/closed state). Parallel molecular dynamics (MD) simulations were performed on the myristylated and nonmyristylated C-subunit in the presence and absence of ligands with a recent crystal structure of the N-myristylated protein (Bastidas et al., 2012). These fluorescence and MD experiments identified a stabilizing effect of myristylation at the N-terminus and myristate pocket and identified long-range allosteric effects of this

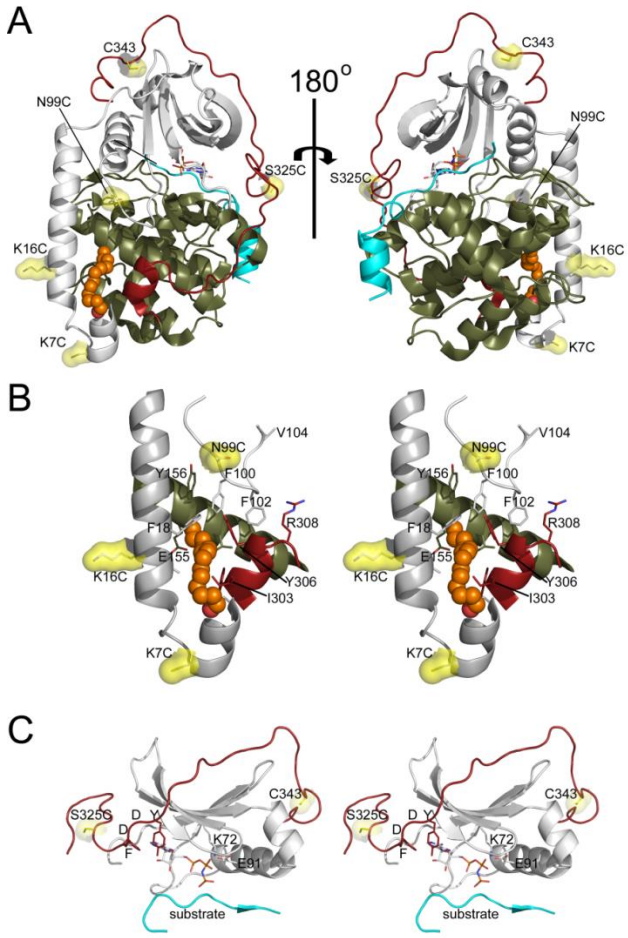

Figure 3.1. Sites of FM conjugation in the C-subunit. A. The structure of the N-myristylated C-subunit of PKA (PDB: 4DFX (Bastidas et al., 2012)) is displayed in cartoon representation with the small lobe (1−126) in gray, large lobe (127−300) in olive, C-tail (301−350) in red, inhibitor peptide in cyan, myristic acid in orange as a stick representation, and sites of mutation in yellow as a stick and surface representation. **B**. A stereoview of the A-helix and myristate pocket is shown in cartoon representation with the regions of the protein and sites of FM conjugation depicted and colored as in (A). Several other residues within or near the myristate pocket are also shown in stick representation, and myristic acid is shown in sphere representation. **C**. A stereoview of regions of the protein near the other sites of labeling is shown in cartoon representation with the regions of the protein and sites of fluorescent labeling depicted and colored as in (A).

modification and ligand binding.

3.2 Experimental Procedures

Purification of the C-Subunit Proteins. All mutations were generated using a Quikchange mutagenesis kit (Stratagene). The K7C and K16C mutations were introduced into the WT C-subunit vector. The N99C and S325C mutations were introduced into vectors containing a C199A mutation. Finally, the C199A mutation was introduced into the WT vector so that the endogenous C343 could be selectively labeled. The nonmyristylated C-subunit was expressed and purified as described previously (Herberg et al., 1993). The myristylated C-subunit was prepared by coexpression with yeast NMT as described previously (Duronio et al., 1990) and purified using a protocol described previously (Bastidas et al., 2012). Three of these mutations, K7C, K16C, and C199A were characterized previously and shown not to negatively affect C-subunit activity (Bastidas et al., 2012; Gangal et al., 1998), and the activity of the other mutants, N99C and S325C, were tested with a spectrophotometric assay as described by Cook et al. with the soluble substrate kemptide (LRRASLG), which showed similar levels of activity as the WT protein (data not shown), suggesting that the mutations did not alter normal C-subunit function (Cook et al., 1982).

Fluorescein Maleimide Labeling. The C-subunit samples (12.5−25 nmol) were initially buffer exchanged by elution through a PD10 column (GE Healthcare Bio-Sciences Corp., Piscataway, NJ) equilibrated with 20 mM MOPS and 150 mM KCl,

pH 7.0, at 4 °C. The protein fractions were pooled, and the concentrations of the pooled samples were determined by spectrophotometry using an A280 extinction coefficient of 45,000 $M^{-1}cm^{-1}$ and ranged between 3 and 6 μM. With the exception of the C199A mutant labeling, the reaction mixtures were made with 4 mM ATP and 8 mM $MgCl_2$ to protect from labeling the endogenous cysteine residues (C199 and C343) because it was previously shown that the presence of MgATP prevents labeling of these native cysteine residues in PKA (Nelson and Taylor, 1981). For the N-terminal mutants, the stoichiometry of FM to protein was 2:1, and for the C199A mutants, it was 3:1. The reactions were allowed to proceed for 1 h at room temperature, protected from light, and then eluted through a PD10 column equilibrated with 20 mM MOPS, 150 mM KCl, and 5 mM β-ME, pH 7.0, at 4 °C. Absorbance measurements at 280 and 495 nm were made on each column fraction, and the light absorbing fractions with retention times that corresponded to unmodified catalytic subunit were pooled. The concentration of labeled protein was determined by spectrophotometry using an A495 extinction coefficient of 65 000 $M^{-1}cm^{-1}$, and the concentration of total protein (labeled and unlabeled) was calculated with the expression

$$[\text{catalytic subunit}] = ((A280 - 0.29) \times A495) \div 45000 \quad (1)$$

Time-Resolved Fluorescence Anisotropy. Emission anisotropy was determined as previously described (Hibbs et al., 2006). Samples were excited by using a 484 nm laser diode from HORIBA Jobin Yvon Inc. (Edison, New Jersey, NJ) and a Semrock Inc. (Rochester, NY) single-band bandpass filter (FF01-482/35-25) in the excitation pathway to enhance its monochromaticity. A Semrock Inc. single-band bandpass filter

(FF01-536/40-25) selected the emission and rotatable Glan−Thompson polarizers were placed in the excitation and emission pathways. Unless stated otherwise, emission anisotropy decays were analyzed with the impulse reconvolution method implemented in the DAS6 software package from HORIBA Jobin Yvon Inc. (Edison New Jersey NJ) described elsewhere (Birch and Imhof, 1991). Briefly and simply, this approach splits the analysis into two steps: analysis of the total emission decay, S(t), from the vertically, I||(t), and orthogonally, I⊥(t), polarized emission components followed by analysis of the vertical/perpendicular difference emission decay, D(t). S(t) is the sum of the three axes of emission and is free of anisotropy effects. It is given by the expression

$$S(t) = I_{\parallel}(t) + G \bullet 2I_{\perp}(t) \qquad (2)$$

and is analyzed as a biexponential function. G is a measure of the instrumental polarization bias for each sample, and the values ranged between 0.97 and 0.995 depending on the instrument configuration. D(t), which includes both fluorescence and anisotropy parameters, is given by the expression

$$D(t) = I_{\parallel}(t) - G \bullet I_{\perp}(t). \qquad (3)$$

D(t) is deconvolved with the results from the S(t) analysis as a constraint yielding

$$r(t) = \beta_1 \exp(-t/\phi_{fast}) + \beta_2 \exp(-t/\phi_{slow}), \qquad (4)$$

where r(t) is the time-dependent anisotropy.

Here, β1 and β2 are the amplitudes of the anisotropy at time zero for the fast and slow anisotropy decay processes, respectively. Φfast and Φslow are the fast and slow rotational correlation times of the anisotropy decay, respectively. Φslow usually yields an estimate of the whole-body rotational correlation time when it is less than about

five times the emission lifetime, and when the rate of the segmental motions around the site of reporter group conjugation differs greatly from the rate of the whole-body diffusion. The accuracy of this estimate increases with the proportion of the total decay that is associated with the slow decay processes. A nonassociative model was assumed, where the emission relaxation times are common to all the rotational correlation times. Goodness of fit was evaluated from the values of the reduced $\chi 2r$ and by visual inspection of the weighted-residual plots. All time-resolved anisotropy measurements were performed with samples suspended in 20 mM MOPS, 150 mM KCl, and 5 mM β-ME, pH 7.0, at 22 °C.

Molecular Dynamics Simulations. System Preparation. Four unique systems were set up based on the X-ray refined structure with PDB ID 4DFX (Bastidas et al., 2012). The four systems are defined to have the following configurations: a myristylated N-termini with ATP and SP20 bound, nonmyristylated N-termini with ATP and SP20 bound, myristylated N-termini without ATP and SP20 bound, and nonmyristylated N-termini without ATP and SP20 bound. The myristylated glycine was prepared by first geometry optimizing with Gaussian (g03) (Case et al., 2010), with B3LYP and the 6-31G(d) basis set. Electrostatic potential fits were obtained from Gaussian using the geometry optimized structure and Hartree−Fock level of theory with the 6-31G* basis set. The Restrained Electrostatic Potential (RESP) module within the Antechamber program in AmberTools27 (Salomon-Ferrer et al., 2013a), was used to assign charges to the atoms using the Gaussian output. The H++ webserver (Anandakrishnan et al., 2012) was used to predict the protonation state of the residues in the structure at a pH

of 7. Only one histidine residue had a particularly low pKa in PKA and was modified to be a charged HIP residue. Other histidines were designated as either HIE or HID (with the ϵ or δ nitrogen protonated, respectively) by evaluating the local environments of each side chain in the crystal structure.

Molecular Dynamics Details. Solvation and Equilibration. The systems were prepared using the AMBER ff99SB (Hornak et al., 2006) force field, with the ildn modification for Ile, Leu, Asp, and Asn residues (Lindorff-Larsen et al., 2010). Each system was solvated in a 10.0 Å TIP3P box, and sodium ions were added to neutralize the charge. Systems were heated to 300 K at constant volume (NVT) with restraints on the protein that were gradually reduced from 200 to 0 kcal/(mol Å2) over a period of 150 ps. The langevin thermostat was used with a collision frequency of 1.0 ps−1. The SHAKE algorithm (Ryckaert et al., 1977) was used to constrain bonds to nonpolarhydrogens, and a 2.0 fs time-step was used during dynamics. A 10.0 Å cutoff was used for nonbonded interactions and the Particle Mesh Ewald method (Darden et al., 1993) was used for calculation of longrange electrostatics. Equilibration runs (100 ps) were done in the NPT ensemble using isotropic pressure scaling and a pressure relaxation time of 2.0 ps.

Production Simulations. For each system, six independent simulations were started from different snapshots from the equilibration simulations (taken at arbitrary intervals after the density of the water box was equilibrated) with randomized velocities. All production runs were conducted in the same NVT conditions as equilibration. All

simulations were performed using the PMEMD module within the Amber11 and 12 simulation packages (Case et al., 2010, 2012; Salomon-Ferrer et al., 2013a). Production runs, each 150ns in length, were performed on GTX580 GPUs using the pmemd.CUDA engine (Gotz et al., 2012; Le Grand et al., 2013; Salomon-Ferrer et al., 2013b).

3.3 Results

Myristylation Stabilizes the Most N-Terminal Residues of the C-Subunit.

Focusing first on the N-terminal dynamics of the C-subunit, the anisotropy decay results with the FM-K7C and FM-K16C conjugates, with and without N-terminal myristylation, are illustrated in **Fig. 3.2** panels A and B, and the decay parameters are summarized in **Table 3.1**. Myristylation was only associated with large effects on the anisotropy decay of FM-K7C, where myristylation increased the β2 parameter (amplitude of slower decay processes) from 0.092 to 0.142 in the apo state and from 0.103 to 0.157 in the ternary state (**Table 3.1, Fig. 3.2A**), suggesting a significant reduction in the angular excursion of the reporter, which is consistent with the myristyl moiety binding to the hydrophobic pocket in the core of the C-subunit observed in the crystal structure. Myristylation produced a small increase in the anisotropy decay of FM-K16C, as evidenced by a reduction of the β2 parameter from 0.201 to 0.185 in the apo state and from 0.185 to 0.174 in the ternary state (**Fig. 3.2B, Table 3.1**). There were modest changes in the decay parameters at the K7C and K16C sites upon formation of a ternary complex that are likely not significant. Still, ligand binding and closed state formation caused a slight decrease in mobility near the K7C

site on the basis of increases in the β2 parameter from 0.092 to 0.103 and from 0.142 to 0.157 for the nonmyristylated and myristylated protein, respectively. For K16C, ligand binding showed slight increases in mobility on the basis of the β2 parameter decreasing from 0.201 to 0.174 and from 0.185 to 0.169 going from apo to ternary states for the nonmyristylated and myristylated protein, respectively.

The results of MD simulations analysis of N-terminal dynamics are illustrated in **Fig. 3.2C** and summarized in **Table 3.2**. The MD simulations agree with the time-resolved fluorescence anisotropy results because the root mean squared fluctuation (RMSF) values of the main-chain atoms of the nonmyristylated protein are much greater than the myristylated protein in both apo and ternary states. This is illustrated in **Fig. 3.2C** and in the lower average main-chain atom RMSF values of residues 2−40 for the myristylated compared with the nonmyristylated protein (**Table 3.2**), indicating that the N-terminus is more flexible with the nonmyristylated protein, and this agrees with the anisotropy data at both K7C and K16C. However, there are small differences between the MD and time-resolved fluorescence data because the MD simulations showed slightly higher mobility of the K16 site for the nonmyristylated compared to myristylated protein (**Fig. 3.2C**), and the time-resolved fluorescence anisotropy data showed slightly lower mobility of the K16 site for the nonmyristylated compared to myristylated protein (**Table 3.1**). However, the differences in mobility seen from both methods are very small and likely not significant. In general, both MD simulations and time-resolved fluorescence anisotropy suggest similar levels of mobility of the K16 region for both the myristylated and nonmyristylated enzyme.

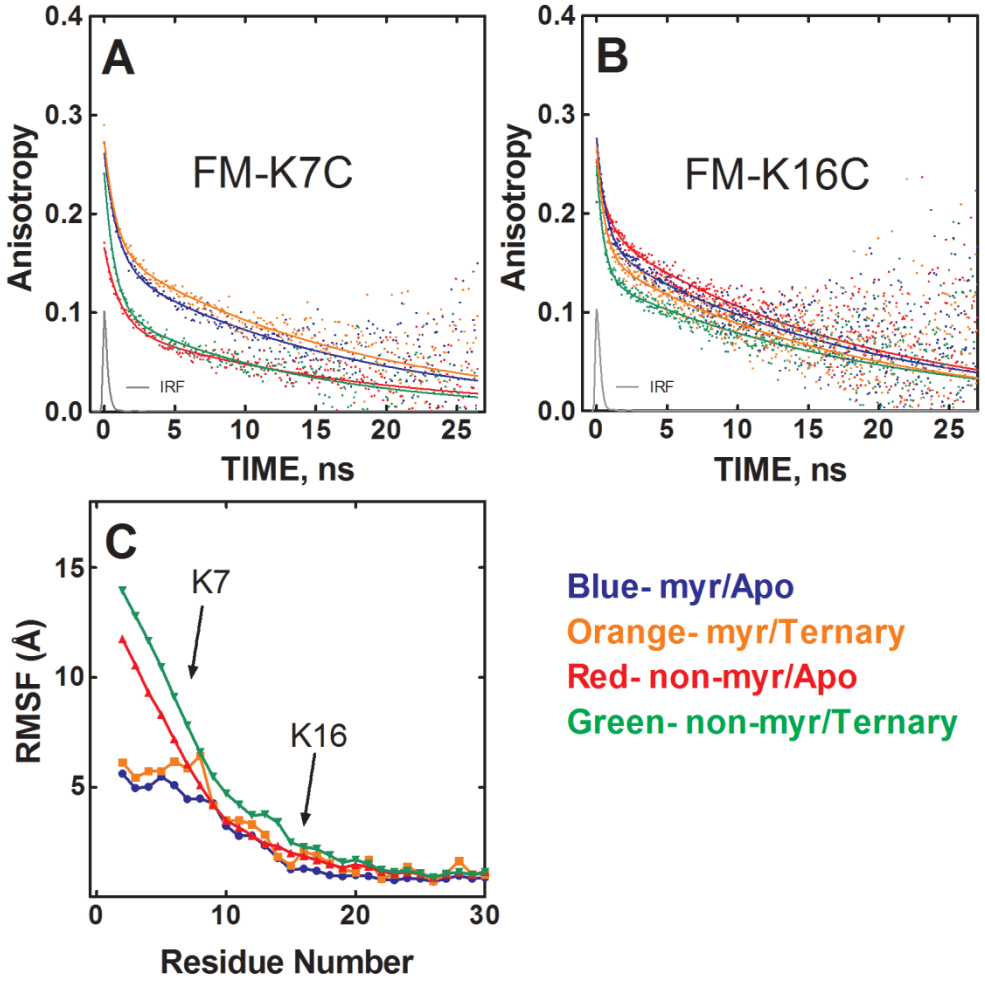

Figure 3.2. Myristylation stabilizes the N-terminus of the C-subunit, measured via time-resolved fluorescence anisotropy and MD simulations. A. Anisotropy decay of FM-K7C in myristylated/apo state (blue), nonmyristylated/apo state (red), myristylated/ternary state (orange), and nonmyristylated/ternary state (green). IRF is the instrument response function. **B**. Anisotropy decay of FM-K16C with the different states colored as in (A). **C**. The root mean squared fluctuation (RMSF) values averaged from six replicate MD simulations of myristylated and nonmyristylated configurations with and without ligands, plotted in angstroms for the A-helix residues (2−30).

Table 3.1. Time-Resolved Fluorescence Anisotropy Parameters of the FM-Conjugates Free in Solution (Apo) or Bound to MgATP and IP20 (Ternary). [a]Amplitude of the fast anisotropy decay processes. [b]Amplitude of the slow anisotropy decay processes. [c]Rotational correlation time of fast anisotropy decay processes. [d]Rotational correlation time of slow anisotropy decay processes. [e]Reduced ψ_r^2 of the anisotropy decay analysis. [f]Amplitude weighted averaged emission lifetime ($\sum\alpha_i\tau_i$, where $\sum\alpha_i=1$). The error terms represent the SEM of the results from three replicate sample preparations each of which was analyzed three times.

Protein	β1[a]	β2[b]	ϕ_{fast} (ns)[c]	ϕ_{slow} (ns)[d]	χ^2_r[e]	<tau>[f]
FM-K7C (Apo)	0.130 ± 0.019	0.092 ± 0.004	0.6 ± 0.2	11.9 ± 4.0	1.4 ± 0.2	3.8 ± 0.2
FM-Myr-K7C (Apo)	0.097 ± 0.007	0.142 ± 0.012	0.6 ± 0.1	14.1 ± 2.3	1.5 ± 0.3	3.6 ± 0.1
FM-K7C (Ternary)	0.117 ± 0.011	0.103 ± 0.001	0.5 ± 0.1	12.2 ± 0.2	1.8 ± 0.0	3.7 ± 0.2
FM-Myr-K7C (Ternary)	0.089 ± 0.003	0.157 ± 0.001	0.7 ± 0.1	17.3 ± 0.3	1.5 ± 0.3	2.8 ± 1.8
FM-K16C (Apo)	0.069 ± 0.007	0.201 ± 0.005	0.5 ± 0.2	14.2 ± 2.4	1.2 ± 0.2	3.5 ± 0.2
FM-Myr-K16C (Apo)	0.085 ± 0.009	0.185 ± 0.005	0.5 ± 0.2	14.0 ± 2.4	1.5 ± 0.4	3.8 ± 0.2
FM-K16C (Ternary)	0.068 ± 0.018	0.174 ± 0.020	0.7 ± 0.2	19.1 ± 0.6	1.1 ± 0.0	3.9 ± 0.0
FM-Myr-K16C (Ternary)	0.093 ± 0.002	0.169 ± 0.000	0.5 ± 0.1	20.3 ± 0.9	1.1 ± 0.1	4.3 ± 0.0
FM-N99C (Apo)	0.099 ± 0.011	0.158 ± 0.024	0.6 ± 0.1	18.3 ± 2.6	1.1 ± 0.1	4.2 ± 0.0
FM-Myr-N99C (Apo)	0.057 ± 0.017	0.200 ± 0.022	1.6 ± 0.3	22.8 ± 1.3	1.0 ± 0.1	4.3 ± 0.2
FM-N99C (Ternary)	0.135 ± 0.026	0.120 ± 0.020	0.3 ± 0.2	17.9 ± 2.2	1.2 ± 0.1	4.2 ± 0.0
FM-Myr-N99C (Ternary)	0.075 ± 0.018	0.181 ± 0.024	0.8 ± 0.3	20.0 ± 0.8	1.1 ± 0.1	4.4 ± 0.1
FM-S325C (Apo)	0.124 ± 0.045	0.154 ± 0.022	0.4 ± 0.2	21.0 ± 0.8	1.0 ± 0.0	4.1 ± 0.1
FM-Myr-S325C (Apo)	0.095 ± 0.014	0.182 ± 0.018	0.6 ± 0.4	19.6 ± 0.7	1.1 ± 0.1	4.1 ± 0.0
FM-S325C (Ternary)	0.150 ± 0.045	0.094 ± 0.013	0.4 ± 0.2	14.9 ± 1.4	1.1 ± 0.1	4.3 ± 0.0
FM-Myr-S325C (Ternary)	0.141 ± 0.022	0.106 ± 0.006	0.4 ± 0.1	13.7 ± 1.1	1.1 ± 0.1	4.3 ± 0.0
FM-C343 (Apo)	0.079 ± 0.003	0.154 ± 0.002	0.9 ± 0.1	19.5 ± 0.6	1.0 ± 0.0	4.3 ± 0.0
FM-Myr-C343 (Apo)	0.087 ± 0.011	0.150 ± 0.008	0.8 ± 0.3	19.4 ± 1.1	1.1 ± 0.1	4.3 ± 0.0
FM-C343 (Ternary)	0.059 ± 0.003	0.174 ± 0.000	1.3 ± 0.2	24.2 ± 0.2	1.0 ± 0.1	4.3 ± 0.1
FM-Myr-C343 (Ternary)	0.089 ± 0.017	0.151 ± 0.015	0.6 ± 0.3	21.6 ± 1.9	1.0 ± 0.1	4.3 ± 0.1

Table 3.2. Average root mean squared fluctuation (RMSF) values in angstroms of the backbone atoms for different regions of the protein from the MD simulations. [a]These simulations are of the protein when it is myristylated at its N-terminal glycine residue. [b]These simulations correspond to the protein that is not myristylated. Apo simulations are of the protein in the absence of ligands, and ternary state corresponds to simulations where the protein was bound to ATP and an inhibitory peptide, SP20.

Region of Protein	Residue Range	[a]Myr Apo (Å)	[a]Myr Ternary (Å)	[b]Apo (Å)	[b]Ternary (Å)
Entire Protein	2-350	1.07	1.16	1.18	1.17
N-terminus/A-helix	2-40	1.97	2.41	2.89	3.40
Core (N/C-lobes)	41-300	0.89	0.95	0.92	0.83
N-lobe	41-126	0.89	0.94	0.95	0.79
C-lobe	127-300	0.89	0.95	0.90	0.86
C-tail	301 to 350	1.31	1.33	1.22	1.15
Myristate Pocket	13-18; 95-105; 150-160; 300-308	0.80	1.04	0.96	1.11
Catalytic Loop	164-172	0.68	0.54	0.68	0.54
DFG motif	184-186	0.97	0.60	0.86	0.55
ATP Site Residues	49-55, 70, 120-127, 327-331	1.19	0.95	1.04	0.84
Activation Loop	192-200	1.15	1.23	1.11	0.97
B-helix	76-81	1.18	1.16	1.39	0.98
C-helix	84-96	0.77	0.92	0.86	0.75
β-strand 2	56-61	0.78	0.89	0.75	0.63
β-strand 3	68-75	0.76	0.78	0.78	0.64
β-strand 4	106-111	0.66	0.78	0.80	0.68
β-strand 5	115-121	0.67	0.76	0.74	0.60

Flexibility of the C-Subunit at the Myristate Pocket.

In addition to the N-terminus, the effects of myristylation and ligand binding on the myristate pocket were examined. On the basis of the X-ray structure, we chose to mutate and conjugate Asn99. The Asn99 residue does not directly interact with the myristyl moiety and is directly above the pocket near Phe100, which forms part of the pocket. We reasoned that if this residue was modified, it should not interfere with the conformational activity of the pocket (**Fig. 3.1A,B**). The results from the FM-N99C mutant are shown in **Fig. 3.3A**. In the absence of ligands, myristylation causes a dramatic decrease in the mobility of this site on the basis of slower anisotropy decay of Φfast and an increase in the β2 parameter (0.158 to 0.200) (**Table 3.1** and **Fig. 3.3A**). Thus, myristylation appears to greatly stabilize the N99C site and presumably the residues near the myristate pocket in an apo state. Interestingly, the addition of MgATP/IP20 to form a ternary complex produced an increase in the mobility of the myristate pocket for both the nonmyristylated and myristylated protein. The increased mobility for the nonmyristylated protein is evidenced by a faster anisotropy decay (Φfast) for the ternary nonmyristylated FM-N99C compared to the apo state (**Fig. 3.3A**) and by the decrease in the β2 parameter (0.158 to 0.120) (**Table 3.1**). Similarly, the β2 parameter decreased for the myristylated protein (0.200 to 0.181) along with Φ1 (1.6 to 0.8 ns), suggesting increased probe mobility with the formation of the ternary complex. Together, myristylation appears to stabilize residues in the myristate pocket compared to the stability of nonmyristylated protein in the presence and absence of ligands, but ligand binding and closed state formation increases the mobility of the myristate pocket for both the nonmyristylated and the myristylated

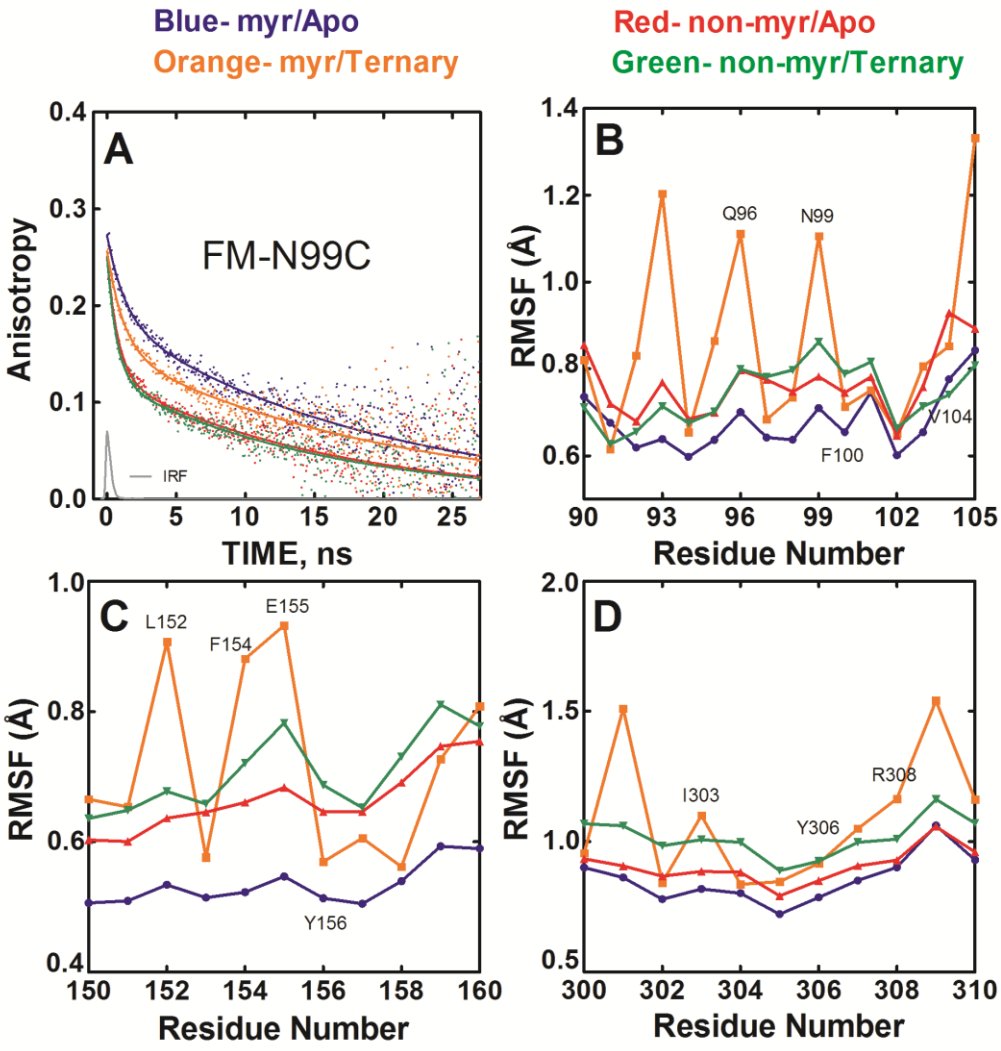

Figure 3.3. Myristylation and ligand binding produces altered mobility of the myristate pocket. A. Anisotropy decay of FM-N99C in myristylated/apo state (blue), nonmyristylated/apo state (red), myristylated/ternary state (orange), and nonmyristylated/ternary state (green). IRF is the instrument response function. (**B−D**) RMSF values of the main-chain atoms from MD simulations for residues 90−105 (B), 150−160 (C), and 300−310 (D).

enzyme.

The results from the MD simulations are in agreement with the fluorescence results and are illustrated in **Fig. 3.3B−D** and summarized in **Table 3.2**. The MD simulations show that Asn99, Glu155, and Tyr306, which are in or near the myristate pocket, exhibit decreased mobility for the myristylated compared to the nonmyristylated protein in an apo state. Also, after forming a ternary complex, the MD simulations show that these regions become more flexible for both the myristylated and nonmyristylated protein (**Fig. 3.3B−D**). Additionally, the average main-chain atom RMSF values of residues at the myristate pocket are lowest for the apo myristylated protein, and the values increase for both the myristylated and nonmyristylated C-subunit going from an apo state to a ternary complex (**Table 3.2**).

Effects of Myristylation and Ligand Binding on the Dynamics of the C-Tail.

Two sites in the C-terminal tail, S325C and the native C343, were examined with fluorescence anisotropy. The S325C site is near the "FDDY" motif that is thought to be important for forming part of the nucleotide binding pocket (Zheng et al., 1993a), and the C343 site is further along the C-tail and closer to the small lobe and A-helix (**Fig. 3.1A,C**). The mobility of the FM-S325C site was unaffected by myristylation but exhibited dramatic increases in mobility following MgATP/IP20 binding. This increased mobility is evident from the sharp decrease in the rate of anisotropy decay in the presence of MgATP/IP20 as illustrated in **Fig. 3.4A** and is based on the large decrease in the β2 parameter (0.154 to 0.094) (**Table 3.1**). The MD simulations did not agree with these results; instead, they showed the highest mobility

for the nonmyristylated protein in an apo state and similar mobility for the other three states (**Fig. 3.4B**).

For the myristylated FM-C343, no significant differences in mobility were observed between apo and ternary states (**Fig. 3.4C**). For the nonmyristylated protein, on the other hand, the probe mobility decreased upon ligand binding. This effect is primarily seen as an increase in the β2 parameter (0.154 to 0.174) (**Table 3.1**). Thus, the mobility of this region was greater for the myristylated protein than the nonmyristylated protein in a ternary complex based on a lower β2 parameter for the myristylated (0.151) compared to the nonmyristylated protein (0.174) in a ternary complex. Here, myristylation blocked the stabilizing effect of ligand binding near the C-terminus. The MD simulations provide some agreement with the experimental results because the nonmyristylated protein in a ternary complex is generally the least mobile and the other three states exhibit similar mobility (**Fig. 3.4D**). Also, the average RMSF values of the entire C-tail suggest a similar result of ligand binding showing minimal effects at the C-tail for the myristylated protein but decreasing mobility for the nonmyristylated protein (**Table 3.2**).

Principal Component Analysis of the MD Simulations.

To further characterize the dynamics of PKA in myristylated and nonmyristylated forms and in the presence and absence of ligands, we utilized principal component analysis (PCA) of the MD simulations to determine the most dominant modes in the dynamics. Specifically, all simulations were combined and the backbone atoms - C, CA, N, and O - on residues 2−350 were used in the analysis. The

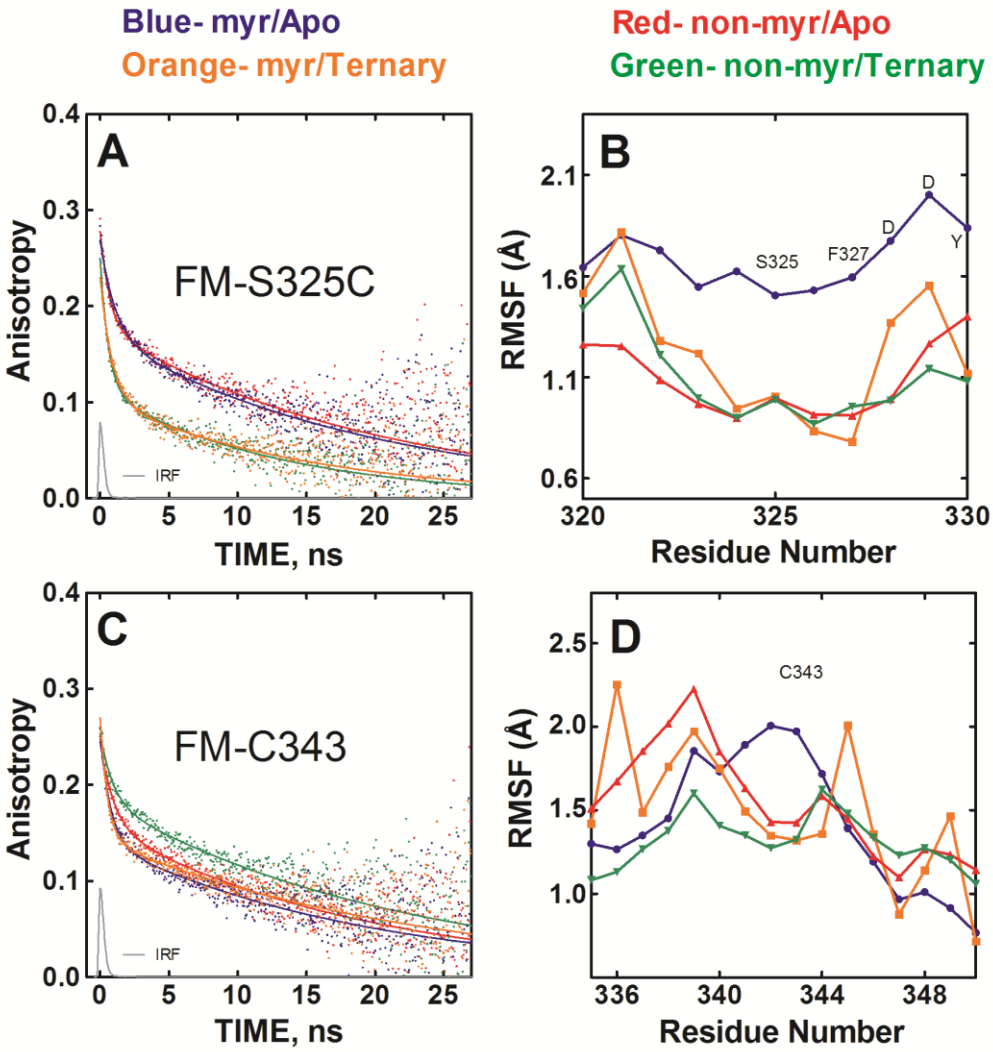

Figure 3.4. Effects of myristylation and ligand binding on the mobility of the C-tail. A. Anisotropy decay of FM-S325C in myristylated/apo state (blue), nonmyristylated/apo state (red), myristylated/ternary state (orange), and nonmyristylated/ternary state (green). IRF is the instrument response function. **B**. RMSF values for the backbone atoms from the MD simulations near the S325 residue. **C**. Anisotropy decay of FM-C343 with the different states colored as in (A). **D**. The RMSF values of the backbone atoms near the C343 residue.

two principal components (PC1 and PC2) are illustrated in **Fig. 3.5A−C**. In this analysis, PC1 and PC2 describe 33% and 15%, respectively, of the total variance of the motions in the simulation. The projections of the PKA simulations are shown in **Fig. 3.5A**, and the starting crystal structure is shown as a red diamond in the figure for reference. The major motions displayed in PC1 showed that as the N-terminus moved vertically, the Gly-rich loop would raise or lower (**Fig. 3.5B,C**). In PC2, the major motions were the rotation of the N-terminus coupled to rotation of the Gly-rich loop (**Fig. 3.5B,C**). The PCA analysis shows a larger range of motion for the nonmyristylated protein than the myristylated protein. Also, the myristylated protein shows mostly PC1 movements unlike the nonmyristylated protein, which has a large range of motions.

3.4 Discussion

The conformational dynamics of the C-subunit are known to be important in the opening and closing of the active-site cleft of the enzyme and potentially in product turnover and allostery (Masterson et al., 2011). We utilized time-resolved fluorescence anisotropy and MD simulations to study the mobility of the C-subunit in myristylated and nonmyristylated configurations and in the presence and absence of ligands. We found that myristylation greatly stabilizes the most N-terminal residues of the A-helix and stabilizes the myristate pocket residues, which is consistent with recent crystal structures of the myristylated C-subunit that display an ordered N-terminus with myristic acid stably bound within its hydrophobic pocket (Bastidas et al., 2012). We also found that the myristylated protein exhibits increased dynamics of

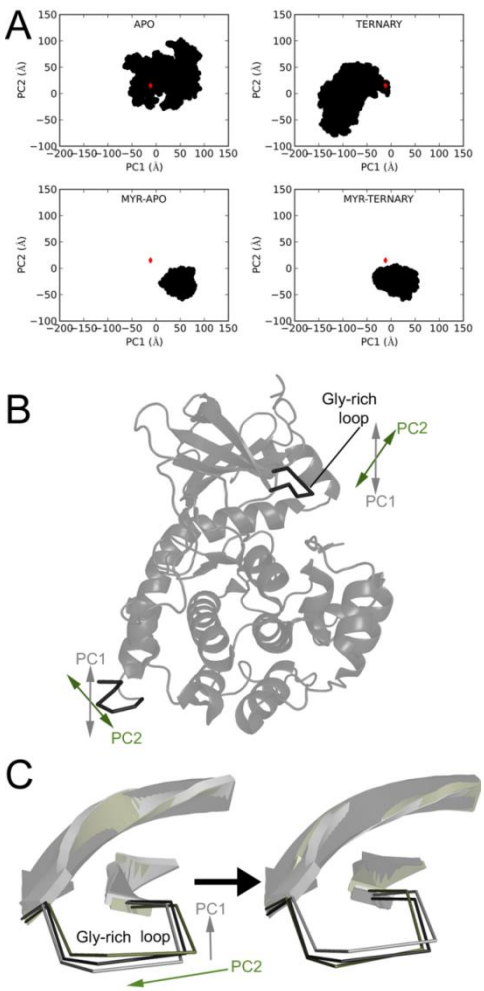

Figure 3.5. PCA analysis of the MD simulations of the C-subunit. The first two principal components were calculated from the backbone atoms of all MD simulations. **A**. Structural ensembles of the backbone atoms for the nonmyristylated C-subunit in apo and ternary states and myristylated C-subunit in apo and ternary states are shown. **B**. Major movements associated with PC1 and PC2 are depicted on the C-subunit. PC1 is associated with a vertical movement of the N-terminus and Gly-rich loop, and PC2 involves a rotation of the N-terminus and Gly-rich loop. **C**. Changes in the Gly-rich loop are shown for PC1 (gray) and PC2 (olive) through the projections aligned with the crystal structure 4DFX (black).

some regions of the protein in the presence of ligands compared to the dynamics of nonmyristylated protein.

We investigated the mobility of residues at the N-terminus and near the myristyl binding pocket for effects of N-myristylation and ligand binding. N-myristylation greatly stabilized the first 10−12 residues at the N-terminus but exhibited less of an effect further along the A-helix near K16 (**Fig. 3.2A−C**). Also, ligand binding did not greatly alter the mobility of the N-terminus. To test for mobility of the myristate pocket, we labeled N99C in the αC-β4 loop. The αC- β4 loop contains many highly conserved residues among AGC kinases including Phe100, Pro101, Phe102, Val104, and L106 (Kannan et al., 2007). Also, this region of the protein serves as a key link between the N- and C-lobes, and it is the only segment of the N-lobe that tracks with the C-lobe when the rigid-body movements of the C-subunit were analyzed (Tsigelny et al., 1999). The myristylated FM-N99C protein and N99 site showed much lower mobility than the nonmyristylated protein, but the flexibility of the pocket increased for both the myristylated protein and nonmyristylated protein upon ligand binding (**Fig. 3.3A−D**). This increase in dynamics at the myristate pocket in a ternary complex observed experimentally and with MD simulations suggests that the myristate pocket and active site may exhibit crosstalk consistent with recent X-ray crystallography (Bastidas et al., 2012), NMR (Gaffarogullari et al., 2011), and MD simulation studies (Cembran et al., 2012).

The increased mobility near N99C and at the myristate pocket upon ligand binding may seem surprising because Val104 in this loop helps to form the binding pocket for the adenine ring of ATP (**Fig. 3.6A**). However, we believe this result may

be explained on the basis of which regions are likely to be stabilized by ATP binding. Val104 forms part of the adenine binding pocket, and its dynamics are likely quenched by ATP binding. Additionally, the C-helix is also likely anchored by ATP binding because of Glu91 in the helix that helps to position ATP (**Fig. 3.6A**). The N99C site is centered between these two regions that likely become anchored by nucleotide binding. We believe that anchoring of both the N- and C-terminal portions of this loop may be compensated for by increased movements of the loop itself. This is one possible explanation for how ATP binding could increase movements of the N99C site and of the myristate pocket in general.

There is mounting evidence that N-myristylation may influence the mobility of different regions within the C-subunit, including the active site, and could be involved in allosteric regulation of the C-subunit. NMR experiments displayed altered chemical shifts at the active site with the myristylated protein (Gaffarogullari et al., 2011). X-ray crystal structures showed that the structure of the N-terminus is influenced by ligand binding (Bastidas et al., 2012), and previous MD simulations showed that the conformation of the N-terminus is coupled to dynamics at the active site of the enzyme (Cembran et al., 2012). It was hypothesized, on the basis of the X-ray crystal structures, that effects of N-myristylation could be transmitted to the active site via interactions between Trp30 on the A-helix, Arg190 on the activation loop, and Arg93 on the C-helix (**Fig. 3.6A**) (Bastidas et al., 2012), and the previous MD simulations of the N-myristylated protein supported this hypothesis (Cembran et al., 2012). The MD simulations analyzed here also support this finding. There is increased dynamics of the C-helix, activation loop, and many of the β-strands in the N-lobe of the C-subunit for

the myristylated protein in a ternary state, whereas the flexibility of these regions decreases for the nonmyristylated C-subunit (**Table 3.2**). Thus, these MD simulations also support increased dynamics of regions near the active site and support the hypothesis that Arg190 and Arg93 could help to mediate these effects on the basis of increases in flexibility of the activation loop and C-helix for the myristylated protein in a ternary complex. Additionally, other important regions at the active site of the C-subunit including the catalytic loop, the DFG motif, and residues involved in ATP binding show similar decreases in mobility going from apo to ternary states for the myristylated and nonmyristylated protein (**Table 3.2**). Therefore, this result suggests that the C-helix, activation loop, and β-strands are unique in displaying increased movements at the active site with the myristylated protein, and it is not simply increased dynamics for the entire active site with the myristylated protein.

The Trp30, Arg190, or Arg93 interaction is one way that the active site and N-myristylation could influence each other. Another way that myristylation and the active site could communicate is via the regulatory spine (R-spine). Leu106 is another residue that is near the N99C site, and it is a key hydrophobic contact to the R-spine. The R-spine is a stack of four hydrophobic residues that are assembled in every active kinase, typically as a consequence of phosphorylation of the activation loop (Kornev et al., 2006; Steichen et al., 2012; Taylor and Kornev, 2011). The adenine ring of ATP completes the parallel C-spine (**Fig. 3.6B,C**) (Kornev et al., 2008). It may be possible that myristylation could influence these spines, especially the regulatory spine, because of its closer proximity to the myristyl moiety. If myristylation influences

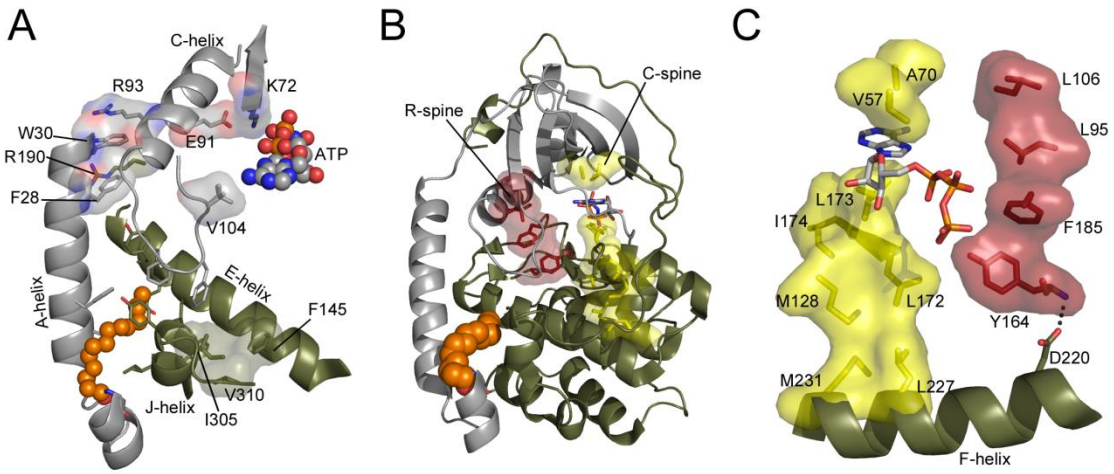

Figure 3.6. Possible modes of crosstalk between the myristate pocket and active site. A. The N-lobe is gray, C-lobe and C-tail are olive, the myristic acid group is shown in sphere representation in orange, and ATP is shown in sphere representation and colored by element. Several residues that may mediate crosstalk between the myristate pocket and active site are shown in stick representation or stick and surface representation. Some residues in the myristic acid pocket are not labeled for viewing clarity but are labeled in Fig. 3.1B. **B**. The protein is colored as in (A). ATP is shown in stick representation. The regulatory and catalytic spines (R-spine and C-spine) are shown in stick and surface representation in red and yellow, respectively. **C**. The C-spine and R-spine are colored and depicted as in (B), and one connection between the F-helix and R-spine is shown.

either or both spines, then it could influence mobility of the entire protein because these residues span both lobes of the kinase.

To further address how myristylation can influence the dynamics of the C-subunit and how N-myristylation may impact the active site, we performed principal component analysis (PCA) of the MD simulations. The movements associated with the two principal components PC1 and PC2 are shown in **Fig. 3.5B,C**. PC1 and PC2 illustrate that the movements of the N-terminus are coupled with movements at the active site and with the global conformation of the protein. PC1 shows that as the N-terminus moves vertically away from the protein, the Gly-rich loop rises and the C-subunit adopts a more open conformation. PC2 shows that a rotation of the N-terminus away from the core of the protein is coupled to rotation of the Gly-rich loop and N-lobe. Also, projecting the motions of the myristylated and nonmyristylated protein onto the PC space shows that the nonmyristylated protein adopts a much wider range of motions than the myristylated protein (**Fig. 3.5A**). Furthermore, the myristylated protein adopts more PC1 movements than the nonmyristylated protein. These results suggest that, by stabilizing the N-terminus and its possible conformations, N-myristylated stabilizes the amount and types of global conformations and movements of the protein. Also, the global dynamics and active site dynamics that are experienced by the myristylated protein are largely opening and closing of the Gly-rich loop and not rotations of the active site.

The implications of the PCA results are interesting to consider in terms of what they suggest about the possible role of N-myristylation on C-subunit activity or interactions. The results suggest that N-myristylation may prevent or limit drastic

conformational changes of the enzyme, possibly due to stabilization of the N-terminus. This is supported by the relatively small range of motions adopted by the myristylated protein in apo and ternary states on the basis of PCA analysis (**Fig. 3.5A**). Therefore, N-myristylation may keep the C-subunit in a relatively stable conformation, which could be important for ligand binding and activity. This possibility is exemplified in the PCA plots (**Fig. 3.5A**) because the range of motions exhibited by the nonmyristylated protein in an apo and ternary state are very different, but for the myristylated protein, on the other hand, the motions adopted in apo or ternary states are very similar. Therefore, N-myristylation may help to lock the enzyme in conformations that are more representative of the active state of enzyme, because the ternary complex is more likely to adopt conformations suitable for catalysis. Also, because the PCA analysis shows that the motions adopted by the N-myristylated protein are mostly opening and closing of the Gly-rich loop, this result suggests that N-myristylation could influence the ability for substrates to bind and be turned over by the enzyme by modulating opening and closing of the active site. Finally, in general, the PCA results further imply that the active site and the myristyl moiety as well as its binding pocket may influence each other.

In addition to the myristate pocket, N-terminus, and possibly the active site, the flexibility of other regions may be influenced by N-myristylation. For instance, another site that we labeled for time-resolved fluorescence anisotropy was the native C343. This region is more mobile in a ternary complex for the myristylated C-subunit than the nonmyristylated enzyme (**Fig. 3.4C**). The mobility of this region is not greatly influenced by ligand binding for the myristylated protein but becomes less

mobile upon ligand binding for the nonmyristylated protein on the basis of time-resolved fluorescence anisotropy, and this result is also in agreement with the MD simulations based on the average RMSF values of the C-tail, which are very similar for the myristylated protein in apo and ternary states but decrease from apo to ternary states for the nonmyristylated protein (**Table 3.2**). Myristylation, thus, prevents the stabilizing effect caused by ligand binding that occurs with the nonmyristylated protein and, effectively, results in increased mobility of this region in a ternary state relative to the nonmyristylated protein.

Additionally, the average main-chain atom RMSF values from several regions throughout the C-subunit suggest that ligand binding increases flexibility in the myristylated enzyme but decreases dynamics for the nonmyristylated C-subunit (**Table 3.2**). For instance, the N-lobe, the C-lobe, and the C-tail all show increases in average RMSF values, indicating increased flexibility, for the myristylated protein going from an apo to ternary state (**Table 3.2**). The nonmyristylated protein, on the other hand, shows decreases in average RMSF values for these same regions, indicating decreased mobility, going from apo to ternary state (**Table 3.2**). Thus, the flexibility of the myristylated protein is generally increased upon ligand binding and generally decreased upon ligand binding for the nonmyristylated protein. These results suggest that myristylation can influence other regions within the C-subunit following ligand binding including, potentially, the active site.

We also wanted to test the mobility of the C-tail region near the FDDY motif that forms part of the ATP binding site (**Fig. 3.1C**). To do this, we investigated the S325 site. This is an important region because the S325C site is near the PxxP motif in

the C-tail (residues 313−316 in PKA), which is a known protein binding site in another AGC kinase, PKC, and may be a binding site in PKA as well (Gould et al., 2009). Furthermore, 3-phosphoinositide dependent protein kinase 1 (PDK1), which phosphorylates the activation loop of different kinases, binds to the C-tail of PKA near this region (Romano et al., 2009). With time-resolved fluorescence anisotropy, the FM-S325C site showed large changes in mobility upon ligand binding for both the myristylated and nonmyristylated protein (**Fig. 3.4A**), but the MD simulations displayed increased mobility for the apo myristylated protein with similar mobility for the other states (**Fig. 3.4B**). Obviously, the discrepancy between the MD and fluorescence data at the S325C site is disappointing. There are some possible explanations for the different results between the two methods. For example, it is possible that the time-resolved fluorescence anisotropy results are distorted by the fluorophore, fluorescein-5-maleimide, altering the natural mobility of the C-tail. It is possible that the fluorophore could interact with other residues in the C-tail or near the active site, and this could cause the increased mobility upon formation of a ternary complex that may not represent natural mobility of the site. Alternatively, there could be problems with the MD simulation results. One possible explanation for discrepancies in the MD simulation results is problems with sampling. It is possible that these simulations may represent outliers in possible motions of the C-tail, and if more simulations were performed or longer simulations were performed, the final RMSF values may change and could be closer to the experimental findings. Additionally, one should keep in mind that the MD simulations are not "measuring" the same things as time-resolved fluorescence anisotropy (TRFA). The MD

simulations are estimating spatial displacement of the main-chain atom over time, whereas TRFA monitors motions of a reporter at the end of a cysteine side chain. (The motions of the reporter group are influenced by (1) the torsional motions of the side chain and linking tether arm, (2) the backbone motions of the peptidyl chain around the conjugated cysteine, and (3) the whole-body rotation diffusion of the protein.) Clearly, caution should be used in interpreting the results from either method.

Beyond adding insight into the conformational dynamics of the C-subunit, the general but not complete consistency between the fluorescence anisotropy and MD simulations and previous NMR and X-ray crystallographic results adds credence to the use of fluorescence anisotropy to measure protein conformational dynamics. Clearly, there are limitations to its use. One such limitation is the possibility that the mutation and conjugation significantly perturb local dynamics and/or function. For instance, if the native C199A site in PKA is labeled, then PKA loses catalytic activity (Nelson and Taylor, 1981). Fortunately, with PKA, labeling of the native cysteine residues is prevented with the addition of MgATP, but with other proteins, the native cysteine residues may need to be mutated in order to perform time-resolved fluorescence anisotropy. Also, if mutation of the cysteine residues negatively impacts the protein's natural function or interactions, then time-resolved fluorescence anisotropy experiments become impractical. Additionally, MD simulations also have limitations and should ideally be verified with experimental findings because artifacts from MD simulations are possible due, for example, to short simulation times or very few simulations. When only a small number of simulations and/or short simulation times are utilized, then it is possible to see artifacts in the simulations. Like other techniques,

it is ideal to perform replications to ensure that results are representative of actual motions and do not represent outliers in possible dynamics. Additionally, MD simulations are reliant on a solved crystal structure. Therefore, it is possible for MD simulations to be biased by the starting crystal structure especially if the structure does not represent a typical conformation of the protein in solution. Therefore, there are some limitations to both MD simulations and time-resolved fluorescence anisotropy, so some caution should be used in the interpretation of results from these approaches. Ideally, cross validation should be utilized for either method, and the general agreement in these studies between the MD simulations and fluorescence anisotropy results supports the use and findings obtained from each method.

In summary, the results of these studies provide new insights into the motions adopted by the C-subunit in response to N-myristylation and ligand binding. As several studies showed previously (Bastidas et al., 2012; Cembran et al., 2012; Gaffarogullari et al., 2011), we also find that N-myristylation stabilizes the N-terminus and myristate pocket, and N-myristylation also may exhibit crosstalk with the active site of the enzyme. We found that ligand binding increases movements at the myristate pocket, and myristylation in combination with ligand binding showed modest increases in dynamics near the active site. Together this suggests that N-myristylation may impart allosteric regulation of the C-subunit.

Chapter 3, in full, was published as Influence of N-myristylation and Ligand Binding on the Flexibility of the Catalytic Subunit of Protein Kinase A. Bastidas AC, Pierce LC, Walker RC, Johnson DA, Taylor SS. *Biochemistry* 2013 Sep 17; 52

(37):6368-79. The dissertation author was the primary investigator and author of this work.

Chapter 4

Phosphoryl Transfer by Protein Kinase A is Captured in a Crystal Lattice

4.1 Introduction

One of the major mechanisms of cell signaling and gene regulation is protein phosphorylation. Phosphorylation is catalyzed by protein kinases, which transfer the γ-phosphate of ATP onto substrate proteins on serine, threonine, and tyrosine residues. Because of their roles in cancer and other diseases, kinases have become an important pharmaceutical target (Manning et al., 2002). One of the best characterized protein kinases is the Ser/Thr kinase cAMP-dependent protein kinase (protein kinase A (PKA)), which serves as a prototype for the entire kinase family (Johnson et al., 2001; Tasken et al., 1997; Taylor et al., 2012b). Under non-activating conditions, PKA exists as a heterotetrameric holoenzyme complex composed of a regulatory (R) subunit dimer that binds to and inactivates two catalytic (C) subunit monomers (R_2C_2). PKA is activated by cAMP, which binds to the R-subunits causing a conformational change unleashing the active C-subunits, which can then phosphorylate protein substrates (Kim et al., 2007).

The C-subunit of PKA was the first kinase structure to be solved (Knighton et al., 1991a) and has served as a prototype for protein kinases because of the multiple biophysical, structural, and computational studies of PKA (Taylor et al., 2012b). PKA serves as a model for all kinases because the core of the enzyme, residues 40−300, is highly conserved. This conserved core forms a bean shaped structure consisting of the small lobe (or N-lobe) (residues 40−126 in PKA) and the large lobe (or C-lobe) (residues 127−300 in PKA). ATP binds in the cleft formed between these two lobes (Zheng et al., 1993c), and recent NMR studies show how binding of the nucleotide

acts to dynamically couple the two lobes making it “committed” to catalysis (Masterson et al., 2011).

The precise mechanism of phosphoryl transfer and the detailed structural validation of the individual steps involved in catalysis are still not well understood for PKA or kinases in general. PKA, like most kinases, requires magnesium ions to catalyze phosphoryl transfer, and magnesium increases the affinity of the enzyme for ATP (Armstrong et al., 1979). Other metals such as manganese can also be utilized by kinases *in vitro* (Grace et al., 1997; Zheng et al., 1993c), but because of cellular concentrations, magnesium is thought to be the physiological metal cofactor. There are two magnesium binding sites in PKA (Bossemeyer et al., 1993; Herberg et al., 1999; Zheng et al., 1993c). One magnesium ion is coordinated by the β- and γ-phosphates of ATP, by Asp184 in a bidendate manner, and by two water molecules and was previously termed Mg1 and activating. The other magnesium ion is coordinated by Asn171, one oxygen atom of Asp184, the α- and γ- phosphates of ATP, and one water molecule and was termed Mg2 and inhibiting (Adams and Taylor, 1993; Zheng et al., 1993a). The active site water molecules that help to coordinate the magnesium ions were shown to be highly conserved among many protein kinases likely due to conservation of key active site residues (Shaltiel et al., 1998). The activating/ inhibiting terminology used to describe the magnesium ions arises from the fact that low concentrations of magnesium (0.5 mM) yield higher k_{cat} values than high magnesium concentrations (10 mM) suggesting an inhibitory effect attributed to one of the two magnesium ions (Adams and Taylor, 1993; Cook et al., 1982; Shaffer and Adams, 1999a). However, this terminology is slightly misleading because binding two

magnesium ions does not actually influence the rate of phosphoryl transfer but, instead, affects the rate of ADP release which is the rate-limiting step at high magnesium concentrations (Adams and Taylor, 1993; Shaffer and Adams, 1999a). The identity of Mg2 as the secondary and inhibitory ion may arise partially from an early report which suggested that low resolution structures obtained under low magnesium concentration displayed density mostly for Mg1 with very little density for Mg2 (Zheng et al., 1993a). Therefore, Mg1 was thought to bind first and with higher affinity with ATP and was thought to be the more important ion for phosphoryl transfer. With ADP, the two magnesium ions were thought to bind with equal affinity, which may explain why the ADP off rate limits turnover at higher magnesium concentration (Armstrong et al., 1979). However, recently, another structure obtained under low magnesium concentration showed density for only Mg2 (Kovalevsky et al., 2012). Additionally, computational studies of the PKA transition state and phosphoryl transfer mechanism suggest that Mg2 yields greater stabilization of the transition state than Mg1 and may thus be more important for catalysis (Cheng et al., 2005; Szarek et al., 2008; Valiev et al., 2007). Therefore, there is some uncertainty about the roles of the two magnesium ions.

Adding further importance to understanding the roles of the magnesium ions is the fact that ATP exists as a complex with magnesium in physiological settings, and in many crystal structures only one metal ion is present. Often, however, the γ-phosphate in these structures does not seem to be ideally oriented for phosphoryl transfer (Tereshko et al., 2001; Wu et al., 2008). In PKA and some other kinases, two metal ions are bound. More recently a comprehensive analysis of cyclin dependent kinase 2

(CDK2) showed that two metal ions are required for the phosphoryl transfer reaction (Bao et al., 2011; Jacobsen et al., 2012). CASK is a highly unusual kinase, the only one known so far, which requires no magnesium ions (Mukherjee et al., 2008). Some kinases, such as PKA and CDK2, are inhibited by increases in magnesium concentration while others show no effect or increased activity in the presence of excess magnesium (Adams, 2001; Adams and Taylor, 1993; Bao et al., 2011; Jacobsen et al., 2012). Therefore, magnesium ions can display complex regulatory roles on protein kinase function. A more detailed understanding of the different roles for magnesium ions in different protein kinases may provide a better understanding of kinase function which could aid in our understanding of activating mutations involved in disease or improve the design of inhibitors of kinases for therapeutic purposes.

In addition to the magnesium ions, there are several conserved residues that are important for phosphoryl transfer. Asp166, which is completely conserved in kinases and may act as a catalytic base, is thought to position the substrate for phosphoryl transfer, and mutation of this residue causes severe defects in phosphoryl transfer (Gibbs and Zoller, 1991; Valiev et al., 2003). Additionally, Lys72 in β-strand 3 forms a salt bridge with Glu91 from the C-helix, and Lys72 helps position ATP for phosphoryl transfer by binding to the α- and β-phosphates of ATP. This lysine residue is essential for catalysis, and it is often mutated in kinases to make "kinase dead" mutants even though this mutation does not abolish ATP binding (Gibbs and Zoller, 1991; Iyer et al., 2005a; Iyer et al., 2005b; Zoller et al., 1981). Furthermore, Lys168 forms a hydrogen bond with the γ-phosphate of ATP and may stabilize the transition

state or possibly aid in the phosphoryl transfer reaction (Cheng et al., 2005; Madhusudan et al., 2002).

To better understand substrate binding and catalysis by PKA, the catalytic subunit was crystallized with a substrate peptide SP20 corresponding to the 20 amino acid inhibitor peptide derived from the endogenous protein inhibitor PKI (5−24) with two mutations that convert it from an inhibitor to a substrate (N20A, A21S) (Madhusudan et al., 1994; Olsen and Uhler, 1991). In addition to SP20, the protein was crystallized with adenosine-5′-(β,γ-imido)triphosphate (AMP-PNP), which is a generally nonhydrolyzable analog of ATP where the atom bridging the β- and γ-phosphates is replaced with a nitrogen (Yount et al., 1971). To our surprise, despite using AMP-PNP, protein crystals grown under certain conditions displayed clear phosphoryl transfer of the γ-phosphate of AMP-PNP onto the P-site serine. Although AMP-PNP is generally used as a nonhydrolyzable analog of ATP, there are some reports of AMP-PNP being hydrolyzed and serving as a substitute for ATP although no kinases are reported to utilize AMP-PNP to our knowledge (Suzuki et al., 1997; Taylor, 1981; Tomaszek and Schuster, 1986; Yount et al., 1971).

We obtained two crystal structures of the C-subunit where both products are trapped in the crystal lattice. One structure refined to 1.55 Å resolution of a crystal analyzed approximately 3 months after appearance displays two states of the protein. 55% of the protein is modeled with intact AMP-PNP and an unphosphorylated substrate, and 45% is modeled with the products of phosphoryl transfer which are AMP-PN and a phosphorylated substrate. Another structure of a crystal harvested approximately 5 months after appearance was refined to 2.15 Å resolution and

displays complete phosphoryl transfer. These structures offer unprecedented insights into the midpoint and end point of kinase phosphoryl transfer allowing for a characterization of the roles of the magnesium ions and yielding information about the steps and mechanisms involved in the reaction turnover. We conclude that, contrary to some previous reports, Mg2 likely binds within the active site first followed by Mg1 and binding of both ions not only is necessary for optimum phosphoryl transfer but also slows product release following transfer. Following transfer, Mg1 leaves the active site which then allows for Mg2-ADP release. Release of Mg1 is likely an important aspect of product release and likely explains why ADP release is rate-limiting at high magnesium concentrations due to the continued occupancy of both magnesium binding sites following phosphoryl transfer.

4.2 Experimental Procedures

Purification of the C-Subunit Proteins. The nonmyristylated WT protein was expressed and purified as described previously (Herberg et al., 1993). The myristylated C-subunit protein was prepared by coexpression with yeast NMT as described previously (Duronio et al., 1990) and purified using a protocol described previously (Bastidas et al., 2012). The myristylated C-subunit utilized for crystallography was a mixture of doubly and triply phosphorylated protein with all protein phosphorylated on Thr197 and Ser338 and about 50% phosphorylated on Ser139. The nonmyristylated C-subunit utilized for crystallization was triply phosphorylated on Ser10, Thr197, and Ser338.

Crystallization. The AMP-PNP, Mg^{2+}, and SP20 complexes were crystallized under similar conditions utilized for previous C-subunit structures (Bastidas et al., 2012; Wu et al., 2005; Yang et al., 2004). The C-subunit protein was dialyzed overnight into 50 mM bicine, 150 mM ammonium acetate, and 10 mM DTT at pH 8.0. This protein was concentrated to 8−10 mg/mL. Immediately preceding crystallization, the protein was combined in an approximately 1:10:20:5 molar ratio of protein:AMP-PNP:Mg^{2+}:SP20 with the AMP-PNP dissolved in 0.1 M Tris pH 7.0 and the Mg^{2+} and SP20 dissolved in water. The protein was crystallized using hanging drop vapor diffusion with 2−6% 2-methyl-2,4-pentanediol (MPD) dissolved in DI water as the well solution. An important note is that phosphoryl transfer of AMP-PNP was only seen when low percentages of MPD were used in the well solution (6% MPD or less) and transfer was not seen with higher MPD percentages (Bastidas et al., 2012). The protein was crystallized using 8 μL drops of 1:1 protein to well solution, and 80−150 μL of methanol were added to the 1 mL well solution immediately before sealing the well. These crystals were grown at 4 °C. Both crystal structures presented here were obtained from drops with the well solution containing 2% MPD. 80 μL of methanol were added to the well for the 1.55 Å structure, and 125 μL of methanol were added to the well for the 2.15 Å structure.

Although it is unclear why low MPD concentrations seem to be required for significant phosphoryl transfer in the crystals, the crystallization conditions may be a contributing factor. High MPD concentrations increase the viscosity of the solution which may inhibit the movement and possible conformations that can be adopted by the protein, and this may have prevented phosphoryl transfer in our earlier structures

(Bastidas et al., 2012). Another possibility is that MPD, a nonpolar compound, will decrease the polarity of the crystal solution. By decreasing the polarity of the solution, MPD may effectively inhibit phosphoryl transfer by neutralizing the magnesium ions or protein residues which are critical for phosphoryl transfer. Additionally, the decreased polarity would also inhibit phosphoryl transfer because polar solvents would be preferred to stabilize the transition state and provide solvent molecules to aid in the reaction.

Data Collection and Refinement. The crystals were flash cooled in liquid nitrogen with cryoprotectant solution (12% MPD and 15% glycerol). The 1.55 Å data set was collected on a crystal harvested approximately 3 months after initial appearance, and the 2.15 Å data set was from a crystal harvested approximately 5 months after initial appearance. The crystal structures were each obtained from one crystal: however, the 2.15 Å structure is from two separate data sets of the same crystal that were merged. Because one data set used a longer exposure time, it allowed refinement to a slightly higher resolution than the first set. The two sets were merged to increase the completeness of the data set. Data were collected on the synchrotron beamline 8.2.1 for the 1.55 Å structure and on beamline 8.2.2 for the 2.15 Å structure of the Advanced Light Source, Lawrence Berkeley National Laboratories (Berkeley, California). For each crystal structure, the data were integrated using iMOSFLM (Battye et al., 2011). Both complexes crystallized in the $P2_12_12_1$ space group similar to previous structures. Molecular replacement was carried out using Phaser (McCoy et al., 2007) with 3FJQ (Thompson et al., 2009) as a search model. The refinement was

performed using refmac5 (1994), and model building was done in Coot (Emsley and Cowtan, 2004). Clear density was visible for phosphoryl transfer in both structures. The 1.55 Å structure showed electron density representing two states of the protein which were with and without phosphoryl transfer. The structure was refined using different percentages of reactant and product states, and 45% phosphoryl transfer yielded the best fit to the electron density. The 2.15 Å structure only showed density for phosphoryl transfer with no density for the intact γ-phosphate of AMP-PNP. However, there was some negative density at the P-site phosphate with full transfer modeled, and therefore, the structure was modeled with 70% phosphoryl transfer. The negative density may arise from some AMP-PNP that hydrolyzed prior to crystallization or that hydrolyzed without phosphoryl transfer. Another note about the refinement is that the Gly-rich loop in the 1.55 Å structure shows some positive electron density that may represent the presence of some molecules that adopt a lower conformation of the loop. Multiple conformations may be adopted due to the presence of both phosphoryl transfer and no transfer, but the majority of the protein is in the conformation modeled. The structures were refined to R_{work}/R_{free} of 17.2%/19.4% and 18.7%/22.8% for the 1.55 Å (4HPU) and 2.15 Å (4HPT) structures respectively. Data collection and refinement statistics are shown in **Table 4.1**.

Table 4.1. Data collection and refinement statistics of partial and complete phosphoryl transfer structures. Data collection was performed at ALS laboratory in Berkeley, CA on beamline 8.2.1 or 8.2.2. [a]Values in parenthesis correspond to the highest resolution shell. [b]5% of the data was excluded from the refinement to calculate the R_{free}. [c]Ramachandran plot quality as defined in MolProbity (Davis et al., 2007).

	1.55 Å Structure	**2.15 Å Structure**
PDB ID	4HPU	4HPT
Data Collection		
Space group	$P2_12_12_1$	$P2_12_12_1$
Cell dimensions		
a, b, c (Å)	57.69, 79.80, 98.14	71.54, 79.06, 80.09
Unique reflections	66,294 (9,505)	21,475 (2,363)
Multiplicity	5.7 (5.7)	7.2 (3.8)
Resolution range (Å)	33.85-1.55 (1.63-1.55)[a]	44.35-2.15 (2.27-2.15)[a]
R_{merge} (%)	7.6 (44.6)	10.0 (44.4)
$I/\sigma I$	12.8 (3.2)	12.4 (2.8)
Completeness (%)	99.7 (99.2)	85.7 (66.2)
Refinement		
R_{work}/R_{free} (%)[b]	17.2/19.4	18.7/22.8
Average B factor (Å^2)	15.15	35.32
Ramachandran angles (%)[c]		
Favored regions	98.57	97.99
Allowed regions	100	100
r.m.s. deviations		
Bond lengths (Å)	0.009	0.009
Bond angles (°)	1.33	1.16

Mass Spectrometry Analysis of Protein Crystals. Preceding mass spectrometry analysis, the protein crystals were washed by sequentially transferring the crystals through 5 drops of fresh well solution (2% MPD) to remove any protein/peptide arising from the solution rather than the crystal. The sample was loaded to a C18 precolumn (360 μm O.D. × 100 μm I.D., 5 μm Zorbax SB-C18, 10 cm packing). The precolumn was connected via Teflon tubing to a C18 analytical column (360 μm O.D. × 75 μm I.D., 5 μm Zorbax SB-C18, 10 cm packing) with an integrated emitter tip (2−4 μm I.D.). Peptides were eluted into an LTQ Orbitrap mass spectrometer (ThermoFisher Scientific, San Jose, CA) with an Agilent 1100 HPLC system. A precolumn splitter was used so that the flow rate out of the emitter tip was about 100 nL/min throughout the gradient. The HPLC gradient was 0−40% B in 30 min (Buffer A: 0.1% formic acid; Buffer B: 90% ACN in 0.1% formic acid). The mass spectrometer was operated in a targeted mode where m/z ratios of +2, +3, and +4 of both the phosphorylated and nonphosphorylated peptide were targeted throughout the entire HPLC gradient. The isolation window for precursor masses were set to 0.5 Da. The dynamic exclusion option was selected with a repeat count of 1, a repeat duration of 0.5 min, and an exclusion duration of 1 min. For data analysis, the m/z ratios for +2, +3, and +4 of the phosphorylated and nonphosphorylated peptides were extracted.

Generating Fo − Fc Omit Maps. The maps displayed in **Fig. 4.2** and **Fig. 4.5C** were generated by omitting different elements from the final model of the structures. The structures were then refined with the components omitted using 10 or more cycles of

restrained refinement, and Fo − Fc maps were generated using the FFT program in the CCP4 suite (1994).

Measurement of Phosphoryl Transfer of AMP-PNP to RIIβ in vitro. The purified C-subunit of PKA was incubated with purified RIIβ; purification of RIIβ is described elsewhere (Zhang et al., 2012), alone and with ATP or AMP-PNP in 0.1 M MOPS, 10 mM MgCl2 at pH 7.0. The concentration of ATP and AMP-PNP used in the reaction buffer was 1 mM when the nucleotides were included. The reaction mixture contained approximately 300 nM C-subunit and 300 nM RIIβ. The reaction was incubated at room temperature for the first 30 min and was then kept at 4 °C. Time points of the reaction were quenched at 30 min, 1 day, and 2 days by taking samples of the reaction mixture, mixing 1:1 with SDS−PAGE sample buffer, and heating the samples for 10 min at 70 °C. These samples were analyzed by Western blot with antibodies against the C-subunit (BD Biosciences), RIIβ (Biomol), and against R-R-X-phosphorylated S/T, the PKA consensus sequence which RIIβ contains at its inhibitor site (Zhang et al., 2012) (Cell Signaling Technology). The level of phosphorylation with AMP-PNP was quantified using ImageJ with the amount of phosphorylated RIIβ for each time point with ATP treated as 100% phosphorylation and with the values normalized to the total amount of RIIβ.

4.3 Results

1.55 Å Structure Displaying Partial Phosphoryl Transfer of the γ-Phosphate of AMP-PNP.

The myristylated C-subunit was crystallized with AMP-PNP, magnesium, and SP20, and the structure was refined to 1.55 Å resolution (**Fig. 4.1A**). Despite using AMP-PNP, the structure shows clear phosphoryl transfer of the γ-phosphate of AMP-PNP onto the substrate serine residue. There is density both for the γ-phosphate on AMP-PNP and for phosphorylated serine on SP20 (**Fig. 4.1B**). Therefore, these crystals contain some protein that has undergone phosphoryl transfer and some that remains in the reactant state with intact AMP-PNP and the unphosphorylated substrate. The structure was refined with different percentages of phosphoryl transfer, and 45% phosphoryl transfer, 55% reactant state yielded the best fit to the electron density.

One previously reported crystal structure, 1RDQ, showed partial hydrolysis of ATP, but since 1RDQ was crystallized with IP20 which contains Ala at the P-site, the phosphate remained as free phosphate within the structure (Yang et al., 2004). To verify that the structure reported here corresponds to phosphoryl transfer and not hydrolysis, we aligned the free phosphate from 1RDQ with this structure. This alignment clearly shows that the hydrolyzed phosphate, as observed in 1RDQ, does not fit the electron density in this structure (**Fig. 4.1C**). To further verify phosphoryl transfer, the structure was modeled and refined with AMP-PNP and no phosphoryl transfer. The resulting Fo − Fc map shows positive electron density on the P-site serine (**Fig. 4.2A**). Alternatively, if the structure is refined with ADP and phosphorylated SP20, the Fo − Fc map shows positive electron density for the γ-phosphate of AMP-PNP (**Fig. 4.2B**). Finally, if the structure is modeled without phosphoryl transfer and with ADP, the Fo − Fc map shows positive electron density

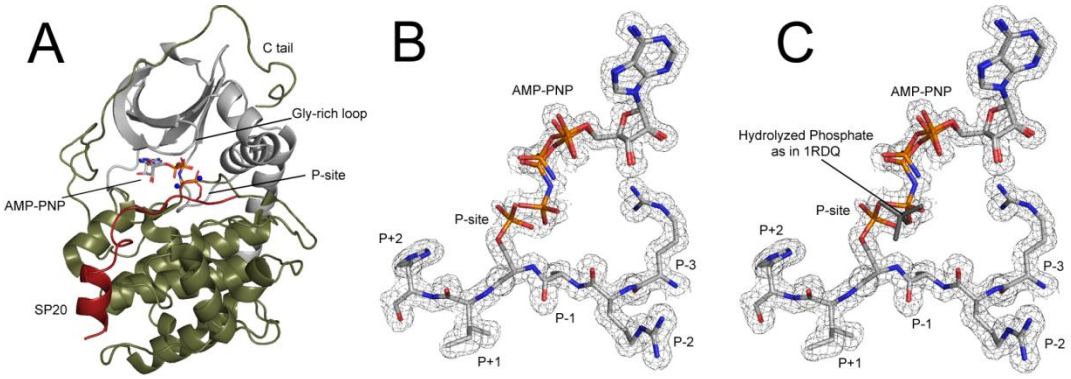

Figure 4.1. Crystal structure of PKA displays partial phosphoryl transfer of AMP-PNP onto a substrate peptide. A. The overall 1.55 Å PKA structure,4HPU, is displayed in cartoon representation with the small lobe (12−126) colored white, large lobe (127−350) colored olive, SP20 colored red, P-site serine and ANP-PNP shown in stick representation and colored by element, and magnesium ions shown as spheres and colored blue. **B**. The $2F_o - F_c$ electron density map contoured to 1 σ is displayed showing partial phosphoryl transfer and partial intact AMP-PNP. The structure is modeled with 45% phosphoryl transfer, 55% reactants. **C**. The same density as in B with the free phosphate from 1RDQ (Yang et al., 2004) displayed in gray to illustrate that the electron density corresponds to phosphoryl transfer and not hydrolyzed, free phosphate.

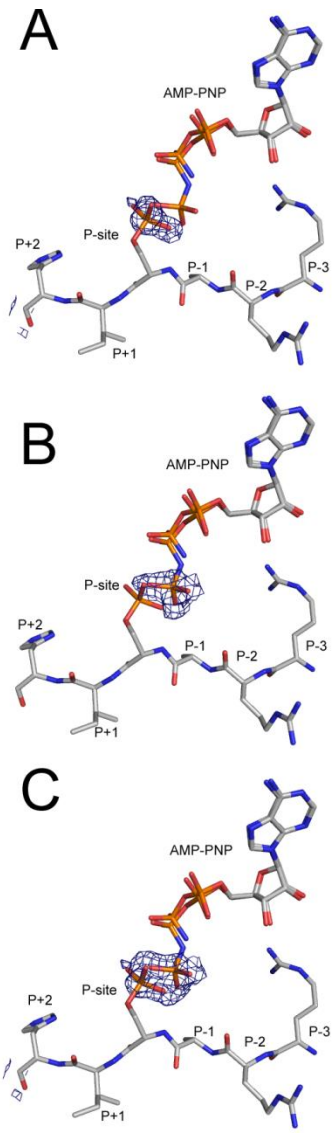

Figure 4.2. Partial phosphoryl transfer is further verified with $F_o - F_c$ maps with different components omitted. The $F_o - F_c$ electron density maps contoured to 3σ are shown when AMP-PNP and no phosphoryl transfer are modeled (**A**); when complete phosphoryl transfer to the P-site serine and ADP are modeled (**B**); and when no phosphoryl transfer and ADP are modeled (**C**). When either P-site phosphorylation (A) or the γ-phosphate of AMP-PNP (B) are excluded from the model, the electron density map clearly shows positive electron density that corresponds to each phosphate group. This finding is also confirmed when both P-site Ser phosphorylation and the γ-phosphate of AMP-PNP are excluded from the model (C).

for both phosphoryl transfer and the γ-phosphate of AMP-PNP (**Fig. 4.2B**). To further confirm the presence of phosphoryl transfer and to ensure that the transfer was present in the crystal and not a result of radiation damage on the X-ray beam, protein crystals were harvested, washed thoroughly, and analyzed by mass spectrometry. Mass spectrometry confirmed the presence of both phosphorylated and unphosphorylated SP20 within the crystal (**Fig. 4.3, Table 4.2**) verifying the results from the crystal structure.

To further verify that AMP-PNP can be utilized for phosphoryl transfer by the C-subunit, the C-subunit was incubated with AMP-PNP and RIIβ *in vitro*. RIIβ contains a C-subunit phosphorylation site at its inhibitor site (Zhang et al., 2012). Phosphorylation of RIIβ with AMP-PNP was monitored by Western blot analysis using an antibody against the phosphorylated PKA substrate. AMP-PNP promoted the phosphorylation of RIIβ in a time-dependent manner, albeit very slowly (**Fig. 4.4**). However, the transfer appears to occur much more quickly with RIIβ in solution than it did with SP20 in the crystallization conditions yielding about 80% transfer compared to ATP after 2 days. The different rates may be due to the different conditions used for crystallization such as different pH values, pH 8.0 during crystallization versus pH 7.0 in solution, and the presence of MPD and methanol during crystallization, which are all likely to affect the transfer rate. It is also possible that RIIβ is phosphorylated with AMP-PNP more readily than SP20. Additionally, turnover may proceed more slowly in a crystalline state, once the protein crystallizes, than in solution due to conformational constriction. However, both the

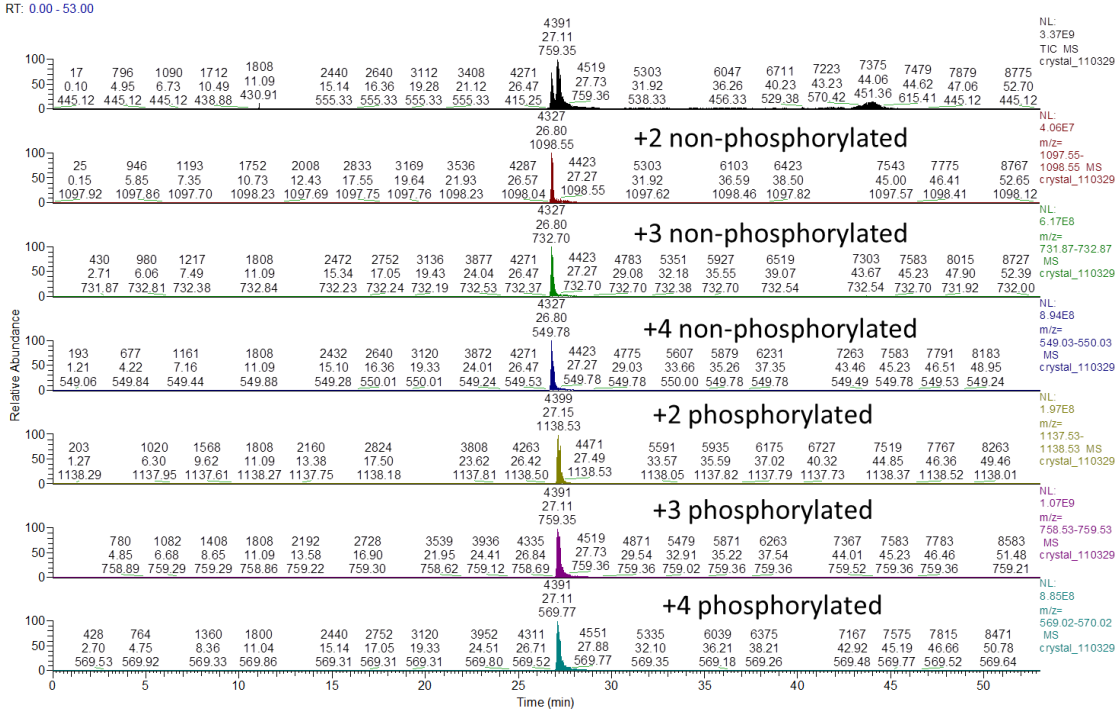

Figure 4.3. Mass spectrometry analysis of peptide from the protein crystal shows the presence of both phosphorylated and unphosphorylated peptide confirming the results from the crystal structure. See **Table 4.2** for more information.

Table 4.2. Theoretical and experimental masses (Da/mol) of phosphorylated and unphosphorylated SP20 peptide from the analyzed protein crystals. Masses listed are in Da/mol. pS: phosphorylated serine

Peptide	TTYADFIASGRTGRRASIHD		TTYADFIASGRTGRRA**pS**IHD	
Charge	**Theoretical Mass**	**Experimental Mass**	**Theoretical Mass**	**Experimental Mass**
+2	1098.05	1098.55	1138.03	1138.53
+3	732.37	732.70	759.03	759.35
+4	549.53	549.78	569.52	569.77

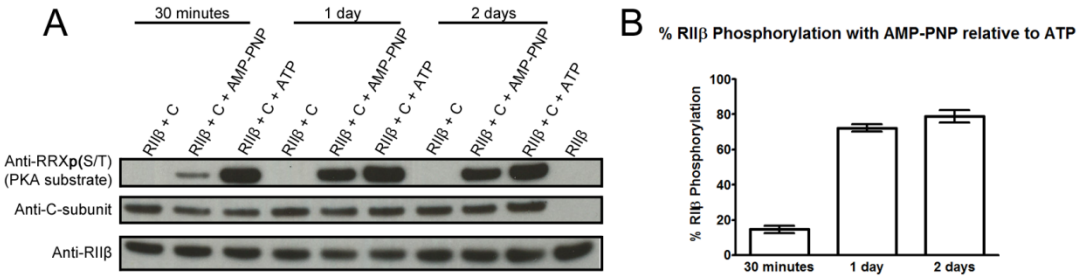

Figure 4.4. The C-subunit phosphorylates RIIβ using AMP-PNP in a time-dependent manner *in vitro*. A. Shown is a representative Western blot from three replicate experiments where the C-subunit (abbreviated C in the figure) was incubated with RIIβ alone, with RIIβ and AMP-PNP, or with RIIβ and ATP, and the phosphorylation status of RIIβ was monitored at 30 minutes, 1 day, and 2 days. The starting RIIβ sample is shown in the last lane showing no phosphorylation before incubation with C-subunit and nucleotide. Also, no phosphorylation was observed when the C-subunit and RIIβ were incubated without nucleotide suggesting that it is not ATP contamination of either protein sample that contributes to RIIβ phosphorylation. Finally, the sample with AMP-PNP shows clear phosphorylation of RIIβ that increases over time. **B**. A quantification of the Western blots showing average RIIβ phosphorylation at each time point with AMP-PNP compared to ATP and normalized by total RIIβ in each sample from the three replicate experiments. Error bars represent SEM from the three replicate experiments.

crystal structure and solution studies show that the C-subunit can utilize AMP-PNP for phosphoryl transfer but at a much slower rate than with ATP.

2.15 Å Structure Displays Complete Phosphoryl Transfer of AMP-PNP.

The 1.55 Å crystal structure was of the myristylated WT protein and shows strong density for 10 of the 14 carbon atoms of myristic acid. To test whether phosphoryl transfer was a result of myristylation and whether phosphoryl transfer increases over time in the crystal as it does in solution (**Fig. 4.4**), the nonmyristylated WT protein was crystallized and data were collected on a crystal approximately 5 months after initial appearance compared to 3 months after crystal appearance for the 1.55 Å structure. This structure was refined to 2.15 Å resolution and displays complete phosphoryl transfer.

The electron density map of the phosphorylation site shows density for phosphoryl transfer with no density for an intact γ-phosphate on AMP-PNP (**Fig. 4.5A**). Also, again, the density corresponds to phosphoryl transfer and not hydrolysis as seen in 1RDQ (Yang et al., 2004) (**Fig. 4.5B**). To further confirm complete phosphoryl transfer, the crystal structure was refined using a model without P-site serine phosphorylation and with ADP modeled in the active site. The resulting Fo − Fc electron density map from this structure is shown in **Fig. 4.5C**. This map only shows positive electron density for phosphoryl transfer with no density for the γ-phosphate of AMP-PNP confirming complete phosphoryl transfer. An important note is that the 2.15 Å structure is modeled with 70% phosphoryl transfer because, despite the lack of density for the γ-phosphate of AMP-PNP, there was some negative density at the

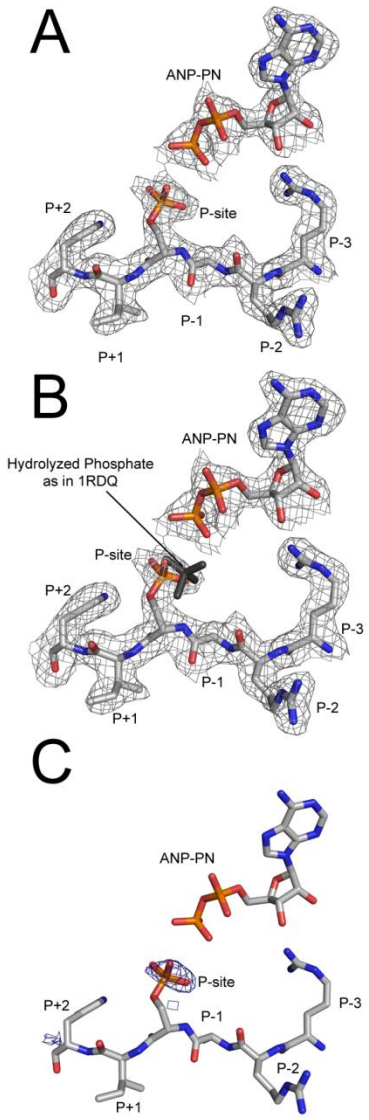

Figure 4.5. The 2.15 Å crystal structure displays complete phosphoryl transfer of AMP-PNP onto the substrate peptide. A. The $2F_o - F_c$ electron density map at 1σ is displayed for 4HPT showing electron density for complete phosphoryl transfer. **B**. The hydrolyzed phosphate from 1RDQ (Yang et al., 2004) is aligned with this structure and colored gray showing that the electron density corresponds to phosphoryl transfer and not hydrolyzed phosphate. **C**. The $F_o - F_c$ electron density map generated from a model with ADP and no phosphoryl transfer modeled in the structure is displayed at 3σ showing positive electron density for phosphoryl transfer with no density for the γ-phosphate of AMP-PNP.

phosphoryl transfer site with full transfer modeled, which may arise from AMP-PNP that hydrolyzed prior to crystallization or hydrolyzed without transfer.

Changes in the Magnesium Ions with Partial versus Complete Phosphoryl Transfer.

Alignment of the two structures shows mostly overlap between the P-site residues within each structure. However, one interesting difference between the two structures involves the magnesium ions. In the 2.15 Å structure, which has undergone complete phosphoryl transfer, Mg1 is partially, if not completely, absent from the active site. Mg1 is modeled into the structure, but there is much less electron density for Mg1 than typically seen for magnesium ions and much less density compared to the 1.55 Å structure (**Fig. 4.6**). Correspondingly, Mg1 also has much higher B-factors than typically seen for magnesium or manganese ions in PKA structures (**Table 4.3**), and the increased B-factor values are only seen for Mg1 and not Mg2, which indicates that it is not partial loss of both ions but only Mg1. Additionally, Mg1 is moved away from Asp184 compared to most structures (**Table 4.3**), which is not typical for Mg1 and occurs without equivalent changes in Mg2. These findings suggest that Mg1 was partially expelled from the active site following phosphoryl transfer or may have been completely expelled and replaced by a water molecule. The structure was modeled with a magnesium ion because it is potentially coordinated with six elements, as would be expected for a magnesium ion, but likely represents either partial occupancy of this site with Mg1 or may result from complete loss of this ion and replacement with a water molecule.

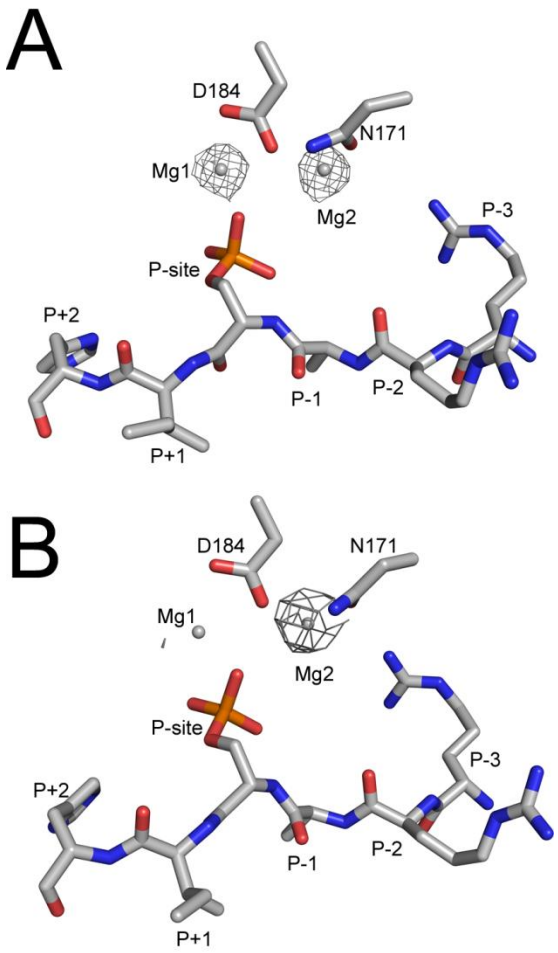

Figure 4.6. Mg1 is expelled from the active site following complete phosphoryl transfer. The $2F_o - F_c$ electron density map at 2σ is displayed for the magnesium ions in the 1.55 Å, partial phosphoryl transfer structure, 4HPU (**A**), and in the 2.15 Å, complete phosphoryl transfer structure, 4HPT (**B**). There is much less electron density for Mg1 than typically seen for magnesium ions in the 2.15 Å complete phosphoryl transfer structure which indicates partial, if not complete, loss of this magnesium ion.

Table 4.3. Summary of Mg (or Mn) B-factor ratios and coordination distances from several PKA structures. 2 – (Madhusudan et al., 2002); 3 – (Zheng et al., 1993c); 4 - (Bossemeyer et al., 1993); 5 - (Yang et al., 2004); 6 – (Kim et al., 2007); 7 – (Brown et al., 2009); 8 – (Yang et al., 2012); 9 – (Bastidas et al., 2012).

	B Factor Ratios		Distance to Asp184 (Å)
PDB ID	**Mg2:All Residues**	**Mg1:All Residues**	**Mg/Mn1-D184**
4HPU	0.44	0.68	2.26/2.28
4HPT	0.62	1.64	2.51/2.74
1L3R[2]	0.54	0.77	2.21/2.32
1ATP[3]	0.57	0.64	2.19/2.35
1CDK[4]	0.50	0.60	1.99/2.11
1RDQ[5]	0.53	0.61	2.20/2.23
2QCS[6]	0.76	0.84	2.32/2.40
3IDB[7]	0.60	0.60	2.34/2.37
3QAL[8]	0.43	0.57	2.19/2.21
3QAM[8]	0.59	0.78	2.08/2.19
4DFX[9]	0.45	0.52	2.21/2.23
4DG0[9]	0.66	0.81	2.34/2.38

Another interesting aspect of these structures is the coordination of the magnesium ions. In the 2.15 Å structure, Mg2 recruits a new water molecule to maintain an octahedral geometry following transfer of the γ-phosphate (**Fig. 4.7 A-B**). Also, this recruited water molecule is present in the 1.55 Å crystal structure that shows partial phosphoryl transfer. Initially there was positive electron density in the 1.55 Å structure near the γ-phosphate that could not be explained, but the 2.15 Å structure helped identify this density as corresponding to this water molecule that is recruited following phosphoryl transfer to maintain an octahedral coordination geometry of Mg2 (**Fig. 4.7C**). Therefore, these results exemplify the strong binding character of Mg2, which supports its role in phosphoryl transfer, as it immediately binds an additional water molecule following phosphoryl transfer. In contrast, Mg1 is partially, if not completely, removed from the active site following phosphoryl transfer despite the fact that this ion should presumably be able to bind since all elements are present for it to maintain similar binding as in the intact AMP-PNP state (**Fig. 4.7 A, C**). Despite transfer of the γ-phosphate, Mg1 should still be able to coordinate with the transferred phosphate and all five other Mg1 binding elements still remain. Also, previous biochemical studies suggested that Mg1 and Mg2 bind with equal affinity with ADP (Armstrong et al., 1979).

4.4 Discussion

By using a substrate version of IP20, which has a much slower off-rate than other peptide substrates, we were able to capture the phosphoryl transfer step in the crystal lattice. The slow off-rate of SP20 may have facilitated the transfer, even with

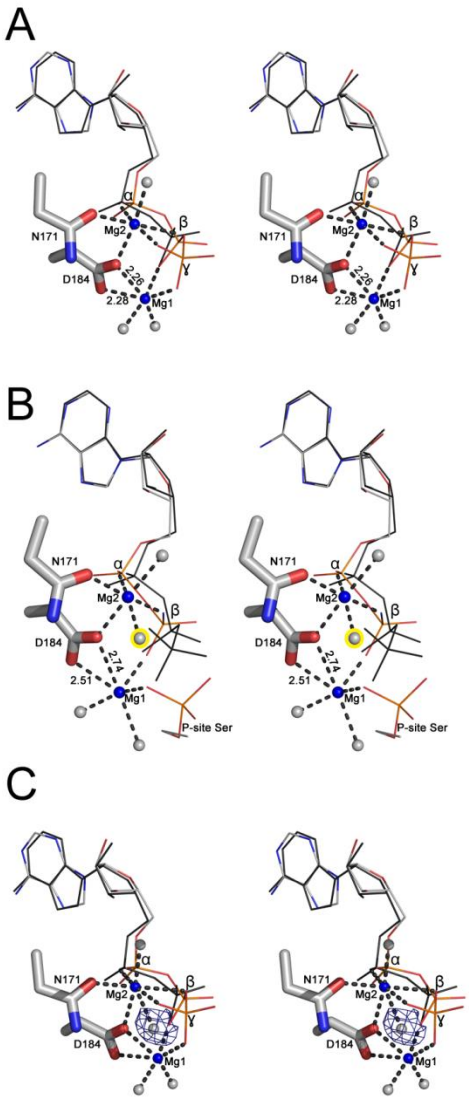

Figure 4.7. Coordination of the magnesium ions before and after phosphoryl transfer. A. A stereoview of the magnesium ions in the 1.55 Å partial phosphoryl transfer structure is displayed. AMP-PNP is colored by element, AMP-PN (without γ-phosphate) is colored black, water molecules are colored gray, and magnesium ions are colored blue. The distances between Asp184 and Mg1 are shown in angstroms. **B**. A stereoview of the magnesium ions in the 2.15 Å complete phosphoryl transfer structure is shown. The AMP-PN from the structure is colored by element, water molecules are colored gray, magnesium ions are colored blue, and AMP-PNP from the 1.55 Å partial phosphoryl transfer structure is aligned and shown in black. Mg2 recruits an additional water molecule that fulfills the vacancy left after transfer of the γ-phosphate highlighted in yellow. **C**. Coloring is the same as in panel A. The $F_o - F_c$ electron density map at 3σ is shown in blue for the area near the new water molecule recruited by Mg2 following phosphoryl transfer in the 1.55 Å partial phosphoryl transfer structure.

AMP-PNP, and the retention of both products. The substrate complex with SP20 solved earlier showed how the Gly-rich loop is perturbed in a minimal way when the P-site Ala is replaced by Ser (Bastidas et al., 2012), and a similar shift was observed in the Gly-rich loop with the RIIβ subunit bound (Brown et al., 2009), which is also a substrate (**Fig. 4.8A-B**). The glycine-rich loop clearly senses what is present at the P-site. The loop changes a bit more following complete transfer of the phosphate to SP20, but the changes are minimal. The fact that neither the backbone geometry nor the temperature factors for the peptide change significantly when SP20 is phosphorylated suggests that both products are trapped. This may be unique to the SP20 structure, which binds with such high affinity and docks to an important hydrophobic groove near the active site. Despite extensive structural, computational, and biochemical studies of PKA, there is still uncertainty and debate about the mechanistic details of catalysis and, in particular, about the roles of the essential magnesium ions in phosphoryl transfer and the steps involved in the rate-limiting step of ADP release. The structures described here allowed us to characterize the reaction progression by PKA. By trapping both products in the crystal lattice we have an opportunity to dissect these critical events in the catalytic process. We obtained one of the highest resolution WT PKA structures to date, which displays 45% phosphoryl transfer. Without these conditions that yield slow phosphoryl transfer of AMP-PNP, it would be difficult to obtain a structure displaying partial phosphoryl transfer. This phosphoryl transfer midpoint structure and the end point 2.15 Å crystal structure displaying complete phosphoryl transfer allowed us to explore in new ways the PKA phosphoryl transfer reaction steps and the roles of the two magnesium ions.

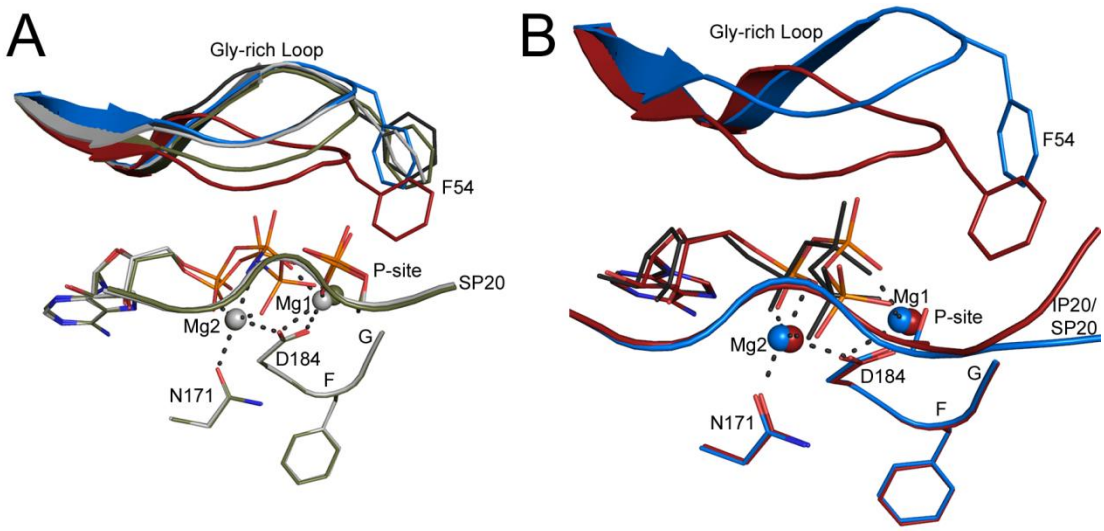

Figure 4.8. Changes in the Gly-rich loop with substrates bound and following phosphoryl transfer. A. The Gly-rich loop is slightly raised in the structures reported here, full transfer (4HPT) depicted in olive and partial transfer (4HPU) depicted in gray, compared to the fully closed structure typically observed with ATP and IP20 (depicted in red from PDB: 3FJQ (Thompson et al., 2009)). The raised loop may result from the presence of a serine rather than alanine residue at the P-site as evident from previous C-subunit structures containing a substrate bound at the active site such as SP20 (depicted in blue from PDB: 4DG0 (Bastidas et al., 2012)) and RIIβ(108−268) (depicted in black from PDB: 3IDB (Brown et al., 2009)). **B**. 4DG0 and 3FJQ are depicted in the same colors as panel A with ATP from 3FJQ colored by element and AMP-PNP from 4DG0 colored black. This alignment highlights that the raised Gly-rich loop may be the result of substrate binding alone and not phosphoryl transfer since 4DG0 which was bound to SP20 but exhibited no phosphoryl transfer also has a raised Gly-rich loop.

We find that Mg2 recruits a water molecule immediately following phosphoryl transfer to maintain an octahedral coordination state. This recruited water molecule is present in both the partial phosphoryl transfer and complete phosphoryl transfer structures due most likely to the strong binding character of Mg2, which may help to catalyze the phosphoryl transfer reaction and/or stabilize the transition state. Additionally, we find that Mg1 is partially, if not completely, expelled following phosphoryl transfer, which implies that it may not bind as strongly and possibly may not influence the active site as much as Mg2. There is no obvious reason why Mg1 should be expelled following phosphoryl transfer since six binding partners of Mg1 are still present. Also, this finding contradicts previous reports that suggested that Mg1 and Mg2 bind with equal affinity with ADP (Armstrong et al., 1979). The concentration of magnesium in the crystal drop is approximately 2.5 mM. This is a relatively high concentration that is much higher than typical physiological concentrations (Kovalevsky et al., 2012; Shaffer and Adams, 1999a) and would, presumably, allow for occupation of the Mg1 site if favorable. Therefore, this structure suggests that Mg1 may not bind as tightly as Mg2 following phosphoryl transfer. Indeed, the inhibitory effects of high magnesium concentrations may arise from occupation of both magnesium sites even after phosphoryl transfer, which may slow down the rate-limiting step of ADP release. This mode of magnesium inhibition was proposed previously (Adams and Taylor, 1993) and seems consistent with the implications of these crystal structures. The single caveat which may promote the release of Mg1 is that we used AMP-PNP instead of ATP, and the nitrogen atom could facilitate the release of Mg1.

Mg1 leaving the active site following phosphoryl transfer may help to answer the important question of how ADP release, the rate-limiting step at high magnesium concentration, is achieved. Computational studies performed to analyze how ADP is released from PKA when two magnesium ions are bound suggested that release was so energetically unfavorable that it would require local unfolding at the active site or large global conformation changes in the protein for release (Khavrutskii et al., 2009). Consequently, the authors argue that one or both magnesium ions may need to be expelled prior to ADP release. Based on the results described here, we propose that Mg1 is the ion that leaves following phosphoryl transfer and this would allow for ADP release.

The structures described here as well as previous crystal structures begin to elucidate the important aspects and steps involved in phosphoryl transfer (**Fig. 4.9**). An important recent result is the crystal structure of PKA obtained under low magnesium concentration, which shows electron density for only Mg2 (Kovalevsky et al., 2012). This structure suggests that Mg2 may bind within the active site first with ATP. It is possible that recognition of the Mg-ATP complex may involve shuttling between the negatively charged residues at the active site including Asp184 and Asp166. Based on the Kovalevsky structure, however, it appears that when Mg-ATP is docked stably into the active site cleft it binds preferentially to the Mg2 site between Asn171 and Asp184. The structures presented here suggest, furthermore, that Mg2 remains in the active site following phosphoryl transfer while Mg1 is expelled, at least in the presence of AMP-PNP. In addition, Mg2 recruits an additional water molecule following phosphoryl transfer to retain an octahedral coordination geometry

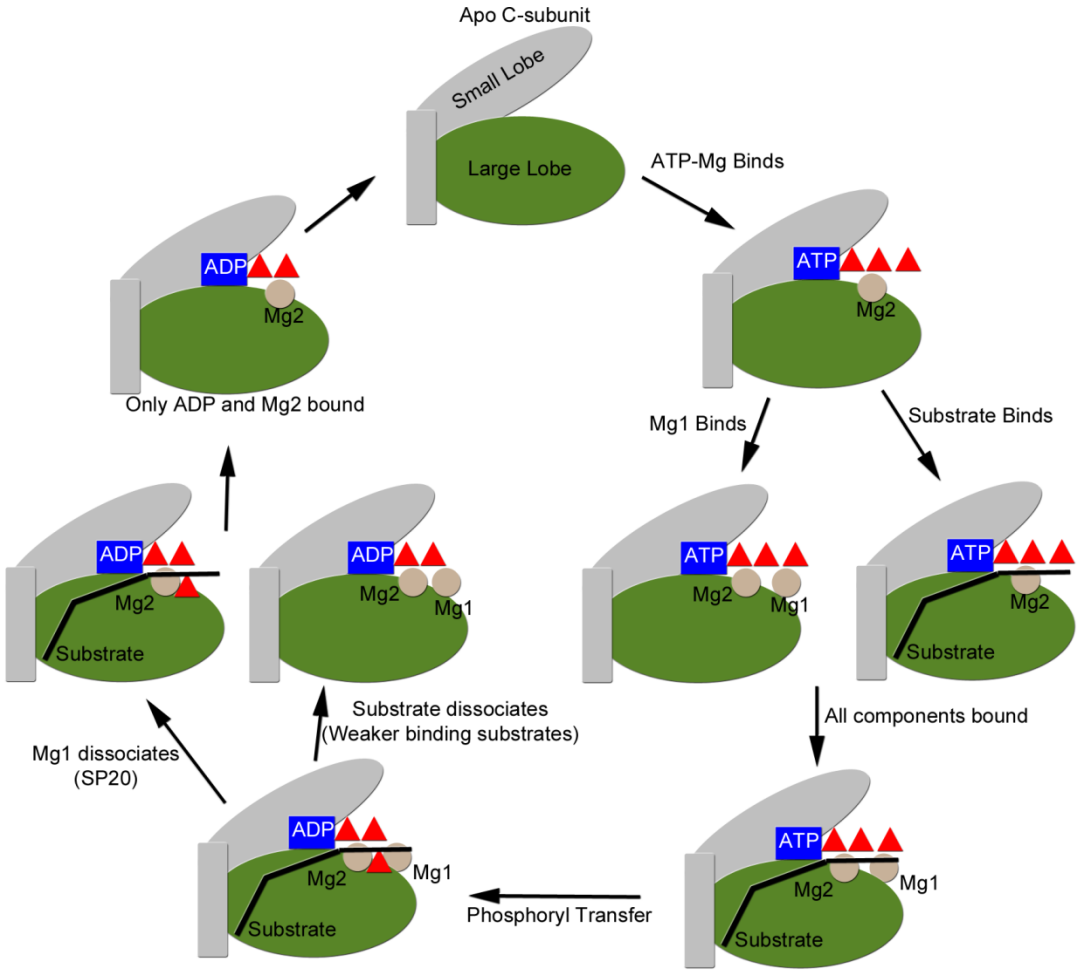

Figure 4.9. Catalytic cycle of PKA. A similar cycle is also predicted for CDK2 (Jacobsen et al., 2012).

(Fig. 4.7B). Taken together, these findings suggest that Mg2 may bind first and exhibits strong binding character. Mg1 helps to position the γ-phosphate of ATP for transfer but is expelled from the active site following phosphoryl transfer to allow for ADP release. ADP and Mg2 are likely to be the last entities remaining in the active site that are most likely released together or may remain until being replaced by another ATP and magnesium ion (**Fig. 4.9**). We cannot comment on the order of the addition of substrates but assume that in the cell with physiological substrates ATP-Mg2 will bind first and then either the peptide or Mg1. With the high affinity phosphorylated SP20 peptide and ADP, it is the Mg1 that is released first. Whether the phosphorylated substrate or the ADP-Mg2 is released next or whether they leave simultaneously is unknown. With physiological substrates, it is likely the phosphorylated protein that will leave first.

This mechanism of phosphoryl transfer progression and turnover may be a general pathway utilized by many, if not all, protein kinases. Given the highly conserved nature of the active site residues of protein kinases, in particular Asp184 of the "DFG" motif and Asp166 the "catalytic base," we predict that all kinases will likely utilize two metal ions, but the details of catalysis and product release may be regulated differently in different kinases. The DFG motif, for example, is highly regulated in many kinases, and it is serving as the "keeper" of Mg1 both positioning it for transfer and also facilitating its release. Recent crystal structures of cyclin dependent kinase 2 (CDK2) suggest a similar process of substrate turnover for this kinase (Jacobsen et al., 2012). Many previous CDK2 crystal structures bound to ATP or ATP-analogues displayed one magnesium ion within the active site, analogous to

Mg2 in PKA structures, suggesting initially that CDK2 may utilize a single metal ion for phosphoryl transfer. However, a crystal structure of a transition state mimic of CDK2 identified two magnesium ions in the active site which are analogous to Mg2 and Mg1 from PKA, and biochemical experiments suggested that the enzyme utilizes two magnesium ions during turnover (Bao et al., 2011). Furthermore, recent structures of CDK2 bound to ADP showed the presence of one or two magnesium ions (Mg2 or Mg1 and Mg2) bound with ADP (Jacobsen et al., 2012). Therefore, these studies independently identified a similar mode of phosphoryl transfer progression in CDK2. The authors also argue that CDK2 binds Mg2 first, but Mg1 must also bind for optimal turnover. After phosphoryl transfer, having two magnesium ions bound to ADP slows product release resulting in a decrease in turnover rate at high magnesium concentration in CDK2 as is also seen in PKA. Based on the two structures of CDK2 bound to ADP, it appears that Mg1 binds less tightly following phosphoryl transfer which then allows for ADP release. Therefore, the findings from our PKA phosphoryl transfer structures may present a general mechanism utilized by many, if not all, protein kinases. Additionally, the structures described here trapped the enzyme at different steps during phosphoryl transfer and trapped both products. The results from these structures are thus likely to represent steps in the reaction progression and are not affected by crystallization soaking conditions that may have yielded the magnesium differences in the CDK2 structures.

The catalytic mechanism of protein kinases, like the roles of the magnesium ions, remains unresolved. There are two mechanisms proposed for phosphoryl transfer by protein kinases which are an associative mechanism and a dissociation mechanism

(Bao et al., 2011; Cheng et al., 2005; Madhusudan et al., 2002; Valiev et al., 2003; Valiev et al., 2007). The main differences between these mechanisms are the transition states and which group accepts the hydrogen atom from the substrate residue. The associative mechanism forms a trigonal bipyramidal transition state with a −3 charge where bond formation with the substrate serine begins before the bond between the β- and γ-phosphate is completely broken, and the proton on the substrate residue is accepted by the incoming γ-phosphate. The dissociative mechanism involves a complete break in the leaving group yielding a metaphosphate with −1 charge, and the conserved aspartate residue, Asp166 in PKA, acts as a catalytic base that accepts the proton from the substrate residue. There has been some debate about the mode of phosphoryl transfer, but the majority of recent studies suggest a dissociative mechanism (Cheng et al., 2005; Valiev et al., 2003; Valiev et al., 2007).

The crystal structures reported here depict the starting point and end point of the phosphoryl transfer reaction and do not represent a transition state, which makes it difficult to make conclusions about the mechanism of phosphoryl transfer. However, there is a PKA transition state mimic structure (Madhusudan et al., 2002) and CDK2 transition state mimic structure (Bao et al., 2011), and when comparing the structures reported here with the transition state structures, some insights may be gleaned about the mechanism of phosphoryl transfer. First of all, the residues at the active site in these phosphoryl transfer structures are very similar to the transition state PKA structure except for the raised Gly-rich loop in these structures (**Fig. 4.8**). However, there are a couple of interesting differences between these structures and the transition state mimic. The biggest difference between these structures and the transition state

mimic, 1L3R (Madhusudan et al., 2002), is the orientation of the substrate serine, Ser21 in the peptide, and the position of Asp166, the putative catalytic base (**Fig. 4.10A-B**). In the transition state mimic structure, the substrate serine is facing Asp166 forming a hydrogen bond with this residue, and in this state, the serine residue is primed for an in-line transfer of the phosphate. By contrast, in these phosphoryl transfer structures the serine residue is flipped away from Asp166 (**Fig. 4.10A-B**).

It could be argued that this flip occurs following phosphoryl transfer as a means to initiate substrate release by, for instance, forcing the Gly-rich loop to rise because this conformation would clash with Phe54 in the fully closed state (**Fig. 4.10A-B**). However, several previous kinase structures bound to the substrate and AMP-PNP showed that the substrate serine residue is flipped away from Asp166 before phosphoryl transfer occurs. In previous structures of the C-subunit bound to SP20 and AMP-PNP without phosphoryl transfer, Ser21 is pointed away from Asp166 (Bastidas et al., 2012) (**Fig. 4.10C**). Additionally, a structure of the C-subunit bound to AMP-PNP and a truncated form of RIIβ, which is a substrate for the C-subunit, also showed the P-site serine facing away from Asp166 (Brown et al., 2009) (**Fig. 4.10C**). Finally, a structure of Akt/PKB bound to a substrate and AMP-PNP also adopted this conformation with the serine residue facing away from the aspartate residue (Yang et al., 2002) (**Fig. 4.10C**). Therefore, this conformation of the substrate residue may precede phosphoryl transfer. However, in the CDK2 (Bao et al., 2011) and PKA (Madhusudan et al., 2002) transition state mimic structures, the substrate residue is facing the putative catalytic base aspartate residue (**Fig. 4.10D**).

The positioning of the serine residue away from Asp166 would seem to

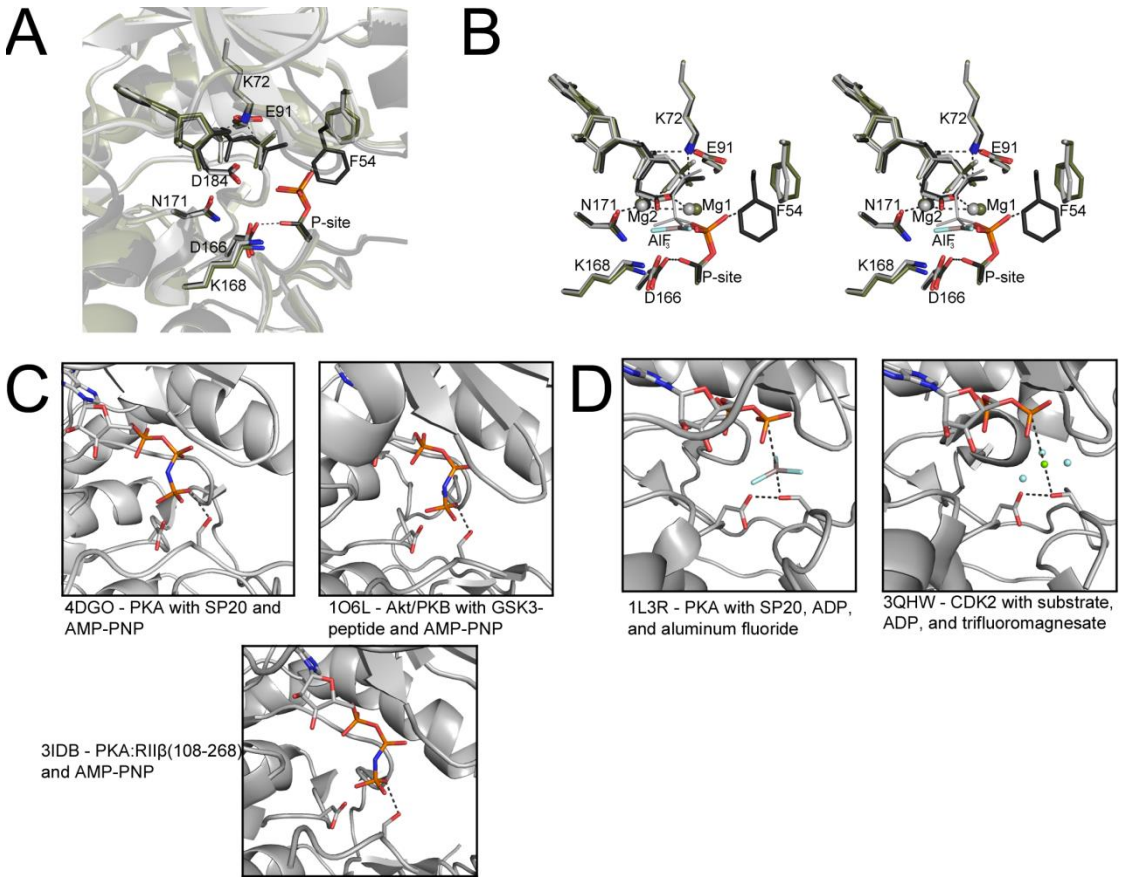

Figure 4.10. Differences between the phosphoryl transfer structures and transition state mimic structure. A. The PKA transition state mimic structure, 1L3R (Madhusudan et al., 2002), is colored black. The partial phosphoryl transfer structure, 4HPU, is colored gray, and the full transfer structure, 4HPT, is colored olive. The protein is shown in transparent cartoon representation and important active site residues are shown in stick representation. The position of Asp166 and the P-site serine is the major difference between the phosphoryl transfer and transition state mimic structures. **B**. A stereo view of the active site residues with the transition state C-subunit structure and phosphoryl transfer structures colored as in (A). **C**. The P-site serine is positioned away from Asp166, the putative catalytic base, in the phosphoryl transfer structures, but this position is present even before transfer as evident from at least three previous structures of PKA (Bastidas et al., 2012; Brown et al., 2009) and Akt/PKB (Yang et al., 2002) bound to a substrate and AMP-PNP. These three structures are displayed with the P-site residue, AMP-PNP, and the conserved aspartate residue shown in stick representation. **D**. Two transition state structures of PKA, 1L3R, and CDK2, 3QHW (Bao et al., 2011), show the P-site residue facing the conserved aspartate. The P-site residue and aspartate residue are shown in stick representation along with ADP and AlF_3, and MgF_3 is shown in sphere representation. This positioning supports the possible role of the aspartate residue as a catalytic base and supports late transfer of the hydrogen atom from the substrate.

contradict the favored dissociative mechanism because the residue is not facing the catalytic base. However, computational studies addressing the mechanism of phosphoryl transfer suggested that the potential hydrogen bond between Asp166 and the substrate residue is actually quite weak in the reactant state and becomes very strong only during the transition state (Valiev et al., 2007). It is not until late in the reaction that Asp166 accepts the proton from the substrate residue. Therefore, these structures may support this mode of reaction progression. It appears that Asp166 does not yield a strong effect on the substrate residue in the reactant state, which may be why the substrate serine is facing away from the aspartate residue to hydrogen bond with an oxygen atom on the γ-phosphate rather than with the aspartate residue (**Fig. 4.10C**). However, following the bond break between the β- and γ-phosphates, Asp166 may exhibit much stronger interactions with the substrate serine which could explain why the substrate then shifts toward the aspartate residue as seen in the PKA and CDK2 transition state mimic structures (**Fig. 4.10D**). Finally, following phosphoryl transfer, these structures suggest that the P-site residue once again flips away from the aspartate residue, which may promote substrate release. Therefore, while the crystal structures reported here do not yield direct evidence of the mechanism of phosphoryl transfer, the structures are consistent with previous computational predictions (Valiev et al., 2007) suggesting a dissociative mechanism where the proton on the substrate residue is accepted late in the reaction.

If a dissociative mechanism does govern phosphoryl transfer, then this may have implications for the findings from these phosphoryl transfer structures. Namely, with a dissociative mechanism it is likely to be the stabilization of the leaving group

that dominates the reaction energetics. It is possible that this could alter the requirements of the magnesium ions because of the use of AMP-PNP rather than ATP, and we should be cautious to make conclusions about the mechanism of reaction progression when using an unnatural ligand. However, a dissociative mechanism involves the formation of a metaphosphate transition state, which would be the same whether the nucleotide is ATP or AMP-PNP. Therefore, the energetics of the transition state should not be altered with AMP-PNP, but it is possible that following phosphoryl transfer AMP-PN may not have the same magnesium requirements as ADP, which could influence magnesium ion binding. However, the similar findings obtained with CDK2 of ADP binding either one or two magnesium ions, with Mg1 being the ion that binds less tightly (Jacobsen et al., 2012), support the findings from this study and make it more likely that this does represent a step in reaction progress by protein kinases. Additionally, even if AMP-PN perhaps requires less magnesium ion stabilization thereby promoting the release of one ion, then this would still suggest that Mg1 is likely to be the ion that binds less tightly and is less important for ADP binding.

In summary, the findings presented here provide structural evidence for kinase catalyzed phosphoryl transfer of AMP-PNP. Because phosphoryl transfer occurred slowly in the protein crystals and because both products were captured in the crystal lattice, we were able to characterize a midpoint and end point in the phosphoryl transfer reaction. These structures provide direct evidence of the steps involved in phosphoryl transfer and yield important advancements in our understanding of kinase reaction progression and mechanism. We find that Mg2 is likely the first and last

magnesium ion present in the active site, while Mg1 is expelled following phosphoryl transfer which may be an important step that precedes ADP release. This sequence of events also appears to govern phosphoryl transfer in CDK2 (Jacobsen et al., 2012), and therefore, it may be a general mechanism for phosphoryl transfer progression in protein kinases that utilize two magnesium ions.

Chapter 4, in full, was published as Phosphoryl Transfer by Protein Kinase A is Captured in a Crystal Lattice. Bastidas AC, Deal MS, Steichen JM, Guo Y, Taylor SS. *JACS* 2013 Mar 27; 135(12):4788-4798. The dissertation author was the primary investigator and author of this work.

Chapter 5

Apo and ADP Bound Structures of Protein Kinase A Provide Insights Into the Mode of Kinase Product Turnover

5.1 Introduction

Protein kinases are an important family of enzymes that govern many signaling processes within cells by transferring the γ-phosphate of ATP onto a substrate protein. The addition of a phosphate group produces large and diverse effects on the modified proteins but is often associated with activating or inhibiting a cellular process. Because of the vast importance of protein kinases in cellular processes, dysfunctional kinase signaling can lead to several diseases including cancer (Manning et al., 2002). Therefore, protein kinases are important drug targets, and better understanding of kinase structure, function, and catalysis may yield advancements in drug targeting.

cAMP-dependent protein kinase also called protein kinase A (PKA) is one of the most well-studied protein kinases, and because of the high conservation of the protein kinase family, it serves as a model for all protein kinases (Johnson et al., 2001). Under non-activating conditions, PKA exists as a heterotetrameric holoenzyme complex composed of a regulatory (R) subunit dimer that binds and inhibits two catalytic (C) subunit monomers. PKA is activated by cAMP, which binds to the R-subunits releasing their inhibition of the C-subunits (Kim et al., 2007). Once released from R-subunit inhibition, the constitutively active C-subunits can phosphorylate target proteins in the cytoplasm and nucleus. The C-subunit of PKA was the first kinase structure solved (Knighton et al., 1991b). This structure identified the bilobal architecture shared by protein kinases. These lobes were termed the N-lobe (or small lobe) and C-lobe (or large lobe). Many subsequent crystal structures defined the wide range of conformations adopted by the dynamic protein kinases. The C-subunit

crystallized in several states termed “open,” “closed,” and “intermediate” based on the relative orientation of the N- and C-lobes. The open conformation adopts the largest distance between the N- and C-lobe and was observed with the apo C-subunit and with the C-subunit bound to an inhibitor peptide IP20 (Akamine et al., 2003; Karlsson et al., 1993; Zheng et al., 1993b). The closed conformation displays tight packing between the N-lobe and the C-lobe which causes a closing of the active site on the substrates, and this conformation is typically seen when the protein is crystallized with IP20 and ATP or ATP-analogues (Knighton et al., 1993; Yang et al., 2004; Zheng et al., 1993c). Finally, the intermediate conformation was observed when the C-subunit was crystallized with adenosine (Narayana et al., 1997). These crystal structures as well as NMR data (Masterson et al., 2011) demonstrate that the C-subunit adopts a wide range of conformations, and these dynamics and conformations could regulate enzyme activity.

The kinetics and phosphoryl transfer reaction by PKA are also well-characterized and improved understanding of kinase reaction progression (Adams, 2001). Pre-steady state and steady-state kinetics of PKA showed that phosphoryl transfer of the γ-phosphate of ATP onto the substrate is a very rapid event; it is other processes that govern the rate of the reaction. These rate-limiting steps are regulated by magnesium ion concentration (Adams and Taylor, 1993). Most protein kinases, including PKA, require magnesium to bind ATP and catalyze phosphoryl transfer. At low magnesium concentration (0.5 mM), PKA has a higher turnover rate than at high magnesium concentration (10 mM), and at the low magnesium concentration, the turnover rate is governed partially by ADP-release and partially by conformational

changes that occur before and after phosphoryl transfer (Lew et al., 1997; Shaffer and Adams, 1999a, b). At high magnesium ion concentrations, PKA reaction rate is governed only by ADP-release (Adams and Taylor, 1993; Cook et al., 1982; Khavrutskii et al., 2009). Therefore, ADP-release is one of the most important steps in PKA reaction turnover and is highly influenced by the magnesium ions.

PKA binds two magnesium ions, which were termed Mg1 and Mg2. Mg1 binds in a bidentate manner with Asp184 of the "DFG" motif as well as the β- and γ-phosphates of ATP. Mg2 coordinates with one oxygen atom of Asp184, with Asn171, and with the α- and γ-phosphates of ATP (Bossemeyer et al., 1993; Zheng et al., 1993a). Each magnesium ion also binds water molecules to fulfill an octahedral coordination state (Shaltiel et al., 1998). The nomenclature of these magnesium ions as Mg1 and Mg2 was made based on an older crystal structure that reported electron density for mostly one magnesium ion when the C-subunit was crystallized with a low concentration of magnesium (Zheng et al., 1993a). Therefore, this ion that showed more electron density was termed Mg1 because it was thought to bind first or more strongly with ATP, and the other ion was termed Mg2. Despite this nomenclature, recent studies suggest that it is possible that the magnesium ions were incorrectly named. Another crystal structure of the C-subunit obtained under low magnesium concentration shows electron density for only one magnesium ion, but the ion observed in the crystal structure corresponds to the Mg2 ion (Kovalevsky et al., 2012). Furthermore, other protein kinases such as CDK2 often crystallize with one magnesium ion, and the ion observed is analogous to Mg2 (Bao et al., 2011). Finally, separate crystal structure studies of reaction progression by PKA and CDK2 both

identify Mg2 as the ion that likely remains in the active site following phosphoryl transfer while Mg1 is lost, suggesting that Mg2 may be the more important and more stably bound ion (Bastidas et al., 2013a; Jacobsen et al., 2012). Also, loss of Mg1 may be an important part of the rate-limiting step of ADP-release and may explain the slower turnover rate at high magnesium concentration due to continued occupancy of both metal binding sites.

To further elucidate reaction progression by PKA and the conformations involved in reaction progression, we obtained the first crystal structure of the C-subunit bound only to ADP by soaking apo crystals with ADP and magnesium. No crystal structures of the C-subunit bound only to ATP or ADP were previously solved as the inhibitor peptide, IP20, is generally necessary to crystallize PKA with nucleotide. There is a structure of the C-subunit bound only to adenosine (Narayana et al., 1997). However, adenosine lacks the phosphate groups, and therefore, it lacks information about the magnesium ions and lacks information on reaction turnover since adenosine is not likely to be a naturally bound product. Here we report the apo structure of the C-subunit refined to 2.9 Å resolution, and the ADP bound structure refined to 3.5 Å resolution. The ADP bound structure supports previous findings that ADP binds with Mg2. Also, the ADP bound structure adopts a conformation that does not conform to the "open," "closed," or "intermediate" state, and therefore, the structure further defines the conformational flexibility of the protein and provides insights into the motions and mechanisms that may govern ADP-release.

5.2 Experimental Procedures

Purification of the myristylated C-subunit protein – The myristylated K7C C-subunit was prepared by co-expression with yeast NMT as described previously (Duronio et al., 1990) and purified following a method described previously (Bastidas et al., 2012). The K7C mutant was used for crystallization because it increases the yield of the myristylated protein. The myristylated protein was used for crystallization because the apo structure was initially obtained to characterize the role of N-myristylation in PKA structure.

Crystallization and ADP soaking – The apo myristylated K7C C-subunit crystallized under similar conditions utilized for the previous apo WT non-myristylated C-subunit structure (Akamine et al., 2003). The protein was dialyzed overnight into 50 mM bicine, 150 mM ammonium acetate, 10 mM DTT, pH 8.0. Then the protein was concentrated to approximately 8-10 mg/mL. The protein was setup for crystallization using the hanging drop vapor diffusion method at 4 °C. The protein was screened against different well solutions with 2-methyl-2,4-pentanediol (MPD) concentrations ranging from 2-18% and with 9-13% methanol added to the well solution immediately before sealing the well. The crystals were obtained using 8 µL drops of 1:1 volume of protein solution to well solution. Crystals typically appeared in 1-2 months, unlike the previous apo C-subunit structure which reported crystal appearance in 6-12 months (Akamine et al., 2003). The apo myristylated K7C C-subunit structure was obtained from a crystal grown with a well solution containing 8% MPD and 9% MeOH added to the well. The protein crystallized contained two sites of phosphorylation on Thr197 and Ser338.

Attempts to co-crystallize the C-subunit with ADP were unsuccessful. Therefore, in order to obtain an ADP bound structure, the apo crystals were soaked with ADP and $MgCl_2$. A solution of ADP and $MgCl_2$ was prepared in 0.1M Tris buffer at pH 7.0 and added to the crystal drop to yield a final drop concentration of approximately 5 mM ADP and 5 mM $MgCl_2$. The crystals were allowed to soak for 24-48 hours before being harvested and flash frozen. The structure reported here was obtained from a crystal soaked with ADP/$MgCl_2$ for 48 hours.

Data collection and refinement – The crystals were flash cooled in liquid nitrogen with cryoprotectant solution (16% MPD and 15% glycerol). Data was collected on the synchrotron beamline 8.2.1 of the Advanced Light Source, Lawrence Berkeley National Labs (Berkeley, California). The crystal structures were integrated using iMOSFLM (Battye et al., 2011). The protein crystallized in the $P2_1$ space group as with the previous apo structure. Molecular replacement was carried out using Phaser (McCoy et al., 2007) with the previously solved apo C-subunit structure PDB ID: 1J3H (Akamine et al., 2003) as a search model for the apo structure and with the apo structure solved here as the search model for the ADP bound structure. The refinement was performed using refmac5 (1994) and model building was done in Coot (Emsley and Cowtan, 2004). Refinement was performed using a TLS and restrained refinement along with non-crystallographic symmetry (NCS) restraints. The TLS groups and NCS restraints used corresponded to the small lobe (residues 10-126 and 327-350) and large lobe (residues 127-326). The apo and ADP bound structures were refined to R_{work}/R_{free} of 24.4%/29.2% and 22.7%/28.4% respectively. The data collection and refinement

statistics are shown in **Table 5.1** with Ramachandran values as defined in MolProbity (Davis et al., 2007).

PDB Deposition: The PDB and structure factors for the apo and ADP bound structures were deposited into the RCSB PDB with accession codes of 4NTS and 4NTT for the apo and ADP structures, respectively.

5.3 Results

Apo C-subunit structure.

The myristylated C-subunit of PKA was crystallized in an apo state because these studies were initially performed to characterize the role of N-myristylation on C-subunit structure, and a K7C mutant protein was utilized because it increases the yield of the myristylated protein (Bastidas et al., 2012). However, the apo crystal structure, refined to 2.9 Å resolution (**Table 5.1, Fig. 5.1A**), did not yield much information about N-myristylation. There is electron density for myristic acid in one of the two molecules in the asymmetric unit (ASU). However, there is only density for 4 of the 14 carbon atoms of myristic acid in the electron density (**Fig. 5.1B**). The lack of electron density for myristic acid implies that the myristic acid group binding within the hydrophobic pocket could be involved in forming a closed state since there is more electron density for the myristic acid group in structures that adopt a closed conformation compared to the open conformation adopted here in an apo state (Bastidas et al., 2012). The lack of density could also be due to lower resolution of the apo structure than the closed structures.

Table 5.1. Crystallography data collection and refinement statistics of apo and ADP bound structures. Data collection was performed at ALS laboratory in Berkeley, CA on beamline 8.2.1.
[a]Values in parenthesis correspond to the highest resolution shell. [b]5% of the data was excluded from the refinement to calculate the R_{free}. [c]Ramachandran plot quality as defined in MolProbity (Davis et al., 2007).

	Apo	**ADP bound**
PDB ID	4NTS	4NTT
Space group	$P2_1$	$P2_1$
Cell dimensions		
a (Å)	50.96	50.48
b (Å)	142.61	143.15
c (Å)	63.16	62.57
α, β, γ (°)	90, 103.61, 90	90, 103.61, 90
Unique reflections	19,014 (2,818)	10,660 (1,572)
Multiplicity	3.1 (3.1)	2.7 (2.7)
Resolution range (Å)	61.38-2.90 (3.06-2.90)[a]	32.15-3.50 (3.69-3.50)[a]
R_{merge} (%)	5.1 (44.1)	10.5 (48.6)
$I/\sigma I$	9.7 (2.1)	5.7 (2.4)
Completeness (%)	97.7 (99.0)	97.5 (98.4)
R_{work}/R_{free} (%)[b]	24.4/29.2	22.7/28.4
Ave.Temp. Factors (B factors) for all atoms ($Å^2$)	ChainA/ChainB	ChainA/ChainB
All residues	72.2/69.0	103.2/99.7
N-lobe (residues 1-126)	72.1/77.8	104.3/104.4
C-lobe (residues 127-300)	65.2/55.1	97.3/91.2
C-tail (residues 301-350)	96.2/96.6	121.4/118.5
Near FDDY (residues 320-335)	117.2/134.4	133.9/130.5
ADP	NA	161.8/124.2
Magnesium	NA	62.2/78.8
Ramachandran angles (%)[c]		
Favored regions	93.66	91.54
Allowed regions	100	100
r.m.s. deviations		
Bond lengths (Å)	0.006	0.007
Bond angles (°)	1.013	1.114

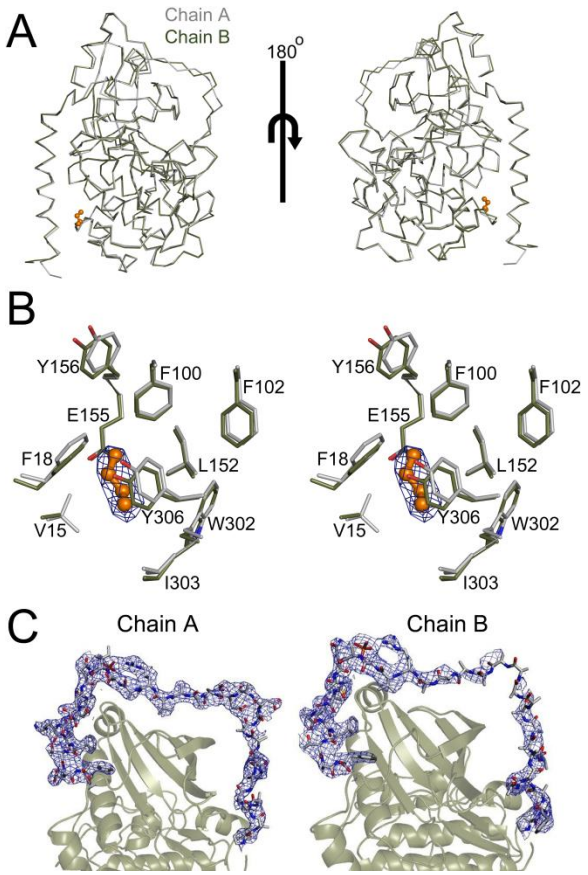

Figure 5.1. Apo structure of the catalytic subunit of PKA. A. The overall apo structure is displayed in ribbon representation with Chain A colored gray and Chain B colored olive and with Chain A and B aligned by the entire protein. **B**. A stereoview of the myristic acid binding pocket for Chain A and Chain B, which are colored as in A, is displayed along with the $2F_o$-F_c electron density at 1σ shown in blue for the myristic acid group from Chain A. There is no electron density for myristic acid in Chain B. **C**. The $2F_o$-F_c electron density at 1σ is shown in blue for the C-terminal tail of Chain A and Chain B.

The overall structure of the myristylated apo C-subunit reported here is in an open conformation similar to the previous WT non-myristylated apo structure (Akamine et al., 2003). There are two molecules in the ASU that are similar with an RMSD of 0.66 between ChainA and ChainB when aligned by the whole protein (**Fig. 5.1A**). The structure is very similar to the previous apo structure with a few small differences. For example, the Cys199 residue was modified with beta-mercaptoethanol in the previous apo structure and is unmodified in this structure. This caused some small shifts in the residues at the activation loop in the structure reported here compared to the previous structure, and the position of the residues in this structure are more likely to represent the native apo conformation. Modification of Cys199 renders the C-subunit inactive (Nelson and Taylor, 1981). Furthermore, the previous structure showed electron density for 2-methyl-2,4-pentanediol (MPD) in the myristic acid pocket, but since these structures used the myristylated protein, this did not occur in the structure reported here. Instead, there is electron density that corresponds to the myristic acid group in ChainA and no electron density in the myristic acid pocket in ChainB. Finally, the C-tail was not modeled in the previous apo structure due to lack of electron density. The electron density of the C-tail in this structure is also very poor with little density from about residues 318-330 in both molecules in the ASU, but the C-tail was modeled into the structure here. However, the C-tail is still not well resolved as evidenced from high B-factor values for the C-tail and seen in the electron density (**Table 5.1**, **Fig. 5.1C**). The C-tail was included but should be interpreted as showing the tentative location of the backbone of this region of the protein. Despite these small differences, the apo structure reported here and the previous structure are

generally very similar, and therefore, our analysis will focus on the new ADP bound structure because the apo structure was characterized and described in great detail previously (Akamine et al., 2003).

Overall ADP bound C-subunit Structure.

The ADP bound structure of the C-subunit was obtained by soaking apo crystals with Mg/ADP. The Mg/ADP structure was refined to 3.5 Å resolution (**Table 5.1**). The overall ADP bound structure is most similar to the apo structure with an RMSD of 0.74 between the apo and ADP bound structures aligned by the entire protein using both molecules in the ASU. Alignment of ChainA/ChainB from the ADP bound structure with a closed, ternary complex, 1RDQ (Yang et al., 2004), yields RMSD values of 1.7 for ChainA and 1.4 for ChainB, and alignment with an intermediate binary complex with adenosine, 1BKX (Narayana et al., 1997), yields RMSD values of 1.5 for ChainA and 1.3 for ChainB. The two molecules in the ASU of the ADP bound structure are similar to each other with RMSD values between ChainA and ChainB for the overall protein of 0.606. ADP and one magnesium ion are present in both molecules in the asymmetric unit (**Fig. 5.2**). The main differences between ChainA and ChainB occur at the Gly-rich loop and C-terminal tail.

As with the apo structure, the electron density of the C-terminal tail is not strong, but there is enough electron density to model the approximate location of the peptide backbone. Also, the C-terminal tail typically forms part of the binding pocket when the C-subunit is bound to nucleotide. In ChainB, there was some positive electron density in the region that Phe327 and Tyr330 typically occupy when bound to

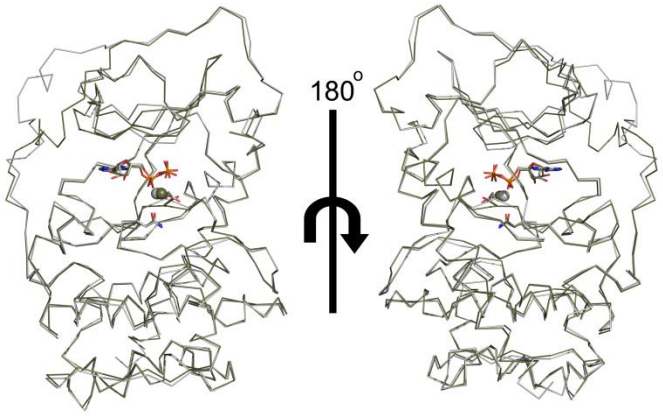

Figure 5.2. ADP bound structure of the C-subunit of PKA. The overall ADP bound structure of the C-subunit is displayed in ribbon representation with Chain A colored gray and Chain B colored olive, and the two molecules from the asymmetric unit are aligned by the entire protein. ADP from each molecule is displayed in stick representation and colored by element, Asn171 and Asp184 that bind to the magnesium are displayed in stick representation and colored by element, and the magnesium ion is colored by chain and displayed in sphere representation.

nucleotide without the C-tail modeled, and there is some electron density with the C-tail modeled with the residue side-chains at this location. Therefore, the side-chains of these amino acid residues are modeled in the structure for ChainB helping to bind ADP (**Fig. 5.3A**). In ChainA, the C-tail does not form part of the binding site, and this is due most likely to crystal packing which prevents the C-tail from forming part of the binding pocket due to close packing at the C-tail with a symmetry related molecule (**Fig. 5.3A-B**). Also, another difference between ChainA and ChainB is the conformation of the Gly-rich loop. Residues 50-53 are much lower in ChainA than ChainB, especially Ser53. It is possible that Ser53 helps to bind to ADP much more in ChainA than ChainB because of the lack of the C-tail forming part of the binding site (**Fig. 5.3C**).

ADP and one magnesium ion are present at the active site in both molecules in the ASU, and there is strong electron density to validate their presence (**Fig. 5.4**). Before ADP and magnesium were included in the structure, there was strong positive electron density for ADP/Mg in both molecules in the ASU, and the final electron density for ADP/Mg, as modeled, is convincing (**Fig. 5.4**). However, the electron density is better in ChainB than ChainA, and correspondingly, the B-factor values are higher for the ADP/Mg in ChainA than ChainB (**Table 1**). It is possible that the better electron density in ChainB is due to the fact that the C-tail can form part of the ADP binding pocket in ChainB but not ChainA. Therefore, this adds credence to the importance of these residues for binding to nucleotide, which was also verified with mutagenesis previously (Batkin et al., 2000) and with hydrogen-deuterium exchanged

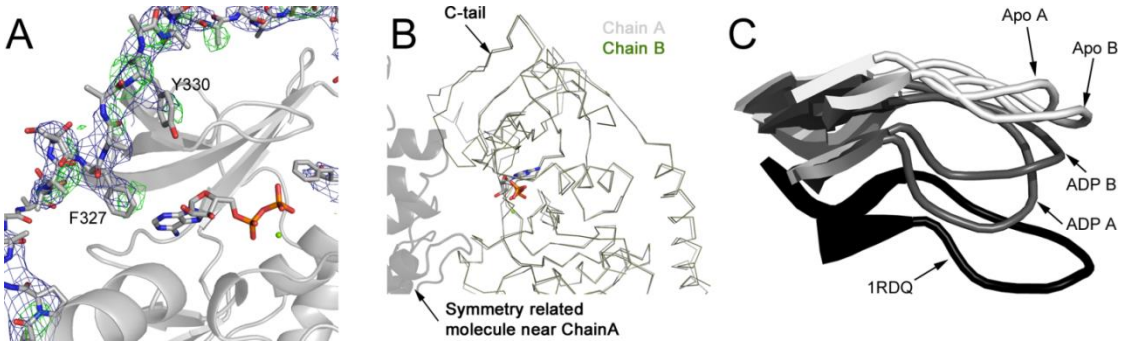

Figure 5.3. Changes at the C-terminal tail and Gly-rich loop in the ADP bound structure. A. The $2F_o$-F_c electron density at 1σ is displayed in blue for the C-terminal tail of Chain B from the ADP bound structure, and the resulting F_o-F_c electron density map contoured to 2.5σ is displayed in green for the C-tail from Chain B when the C-terminal tail is excluded from the final model of the structure. **B**. Chain A, gray, and Chain B, olive, are displayed is ribbon representation and aligned by the entire protein. A symmetry related molecule near the C-terminal tail of Chain A is displayed in black transparent cartoon representation showing that crystal packing prevents Chain A from adopting the C-tail conformation adopted by Chain B. **C**. The Apo structure, ADP bound structure, and a ternary structure, 1RDQ (Yang et al., 2004), were aligned by the entire protein, and the location of the Gly-rich loop from each structure following this alignment is displayed.

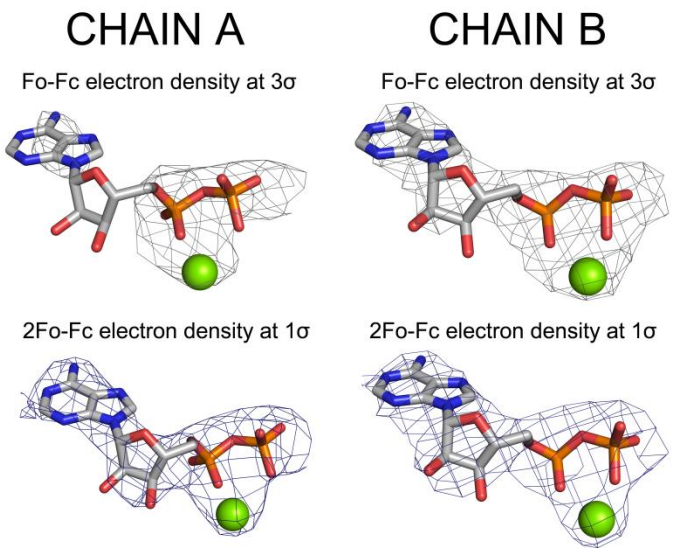

Figure 5.4. Electron density for ADP from each molecule in the asymmetric unit. The F_o-F_c electron density at 3σ from the first refinement of the ADP bound structure without ADP or magnesium modeled into the structure is displayed for Chain A and Chain B (top), and the $2F_o$-F_c electron density of the final model contoured to 1σ is displayed for each chain (bottom).

coupled to mass spectrometry measured with the C-subunit bound to ADP (Hyeon et al., 2009).

Despite binding to ADP, the C-subunit still adopts a largely open conformation. The Gly-rich loop is still raised much more than the closed state. The Gly-rich loop is, however, lowered compared to the apo state (**Fig. 5.5A-B**). Similarly, the C-terminal tail forms part of the binding site for ADP in ChainB, but the C-tail does not close down onto the active site to the same extent in the ADP bound structure as it does in the closed state as shown with 1RDQ (**Fig. 5.5A-B**). Therefore, the ADP bound structure adopts a conformation that does not conform to any of the previously identified states, open, closed, or intermediate. This fact is further illustrated by examining different distances between residues or regions of the protein that characterize the different states (**Table 5.2**). These distances are different in the ADP bound structure than in the open, closed, or intermediate states. Therefore, the ADP bound structure displays a new conformation of the C-subunit that could represent a conformation involved in ADP release.

Mg Binding Site and Implications on Reaction Progression:

There is only one magnesium ion present in the ADP bound structure unlike typical PKA ternary structures which display two magnesium ions at the active site (Yang et al., 2004). The magnesium ion at the active site in the ADP bound structure corresponds to Mg2. Although the location of the magnesium ion does not exactly match the typical position of Mg2, the magnesium ion is clearly situated between Asp184 and Asn171, which would correspond to the Mg2 ion (**Fig. 5.6A**). Also, to

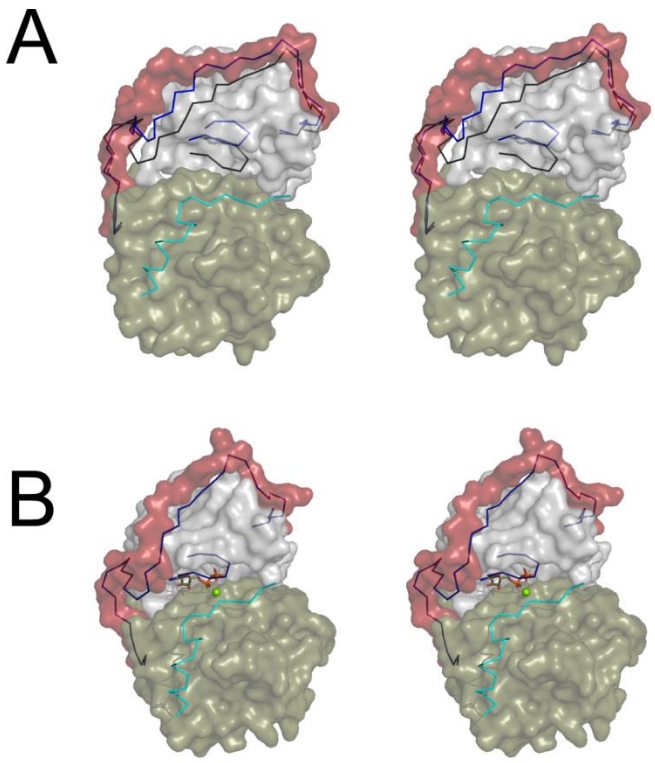

Figure 5.5. The ADP bound structure adopts a unique conformation. A. A stereoview of the apo structure reported here is displayed in surface representation with the N-lobe (residues 1-126) colored gray, large lobe (residues 127-300) colored olive, and C-tail (residues 301-350) colored red. Chain B from the ADP bound structure and a ternary structure, 1RDQ (Yang et al., 2004), are aligned with the apo structure by the entire protein. The C-tail and Gly-rich loop from the ADP bound structure is colored blue and shown in ribbon representation, and the C-tail and Gly-rich loop from the ternary structure are colored black and displayed in ribbon representation. The inhibitor peptide, IP20, from the ternary structure is colored cyan and shown in ribbon representation. **B**. A stereoview of Chain B from the ADP bound structure is displayed in surface representation with the regions of the protein colored as in A. The C-tail and Gly-rich loop from the ternary structure, 1RDQ, aligned with the ADP bound structure by the entire protein are shown in ribbon representation and colored blue. IP20 is depicted as in A.

Table 5.2. Distances within the C-subunit that define different conformations. Adapted from Johnson et al. (Johnson et al., 2001). 1 – Karlsson et al., 1993; 2 – Narayana et al., 1997; 3 – Zheng et al., 1993c; 4 – Knighton et al., 1993; 5 – Bossemeyer et al., 1993.

Conformation:	ADP bound (ChainA/B)	Open	Intermediate	Closed	Closed	Closed
Peptide	None	IP20	None	IP20	IP20	IP20
Nucleotide	ADP	None	Adenosine	ATP	none	AMP-PNP
PDB ID	4NTT	1CTP[1]	1BKX[2]	1ATP[3]	1APM[4]	1CDK[5]
His87-Thr197 (N-PO_4)	6.7/6.3	7.1	3.2	2.7	2.8	2.8
Glu170-Tyr330 (backbone C=O-OH)	NA/12.3	14.6	8.6	8.2	8.2	7.9

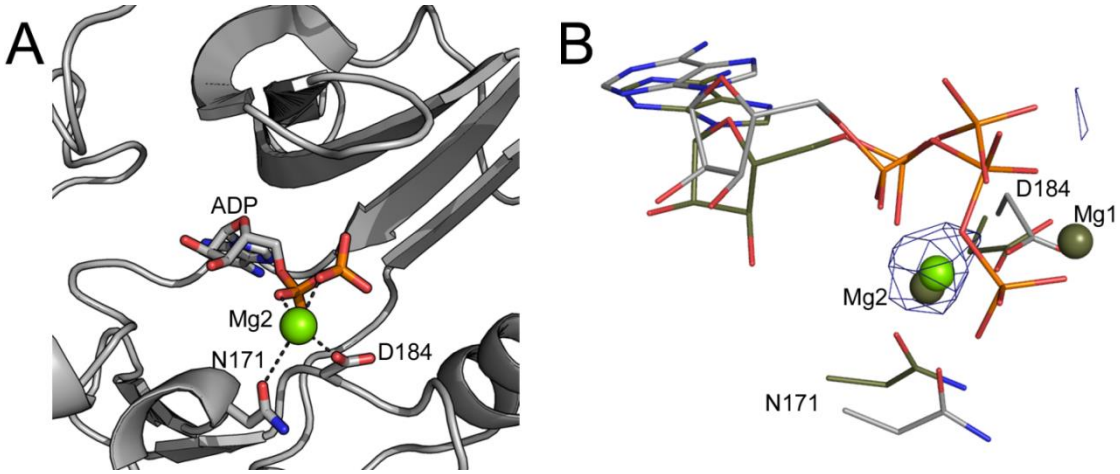

Figure 5.6. ADP binds at the active site with Mg2. A. The active site of Chain B from the ADP bound structure is displayed in cartoon representation with ADP displayed in stick representation and magnesium displayed in sphere representation. The side-chain of Asn171 and Asp184, which chelate the magnesium ions, are displayed in stick representation. **B**. The resulting F_o-F_c electron density map obtained by omitting the magnesium ion from the final ADP bound structure is displayed contoured to 3σ showing strong positive electron density at the Mg2 site with no density for the Mg1 site. The ternary structure, 1RDQ (Yang et al., 2004), colored olive was aligned by the entire protein to the ADP bound structure to illustrate the location of Asn171, Asp184, ATP, and the magnesium ions from the ternary structure.

further verify that the magnesium ion is modeled correctly and corresponds to Mg2, the magnesium ion was removed from the final model of the structure and refined. The corresponding F_o-F_c map shows strong positive electron density at the site where the magnesium ions were modeled, and again, the site corresponds to Mg2 based on its location between Asp184 and Asn171 (**Fig. 5.6B**). Therefore, Mg2 is the ion that binds more strongly with ADP and verifies previous studies suggesting that Mg1 is lost following phosphoryl transfer (Bastidas et al., 2013a; Jacobsen et al., 2012).

5.4 Discussion

The ADP bound structure displays one magnesium ion bound at the active site that corresponds to Mg2 which is situated between Asp184 of the DFG motif and Asn171 (**Fig. 5.6A-B**). This structure suggests PKA binds ADP with Mg2, and therefore, Mg1 must be released following phosphoryl transfer. This mode of reaction progression was seen previously in both CDK2 and PKA (Bastidas et al., 2013a; Jacobsen et al., 2012). Crystal structures showed that ADP can bind with one or two magnesium ions at the active site of PKA or CDK2, and if only one magnesium ion is bound, the ion corresponds to Mg2. Release of Mg1 is therefore hypothesized to be an important part of the rate-limiting step of ADP-release. This structure further supports these previous findings and hypothesis by showing that PKA binds to ADP with Mg2.

An examination of several kinase structures bound to ADP suggests that many kinases may release Mg1 following phosphoryl transfer or bind Mg2 more strongly than Mg1. Several kinase structures crystallized with ADP show two magnesium ions at the active site that correspond to Mg1 and Mg2 (Jacobsen et al., 2012; Kikani et al.,

2010; Lawrence et al., 2012). In many other cases, when a kinase binds one magnesium ion at the active site, the ion bound corresponds to Mg2 (Aoki et al., 2004; Fischmann et al., 2009; Hughes et al., 2012; Jacobsen et al., 2012; McNamara et al., 2009). Therefore, it is likely that many protein kinases bind two magnesium ions to facilitate phosphoryl transfer. Kinases can then retain both ions following phosphoryl transfer or can release one ion, the Mg1 ion, to facilitate ADP-release. There are, however, some kinase structures bound to ADP that bind the magnesium ions in positions that do not correspond to the Mg2 and Mg1 sites from PKA (Ko et al., 2010; Singh et al., 2008), and there are structures with only one magnesium ion bound that binds only to ADP and no amino acid residues (Richards et al., 2009; Westwood et al., 2009). Therefore, these magnesium binding sites and mode of magnesium release may not be universal for all kinases but likely control many kinases.

In addition to validating the potential mode of magnesium release during reaction turnover, the ADP bound structure also provides a glimpse of possible motions and conformation involved in ADP release. The ADP bound structure adopts a mostly open conformation, but it is still more closed than the apo state (**Fig. 5.5A-B**). The Gly-rich loop lowers compared to the apo state to help to bind to ADP at the active site but not as much as in the ternary, closed state. Similarly, the C-tail moves into the active site to bind to ADP with residues Phe327 and Tyr330, as in the closed state, but the C-tail does not move into the active site to the same extent in the ADP bound structure as in the intermediate or closed states (**Fig. 5.5A-B**).

The ADP bound structure provides insights into how ADP release may proceed. ADP release likely occurs with opening of the enzyme via rising of the Gly-

rich loop and C-terminal tail as shown in the ADP bound structure (**Fig. 5.5A-B**). Also, one of the molecules in the asymmetric unit, Chain A, does not show the C-tail binding at the active site because it is blocked by a symmetry related molecule (**Fig. 5.3B**). However, ADP is still present at the active site in Chain A but is not as stably bound as in Chain B based on electron density and B-factor values. Therefore, a possible mode of ADP release involves removal of the C-terminal tail from the active site following general opening of the active site which then destabilizes ADP binding allowing for release. Combining the information about the role of the magnesium ions in ADP release, a potential mode of reaction progression and ADP release by PKA becomes evident. Following phosphoryl transfer, Mg1 is released which destabilizes ADP binding. Subsequently, the active site opens through rising of the Gly-rich loop and C-terminal tail away from the active site. Next, the C-terminal tail may be removed from the active site, which allows for ADP release (**Fig. 5.7**). It is also possible that ADP release is not controlled by movement of the C-tail alone but general opening of both the C-tail and Gly-rich loop together. Therefore, these structures begin to explain how the rate limiting step of ADP release may proceed and identifies conformations and movements involved in this process.

In summary, the ADP bound structure reported here further defines the conformational flexibility of the C-subunit because it does not conform to any of the previously defined states, open, closed, or intermediate. Furthermore, the ADP bound structure provides evidence of how reaction progression may proceed in PKA and kinases in general. ADP binds at the active site with only one magnesium ion corresponding to Mg2, which is consistent with previous reports suggesting that Mg1

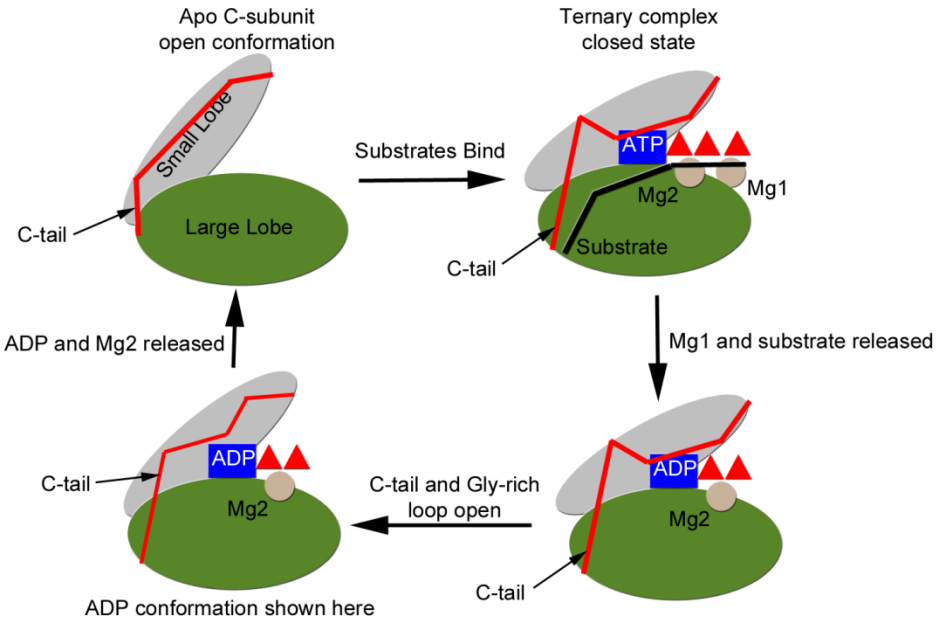

Figure 5.7. Schematic representation of possible steps and conformations involved in reaction turnover by PKA. This depiction highlights conformational changes that may occur including opening of the active site following substrate release. See Bastidas et al. and Jacobsen et al. (Bastidas et al., 2013a; Jacobsen et al., 2012) for more detailed depictions of possible substrate binding and release steps.

is released following phosphoryl transfer, and release of Mg1 may be an important step that precedes ADP release. Additionally, the conformation adopted with the ADP bound structure presents evidence of the conformational changes that may precede ADP release during reaction turnover including opening of the active site by movement of the Gly-rich loop and C-tail away from the active site.

Chapter 5, in full, will be published in the near future with the tentative title of Apo and ADP Bound Structures of Protein Kinase A Provide Insights into the Mode of Kinase Product Turnover. Bastidas AC, Wu J, Taylor SS. The dissertation author was the primary researcher and author of this work.

Chapter 6

Conclusions

Although the ubiquitously expressed Cα subunit of PKA is always co-translationally N-myristylated, there are not many studies of the function and effects of N-myristylation. Few studies of N-myristylation of PKA were performed because the recombinantly expressed protein is not myristylated due to lack of the enzyme N-myristyl transferase (NMT) in *E. coli*. However, by co-expressing the C-subunit with NMT and purifying with a histidine tagged regulatory (R) subunit, we were able to obtain larger quantities of the recombinant N-myristylated protein than previously possible. A major goal of this dissertation was to elucidate how N-myristylation influences the structure, function, and dynamics of the catalytic subunit of PKA.

While studying the effects of N-myristylation of PKA, the serendipitous finding that the generally non-hydrolyzable analog of ATP, AMP-PNP, can be utilized for phosphoryl transfer by PKA in protein crystals yielded another avenue of studies for my dissertation. Therefore, my dissertation also focused on the mechanism of reaction progression by PKA and likely many, if not all, protein kinases. Partial and full phosphoryl transfer structures of AMP-PNP onto a substrate peptide as well as an apo and an ADP bound structure of the C-subunit in the absence of substrate allowed for glimpses of multiple states of PKA during reaction turnover. We obtained the starting state of the enzyme with the apo structure as well as structures bound with nucleotide and substrate without phosphoryl transfer; with partial transfer; with full phosphoryl transfer; and a structure of the C-subunit bound only to ADP, which likely represents the final state in reaction turnover since ADP release is the rate-limiting step in PKA reaction turnover. These multiple structures allowed for thorough analysis of the steps that may govern reaction turnover; identified the release of one of the

magnesium ions following phosphoryl transfer; and identified a new conformation that may be important in ADP-release.

Recombinant N-myristylation of the C-subunit of PKA

One of the first obstacles with studying the N-myristylated C-subunit of PKA and a major reason why there were few studies of this modification is because it is difficult to purify the recombinant N-myristylated C-subunit. In order to myristylate PKA, NMT must be co-expressed with the C-subunit, but NMT interferes with the typical purification methods for the C-subunit. Therefore, another method of purification was required. The method we utilized to purify the C-subunit was through co-lysis of the N-myristylated C-subunit with a histidine tagged R-subunit, which allowed the protein to be purified using Ni resin with elution with cAMP. Furthermore, the preparation produced both myristylated and non-myristylated C-subunit, which were separated on a cation exchange column. Furthermore, another advancement in the purification was achieved with a K7C mutant C-subunit. The K7C mutation alters the PKA recognition sequence at Ser10 and, therefore, prevents phosphorylation of Ser10. Preventing Ser10 phosphorylation resulted in preparations that yielded essentially 100% myristylated protein, and therefore, the K7C mutant could be utilized for crystallization studies as it increased the yield of myristylated protein. In summary, co-lysis of the C-subunit with a histidine tagged R-subunit provided a means of C-subunit purification which is complicated by co-expression with NMT, and preventing Ser10 phosphorylation increased the amount of N-

myristylated protein to be essentially 100% myristylated which greatly aided in these studies and in protein crystallization (Bastidas et al., 2012).

Role of N-myristylation on PKA Structure

The N-myristylated WT and K7C mutant proteins were crystallized bound to a substrate peptide, SP20, (binary complex) and bound to AMP-PNP and SP20 (ternary complex). N-myristylation orders the N-terminus for the WT protein in a binary complex and also for K7C in both binary and ternary complexes. The K7C mutant has a more stable N-terminus than the WT protein, which could be due to protein crystal packing or could be due to the mutation itself. The important finding, however, is that the N-terminus is ordered by N-myristylation in the WT protein but only in a binary complex, and the N-terminus becomes disordered in a ternary complex. This fact suggests that ATP binding causes a disordering of the N-terminus in the WT protein, and furthermore, suggests that there may be crosstalk between the active site and myristate pocket. This, in turn, suggests that N-myristylation and the myristic acid binding pocket may yield allosteric regulation of the C-subunit by influencing mobility of regions distant from the myristic acid pocket including, possibly, the active site of the enzyme.

Role of N-myristylation on PKA Dynamics

To study the effects of N-myristylation on C-subunit dynamics, we utilized a combination of time-resolved fluorescence anisotropy measured on fluorescently labeled cysteine residues introduced throughout the C-subunit along with molecular

dynamics (MD) simulations of a structure solved as part of my thesis work. Both of these techniques were performed in the absence of the ligands (apo, open state) and in the presence of SP20 or IP20 and ATP (ternary complex, closed state). These studies allowed for characterization of the effect that N-myristylation has on C-subunit flexibility and motions in the presence and absence of ligands. The results with MD simulations and time-resolved fluorescence anisotropy generally showed good agreement. Both methods showed that in the presence and absence of ligands N-myristylation stabilizes the first 10-12 residues at the N-terminus but exhibits less of an effect further along the N-terminus, and N-myristylation stabilizes the residues within the myristic acid binding pocket as would be expected due to the myristic acid group stably binding in this pocket in the crystal structures. Interestingly, in the presence of ligands, the dynamics of residues within the myristic acid binding pocket increased for both the myristylated and non-myristylated protein further suggesting, as with the crystal structures, that the myristic acid binding pocket and active site may exhibit crosstalk. Finally, the myristylated protein also generally showed overall increased dynamics based on MD simulations, and the active site showed increased flexibility for the myristylated compared to the non-myristylated protein adding further evidence of influences between the myristate pocket and active site (Bastidas et al., 2013b).

Reaction Progression by PKA

An unexpected finding from these studies was that AMP-PNP can be utilized for phosphoryl transfer by PKA but at a much slower rate than with ATP, and this

allowed for crystal structures of the C-subunit displaying partial and complete phosphoryl transfer. Comparison of the midpoint and final result of phosphoryl transfer yielded information about the mode of reaction turnover. The full transfer structure showed less density for one magnesium ion, previously termed Mg1, than typically observed in crystal structures and much less density for Mg1 than Mg2. This result suggests that much if not all of the Mg1 ion vacated the active site in the complete transfer structure. Therefore, a likely mode of reaction progression involves release of the Mg1 ion following phosphoryl transfer, which is likely a necessary event that precedes the rate-limiting step of ADP release (Bastidas et al., 2013a).

Furthermore, my dissertation included crystallization of the apo C-subunit, and these apo crystals were then used to obtain the first ADP bound structure of the C-subunit by soaking the apo crystals with ADP and magnesium. The ADP bound structure further supports the release of Mg1 as a necessary step during ADP release because the ADP bound structure shows electron density for only Mg2. Therefore, this structure supports the AMP-PNP phosphoryl transfer structures. Additionally, the ADP bound structure provides insights into the motions that may accompany ADP release. The ADP bound structure adopts a new conformation. The structure is more open than the closed or intermediate states but more closed than the open state. The ADP bound structure suggests that ADP release proceeds through rising of the Gly-rich loop and C-tail, which then allows for ADP release. Taken together, my dissertation revealed that Mg1 is released following phosphoryl transfer, and release of Mg1 is a likely step that precedes the rate-limiting step of ADP release. Following Mg1 release and substrate release, ADP release proceeds via rising of the Gly-rich

loop and C-terminal tail which then allow for release of ADP and Mg2. Therefore, this dissertation provides structural evidence of the steps and possible conformations involved in phosphoryl transfer.

Future Work

Determining the physiological effects of N-myristylation of PKA

Much of this dissertation focuses on the structural and biochemical effects of N-myristylation on the C-subunit of PKA, which are an important initial step in understanding the roles of this modification. However, this dissertation does not address what role this modification may have physiologically in terms of influences on, for instance, C-subunit localization or interactions. Therefore, important follow up studies could include investigating the role of N-myristylation on the cellular localization of the C-subunit; effects on protein interactions and protein substrates; and other possible downstream effects such as CREB activation. Physiological studies would provide a greater understanding of how this modification and its effects on C-subunit structure and dynamics actually influence cellular events.

Can the myristic acid pocket of PKA be specifically targeted to exhibit a functional effect?

One of the major findings from the studies of N-myristylation is that there appears to be crosstalk between the myristic acid binding pocket and the active site of the enzyme. This was supported by the structural studies as well as the studies of

protein dynamics with time-resolved fluorescence anisotropy and MD simulations. Therefore, an interesting possibility that could be studied is whether or not small molecules can be used to specifically target the myristic acid pocket in PKA to illicit a physiological response. There is a precedent for this possibility because c-Abl, a tyrosine kinase, can be either activated or inhibited by small molecules binding within its myristic acid pocket, and the protein's localization can also be affected by molecules binding in its myristate pocket (Fabbro et al., 2010; Yang et al., 2011). Therefore, it is possible that PKA could be affected by molecules binding in its myristic acid pocket. It would be interesting if molecules could be engineered that bind within the myristic acid pocket, and the effects of this binding could be investigated structurally, biochemically, and in cells.

Verification and Further Characterization of Kinase Reaction Progression

This dissertation provided great advances in understanding reaction turnover by PKA and likely many protein kinases. Mg2 was identified as the more stably bound ion that remains bound to ADP following phosphoryl transfer while Mg1 is released. Release of Mg1 is likely an important step that precedes ADP release. Future studies could be aimed at verifying this mode of reaction progress in PKA and other protein kinases. For example, CDK2 can be crystallized with ADP bound to either 1 magnesium ion or two magnesium ions (Jacobsen et al., 2012). A possible future experiment that could be performed with PKA would be to soak ADP with higher magnesium concentrations into the apo structure to determine whether PKA can also bind to ADP with two magnesium ions. If PKA was crystallized bound to ADP with

two magnesium ions, then that structure would verify that Mg2 is more strongly bound, which is why higher concentrations are necessary to bind to Mg1 because of a lower K_d. Furthermore, the ADP bound structure with two magnesium ions could yield information about how Mg1 is released depending on positioning of residues at the active site and whether or not they are different than the ADP with one magnesium ion structure.

Furthermore, another set of future studies that could be performed based on the results of this dissertation are computational studies to address the movements and mechanism underlying ADP release in PKA. Computational studies of ADP release were performed previously, but the previous studies were performed either in the absence of magnesium (Lu et al., 2005) or in the presence of two magnesium ions (Khavrutskii et al., 2009). Both of these states are unlikely to be the physiological state for ADP release. My dissertation suggests that Mg1 is released prior to ADP release, and therefore, computational studies should be performed with ADP and the Mg2 ion. The computational studies performed with ADP and two magnesium ions suggested that release with two magnesium ions is so energetically unfavorable that it is nearly impossible, and the authors suggest that one or both ions may need to be released before ADP release (Khavrutskii et al., 2009). Mg1 was identified to be the ion released. Consequently, computational studies performed in the presence of ADP and Mg2 may yield further insights into how the rate-limiting step of ADP and Mg2 release is achieved.

References

(1994). The CCP4 suite: programs for protein crystallography. Acta Crystallogr D Biol Crystallogr *50*, 760-763.

Adams, J.A. (2001). Kinetic and catalytic mechanisms of protein kinases. Chem Rev *101*, 2271-2290.

Adams, J.A., McGlone, M.L., Gibson, R., and Taylor, S.S. (1995). Phosphorylation modulates catalytic function and regulation in the cAMP-dependent protein kinase. Biochemistry *34*, 2447-2454.

Adams, J.A., and Taylor, S.S. (1993). Divalent metal ions influence catalysis and active-site accessibility in the cAMP-dependent protein kinase. Protein Sci *2*, 2177-2186.

Akamine, P., Madhusudan, Wu, J., Xuong, N.H., Ten Eyck, L.F., and Taylor, S.S. (2003). Dynamic features of cAMP-dependent protein kinase revealed by apoenzyme crystal structure. J Mol Biol *327*, 159-171.

Ames, J.B., Porumb, T., Tanaka, T., Ikura, M., and Stryer, L. (1995). Amino-terminal myristoylation induces cooperative calcium binding to recoverin. J Biol Chem *270*, 4526-4533.

Anandakrishnan, R., Aguilar, B., and Onufriev, A.V. (2012). H++ 3.0: automating pK prediction and the preparation of biomolecular structures for atomistic molecular modeling and simulations. Nucleic Acids Res *40*, W537-541.

Aoki, M., Yokota, T., Sugiura, I., Sasaki, C., Hasegawa, T., Okumura, C., Ishiguro, K., Kohno, T., Sugio, S., and Matsuzaki, T. (2004). Structural insight into nucleotide recognition in tau-protein kinase I/glycogen synthase kinase 3 beta. Acta Crystallogr D Biol Crystallogr *60*, 439-446.

Armstrong, R.N., Kondo, H., Granot, J., Kaiser, E.T., and Mildvan, A.S. (1979). Magnetic resonance and kinetic studies of the manganese(II) ion and substrate complexes of the catalytic subunit of adenosine 3',5'-monophosphate dependent protein kinase from bovine heart. Biochemistry *18*, 1230-1238.

Bao, Z.Q., Jacobsen, D.M., and Young, M.A. (2011). Briefly bound to activate: transient binding of a second catalytic magnesium activates the structure and dynamics of CDK2 kinase for catalysis. Structure *19*, 675-690.

Bastidas, A.C., Deal, M.S., Steichen, J.M., Guo, Y., Wu, J., and Taylor, S.S. (2013a). Phosphoryl transfer by protein kinase a is captured in a crystal lattice. J Am Chem Soc *135*, 4788-4798.

Bastidas, A.C., Deal, M.S., Steichen, J.M., Keshwani, M.M., Guo, Y., and Taylor, S.S. (2012). Role of N-terminal myristylation in the structure and regulation of cAMP-dependent protein kinase. J Mol Biol *422*, 215-229.

Bastidas, A.C., Pierce, L.C., Walker, R.C., Johnson, D.A., and Taylor, S.S. (2013b). Influence of N-myristylation and ligand binding on the flexibility of the catalytic subunit of protein kinase A. Biochemistry *52*, 6368-6379.

Batkin, M., Schvartz, I., and Shaltiel, S. (2000). Snapping of the carboxyl terminal tail of the catalytic subunit of PKA onto its core: characterization of the sites by mutagenesis. Biochemistry *39*, 5366-5373.

Battye, T.G., Kontogiannis, L., Johnson, O., Powell, H.R., and Leslie, A.G. (2011). iMOSFLM: a new graphical interface for diffraction-image processing with MOSFLM. Acta Crystallogr D Biol Crystallogr *67*, 271-281.

Birch, D.J.S., and Imhof, R.E. (1991). Time-domain fluorescence spectroscopy using time-correlated single photon counting, in Topics in Fluorescence Spectroscopy: Techniques Vol. 1 (New York, NY.: Plenum).

Boettcher, A.J., Wu, J., Kim, C., Yang, J., Bruystens, J., Cheung, N., Pennypacker, J.K., Blumenthal, D.A., Kornev, A.P., and Taylor, S.S. (2011). Realizing the allosteric potential of the tetrameric protein kinase A RIalpha holoenzyme. Structure *19*, 265-276.

Bossemeyer, D., Engh, R.A., Kinzel, V., Ponstingl, H., and Huber, R. (1993). Phosphotransferase and substrate binding mechanism of the cAMP-dependent protein kinase catalytic subunit from porcine heart as deduced from the 2.0 A structure of the complex with Mn2+ adenylyl imidodiphosphate and inhibitor peptide PKI(5-24). EMBO J *12*, 849-859.

Boudeau, J., Miranda-Saavedra, D., Barton, G.J., and Alessi, D.R. (2006). Emerging roles of pseudokinases. Trends in cell biology *16*, 443-452.

Boutin, J.A. (1997). Myristoylation. Cell Signal *9*, 15-35.

Breitenlechner, C., Engh, R.A., Huber, R., Kinzel, V., Bossemeyer, D., and Gassel, M. (2004). The typically disordered N-terminus of PKA can fold as a helix and project the myristoylation site into solution. Biochemistry *43*, 7743-7749.

Brown, S.H., Wu, J., Kim, C., Alberto, K., and Taylor, S.S. (2009). Novel isoform-specific interfaces revealed by PKA RIIbeta holoenzyme structures. J Mol Biol *393*, 1070-1082.

Buetow, L., and Ghosh, P. (2003). Structural elements required for deamidation of RhoA by cytotoxic necrotizing factor 1. Biochemistry *42*, 12784-12791.

Carr, S.A., Biemann, K., Shoji, S., Parmelee, D.C., and Titani, K. (1982). n-Tetradecanoyl is the NH2-terminal blocking group of the catalytic subunit of cyclic AMP-dependent protein kinase from bovine cardiac muscle. Proc Natl Acad Sci U S A *79*, 6128-6131.

Case, D.A., Darden, T.A., Cheatham, T.E., III, Simmerling, C.L., Wang, J., Duke, R.E., Luo, R., Walker, R.C., Zhang, W., and Merz, K.M. (2010). Amber 11 (University of California, San Francisco.).

Case, D.A., Darden, T.A., Cheatham, T.E., III, Simmerling, C.L., Wang, J., Duke, R.E., Luo, R., Walker, R.C., Zhang, W., and Merz, K.M. (2012). Amber12 (University of California, San Francisco).

Cembran, A., Masterson, L.R., McClendon, C.L., Taylor, S.S., Gao, J., and Veglia, G. (2012). Conformational Equilibrium of N-Myristoylated cAMP-Dependent Protein Kinase A by Molecular Dynamics Simulations. Biochemistry *51*, 10186-10196.

Cheng, Y., Zhang, Y., and McCammon, J.A. (2005). How does the cAMP-dependent protein kinase catalyze the phosphorylation reaction: an ab initio QM/MM study. J Am Chem Soc *127*, 1553-1562.

Chida, T., Ando, M., Matsuki, T., Masu, Y., Nagaura, Y., Takano-Yamamoto, T., Tamura, S., and Kobayashi, T. (2013). N-Myristoylation is essential for protein phosphatases PPM1A and PPM1B to dephosphorylate their physiological substrates in cells. Biochem J *449*, 741-749.

Choi, Y., Seeliger, M.A., Panjarian, S.B., Kim, H., Deng, X., Sim, T., Couch, B., Koleske, A.J., Smithgall, T.E., and Gray, N.S. (2009). N-myristoylated c-Abl tyrosine kinase localizes to the endoplasmic reticulum upon binding to an allosteric inhibitor. J Biol Chem *284*, 29005-29014.

Clegg, C.H., Ran, W., Uhler, M.D., and McKnight, G.S. (1989). A mutation in the catalytic subunit of protein kinase A prevents myristylation but does not inhibit biological activity. J Biol Chem *264*, 20140-20146.

Cook, P.F., Neville, M.E., Jr., Vrana, K.E., Hartl, F.T., and Roskoski, R., Jr. (1982). Adenosine cyclic 3',5'-monophosphate dependent protein kinase: kinetic mechanism for the bovine skeletal muscle catalytic subunit. Biochemistry *21*, 5794-5799.

Cui, J., Yao, Q., Li, S., Ding, X., Lu, Q., Mao, H., Liu, L., Zheng, N., Chen, S., and Shao, F. (2010). Glutamine deamidation and dysfunction of ubiquitin/NEDD8 induced by a bacterial effector family. Science *329*, 1215-1218.

Darden, T., York, D., and Pedersen, L. (1993). Particle Mesh Ewald - an N.Log(N) Method for Ewald Sums in Large Systems. J Chem Phys *98*, 10089-10092.

Davis, I.W., Leaver-Fay, A., Chen, V.B., Block, J.N., Kapral, G.J., Wang, X., Murray, L.W., Arendall, W.B., 3rd, Snoeyink, J., Richardson, J.S., and Richardson, D.C. (2007). MolProbity: all-atom contacts and structure validation for proteins and nucleic acids. Nucleic Acids Res *35*, W375-383.

Derewenda, Z.S., and Vekilov, P.G. (2006). Entropy and surface engineering in protein crystallization. Acta Crystallogr D Biol Crystallogr *62*, 116-124.

Duronio, R.J., Jackson-Machelski, E., Heuckeroth, R.O., Olins, P.O., Devine, C.S., Yonemoto, W., Slice, L.W., Taylor, S.S., and Gordon, J.I. (1990). Protein N-myristoylation in Escherichia coli: reconstitution of a eukaryotic protein modification in bacteria. Proc Natl Acad Sci U S A *87*, 1506-1510.

Emsley, P., and Cowtan, K. (2004). Coot: model-building tools for molecular graphics. Acta Crystallogr D Biol Crystallogr *60*, 2126-2132.

Fabbro, D., Manley, P.W., Jahnke, W., Liebetanz, J., Szyttenholm, A., Fendrich, G., Strauss, A., Zhang, J., Gray, N.S., Adrian, F., Warmuth, M., Pelle, X., Grotzfeld, R., Berst, F., Marzinzik, A., Cowan-Jacob, S.W., Furet, P., and Mestan, J. (2010). Inhibitors of the Abl kinase directed at either the ATP- or myristate-binding site. Biochim Biophys Acta *1804*, 454-462.

Fantozzi, D.A., Harootunian, A.T., Wen, W., Taylor, S.S., Feramisco, J.R., Tsien, R.Y., and Meinkoth, J.L. (1994). Thermostable inhibitor of cAMP-dependent protein kinase enhances the rate of export of the kinase catalytic subunit from the nucleus. J Biol Chem *269*, 2676-2686.

Farazi, T.A., Waksman, G., and Gordon, J.I. (2001). The biology and enzymology of protein N-myristoylation. J Biol Chem *276*, 39501-39504.

Fayard, E., Xue, G., Parcellier, A., Bozulic, L., and Hemmings, B.A. (2010). Protein kinase B (PKB/Akt), a key mediator of the PI3K signaling pathway. Curr Top Microbiol Immunol *346*, 31-56.

Fischer, E.H., and Krebs, E.G. (1955). Conversion of phosphorylase b to phosphorylase a in muscle extracts. J Biol Chem *216*, 121-132.

Fischmann, T.O., Smith, C.K., Mayhood, T.W., Myers, J.E., Reichert, P., Mannarino, A., Carr, D., Zhu, H., Wong, J., Yang, R.S., Le, H.V., and Madison, V.S. (2009). Crystal structures of MEK1 binary and ternary complexes with nucleotides and inhibitors. Biochemistry *48*, 2661-2674.

Francis, S.H., and Corbin, J.D. (1994). Structure and function of cyclic nucleotide-dependent protein kinases. Annu Rev Physiol *56*, 237-272.

Fukuda, K., Gupta, S., Chen, K., Wu, C., and Qin, J. (2009). The pseudoactive site of ILK is essential for its binding to alpha-Parvin and localization to focal adhesions. Mol Cell *36*, 819-830.

Gaffarogullari, E.C., Masterson, L.R., Metcalfe, E.E., Traaseth, N.J., Balatri, E., Musa, M.M., Mullen, D., Distefano, M.D., and Veglia, G. (2011). A myristoyl/phosphoserine switch controls cAMP-dependent protein kinase association to membranes. J Mol Biol *411*, 823-836.

Gangal, M., Clifford, T., Deich, J., Cheng, X., Taylor, S.S., and Johnson, D.A. (1999). Mobilization of the A-kinase N-myristate through an isoform-specific intermolecular switch. Proc Natl Acad Sci U S A *96*, 12394-12399.

Gangal, M., Cox, S., Lew, J., Clifford, T., Garrod, S.M., Aschbaher, M., Taylor, S.S., and Johnson, D.A. (1998). Backbone flexibility of five sites on the catalytic subunit of cAMP-dependent protein kinase in the open and closed conformations. Biochemistry *37*, 13728-13735.

Gibbs, C.S., and Zoller, M.J. (1991). Rational scanning mutagenesis of a protein kinase identifies functional regions involved in catalysis and substrate interactions. J Biol Chem *266*, 8923-8931.

Gotz, A.W., Williamson, M.J., Xu, D., Poole, D., Le Grand, S., and Walker, R.C. (2012). Routine Microsecond Molecular Dynamics Simulations with AMBER on GPUs. 1. Generalized Born. J Chem Theory Comput *8*, 1542-1555.

Gould, C.M., Kannan, N., Taylor, S.S., and Newton, A.C. (2009). The chaperones Hsp90 and Cdc37 mediate the maturation and stabilization of protein kinase C through a conserved PXXP motif in the C-terminal tail. J Biol Chem *284*, 4921-4935.

Grace, M.R., Walsh, C.T., and Cole, P.A. (1997). Divalent ion effects and insights into the catalytic mechanism of protein tyrosine kinase Csk. Biochemistry *36*, 1874-1881.

Hantschel, O., Nagar, B., Guettler, S., Kretzschmar, J., Dorey, K., Kuriyan, J., and Superti-Furga, G. (2003). A myristoyl/phosphotyrosine switch regulates c-Abl. Cell *112*, 845-857.

Hemmer, W., McGlone, M., and Taylor, S.S. (1997). Recombinant strategies for rapid purification of catalytic subunits of cAMP-dependent protein kinase. Anal Biochem *245*, 115-122.

Herberg, F.W., Bell, S.M., and Taylor, S.S. (1993). Expression of the catalytic subunit of cAMP-dependent protein kinase in Escherichia coli: multiple isozymes reflect different phosphorylation states. Protein Eng *6*, 771-777.

Herberg, F.W., Doyle, M.L., Cox, S., and Taylor, S.S. (1999). Dissection of the nucleotide and metal-phosphate binding sites in cAMP-dependent protein kinase. Biochemistry *38*, 6352-6360.

Herberg, F.W., Zimmermann, B., McGlone, M., and Taylor, S.S. (1997). Importance of the A-helix of the catalytic subunit of cAMP-dependent protein kinase for stability and for orienting subdomains at the cleft interface. Protein Sci *6*, 569-579.

Hereng, T.H., Backe, P.H., Kahmann, J., Scheich, C., Bjoras, M., Skalhegg, B.S., and Rosendal, K.R. (2012). Structure and function of the human sperm-specific isoform of protein kinase A (PKA) catalytic subunit Calpha2. J Struct Biol *178*, 300-310.

Hibbs, R.E., Radic, Z., Taylor, P., and Johnson, D.A. (2006). Influence of agonists and antagonists on the segmental motion of residues near the agonist binding pocket of the acetylcholine-binding protein. J Biol Chem *281*, 39708-39718.

Hornak, V., Abel, R., Okur, A., Strockbine, B., Roitberg, A., and Simmerling, C. (2006). Comparison of multiple Amber force fields and development of improved protein backbone parameters. Proteins *65*, 712-725.

Hughes, S., Elustondo, F., Di Fonzo, A., Leroux, F.G., Wong, A.C., Snijders, A.P., Matthews, S.J., and Cherepanov, P. (2012). Crystal structure of human CDC7 kinase in complex with its activator DBF4. Nat Struct Mol Biol *19*, 1101-1107.

Huse, M., and Kuriyan, J. (2002). The conformational plasticity of protein kinases. Cell *109*, 275-282.

Hyeon, C., Jennings, P.A., Adams, J.A., and Onuchic, J.N. (2009). Ligand-induced global transitions in the catalytic domain of protein kinase A. Proc Natl Acad Sci U S A *106*, 3023-3028.

Ilouz, R., Bubis, J., Wu, J., Yim, Y.Y., Deal, M.S., Kornev, A.P., Ma, Y., Blumenthal, D.K., and Taylor, S.S. (2012). Localization and quaternary structure of the PKA RIbeta holoenzyme. Proc Natl Acad Sci U S A *109*, 12443-12448.

Iyer, G.H., Garrod, S., Woods, V.L., Jr., and Taylor, S.S. (2005a). Catalytic independent functions of a protein kinase as revealed by a kinase-dead mutant: study of the Lys72His mutant of cAMP-dependent kinase. J Mol Biol *351*, 1110-1122.

Iyer, G.H., Moore, M.J., and Taylor, S.S. (2005b). Consequences of lysine 72 mutation on the phosphorylation and activation state of cAMP-dependent kinase. J Biol Chem *280*, 8800-8807.

Jacobsen, D.M., Bao, Z.Q., O'Brien, P., Brooks, C.L., 3rd, and Young, M.A. (2012). Price to be paid for two-metal catalysis: magnesium ions that accelerate chemistry unavoidably limit product release from a protein kinase. J Am Chem Soc *134*, 15357-15370.

Jedrzejewski, P.T., Girod, A., Tholey, A., Konig, N., Thullner, S., Kinzel, V., and Bossemeyer, D. (1998). A conserved deamidation site at Asn 2 in the catalytic subunit of mammalian cAMP-dependent protein kinase detected by capillary LC-MS and tandem mass spectrometry. Protein Sci *7*, 457-469.

Johnson, D.A., Akamine, P., Radzio-Andzelm, E., Madhusudan, M., and Taylor, S.S. (2001). Dynamics of cAMP-dependent protein kinase. Chem Rev *101*, 2243-2270.

Kannan, N., Haste, N., Taylor, S.S., and Neuwald, A.F. (2007). The hallmark of AGC kinase functional divergence is its C-terminal tail, a cis-acting regulatory module. Proc Natl Acad Sci U S A *104*, 1272-1277.

Karlsson, R., Zheng, J., Xuong, N., Taylor, S.S., and Sowadski, J.M. (1993). Structure of the mammalian catalytic subunit of cAMP-dependent protein kinase and an inhibitor peptide displays an open conformation. Acta Crystallogr D Biol Crystallogr *49*, 381-388.

Khavrutskii, I.V., Grant, B., Taylor, S.S., and McCammon, J.A. (2009). A transition path ensemble study reveals a linchpin role for Mg(2+) during rate-limiting ADP release from protein kinase A. Biochemistry *48*, 11532-11545.

Kikani, C.K., Antonysamy, S.A., Bonanno, J.B., Romero, R., Zhang, F.F., Russell, M., Gheyi, T., Iizuka, M., Emtage, S., Sauder, J.M., Turk, B.E., Burley, S.K., and Rutter, J. (2010). Structural bases of PAS domain-regulated kinase (PASK) activation in the absence of activation loop phosphorylation. J Biol Chem *285*, 41034-41043.

Kim, C., Cheng, C.Y., Saldanha, S.A., and Taylor, S.S. (2007). PKA-I holoenzyme structure reveals a mechanism for cAMP-dependent activation. Cell *130*, 1032-1043.

Kirschner, L.S., Yin, Z., Jones, G.N., and Mahoney, E. (2009). Mouse models of altered protein kinase A signaling. Endocr Relat Cancer *16*, 773-793.

Knighton, D.R., Bell, S.M., Zheng, J., Ten Eyck, L.F., Xuong, N.H., Taylor, S.S., and Sowadski, J.M. (1993). 2.0 A refined crystal structure of the catalytic subunit of cAMP-dependent protein kinase complexed with a peptide inhibitor and detergent. Acta Crystallogr D Biol Crystallogr *49*, 357-361.

Knighton, D.R., Zheng, J.H., Ten Eyck, L.F., Ashford, V.A., Xuong, N.H., Taylor, S.S., and Sowadski, J.M. (1991a). Crystal structure of the catalytic subunit of cyclic adenosine monophosphate-dependent protein kinase. Science *253*, 407-414.

Knighton, D.R., Zheng, J.H., Ten Eyck, L.F., Xuong, N.H., Taylor, S.S., and Sowadski, J.M. (1991b). Structure of a peptide inhibitor bound to the catalytic subunit of cyclic adenosine monophosphate-dependent protein kinase. Science *253*, 414-420.

Ko, T.P., Jeng, W.Y., Liu, C.I., Lai, M.D., Wu, C.L., Chang, W.J., Shr, H.L., Lu, T.J., and Wang, A.H. (2010). Structures of human MST3 kinase in complex with adenine, ADP and Mn2+. Acta Crystallogr D Biol Crystallogr *66*, 145-154.

Kornev, A.P., Haste, N.M., Taylor, S.S., and Eyck, L.F. (2006). Surface comparison of active and inactive protein kinases identifies a conserved activation mechanism. Proc Natl Acad Sci U S A *103*, 17783-17788.

Kornev, A.P., Taylor, S.S., and Ten Eyck, L.F. (2008). A helix scaffold for the assembly of active protein kinases. Proc Natl Acad Sci U S A *105*, 14377-14382.

Kovalevsky, A.Y., Johnson, H., Hanson, B.L., Waltman, M.J., Fisher, S.Z., Taylor, S., and Langan, P. (2012). Low- and room-temperature X-ray structures of protein kinase A ternary complexes shed new light on its activity. Acta Crystallogr D Biol Crystallogr *68*, 854-860.

Kurzrock, R., Shtalrid, M., Talpaz, M., Kloetzer, W.S., and Gutterman, J.U. (1987). Expression of c-abl in Philadelphia-positive acute myelogenous leukemia. Blood *70*, 1584-1588.

Lawrence, H.R., Martin, M.P., Luo, Y., Pireddu, R., Yang, H., Gevariya, H., Ozcan, S., Zhu, J.Y., Kendig, R., Rodriguez, M., Elias, R., Cheng, J.Q., Sebti, S.M., Schonbrunn, E., and Lawrence, N.J. (2012). Development of o-chlorophenyl substituted pyrimidines as exceptionally potent aurora kinase inhibitors. J Med Chem *55*, 7392-7416.

Le Grand, S., Gotz, A.W., and Walker, R.C. (2013). SPFP: Speed without compromise-A mixed precision model for GPU accelerated molecular dynamics simulations. Comput Phys Commun *184*, 374-380.

Lemmon, M.A., and Schlessinger, J. (2010). Cell signaling by receptor tyrosine kinases. Cell *141*, 1117-1134.

Lew, J., Taylor, S.S., and Adams, J.A. (1997). Identification of a partially rate-determining step in the catalytic mechanism of cAMP-dependent protein kinase: a transient kinetic study using stopped-flow fluorescence spectroscopy. Biochemistry *36*, 6717-6724.

Li, D., Agrellos, O.A., and Calderone, R. (2010). Histidine kinases keep fungi safe and vigorous. Current opinion in microbiology *13*, 424-430.

Li, H., Dou, J., Ding, L., and Spearman, P. (2007). Myristoylation is required for human immunodeficiency virus type 1 Gag-Gag multimerization in mammalian cells. J Virol *81*, 12899-12910.

Lindberg, R.A., Quinn, A.M., and Hunter, T. (1992). Dual-specificity protein kinases: will any hydroxyl do? Trends Biochem Sci *17*, 114-119.

Lindorff-Larsen, K., Piana, S., Palmo, K., Maragakis, P., Klepeis, J.L., Dror, R.O., and Shaw, D.E. (2010). Improved side-chain torsion potentials for the Amber ff99SB protein force field. Proteins *78*, 1950-1958.

Lu, B., Wong, C.F., and McCammon, J.A. (2005). Release of ADP from the catalytic subunit of protein kinase A: a molecular dynamics simulation study. Protein Sci *14*, 159-168.

Madhusudan, Akamine, P., Xuong, N.H., and Taylor, S.S. (2002). Crystal structure of a transition state mimic of the catalytic subunit of cAMP-dependent protein kinase. Nat Struct Biol *9*, 273-277.

Madhusudan, Trafny, E.A., Xuong, N.H., Adams, J.A., Ten Eyck, L.F., Taylor, S.S., and Sowadski, J.M. (1994). cAMP-dependent protein kinase: crystallographic insights into substrate recognition and phosphotransfer. Protein Sci *3*, 176-187.

Manning, G., Whyte, D.B., Martinez, R., Hunter, T., and Sudarsanam, S. (2002). The protein kinase complement of the human genome. Science *298*, 1912-1934.

Masterson, L.R., Mascioni, A., Traaseth, N.J., Taylor, S.S., and Veglia, G. (2008). Allosteric cooperativity in protein kinase A. Proc Natl Acad Sci U S A *105*, 506-511.

Masterson, L.R., Shi, L., Metcalfe, E., Gao, J., Taylor, S.S., and Veglia, G. (2011). Dynamically committed, uncommitted, and quenched states encoded in protein kinase A revealed by NMR spectroscopy. Proc Natl Acad Sci U S A *108*, 6969-6974.

Mauro, M.J., O'Dwyer, M., Heinrich, M.C., and Druker, B.J. (2002). STI571: a paradigm of new agents for cancer therapeutics. J Clin Oncol *20*, 325-334.

Mayans, O., van der Ven, P.F., Wilm, M., Mues, A., Young, P., Furst, D.O., Wilmanns, M., and Gautel, M. (1998). Structural basis for activation of the titin kinase domain during myofibrillogenesis. Nature *395*, 863-869.

McCoy, A.J., Grosse-Kunstleve, R.W., Adams, P.D., Winn, M.D., Storoni, L.C., and Read, R.J. (2007). Phaser crystallographic software. J Appl Crystallogr *40*, 658-674.

McNamara, L.K., Watterson, D.M., and Brunzelle, J.S. (2009). Structural insight into nucleotide recognition by human death-associated protein kinase. Acta Crystallogr D Biol Crystallogr *65*, 241-248.

Min, X., Lee, B.H., Cobb, M.H., and Goldsmith, E.J. (2004). Crystal structure of the kinase domain of WNK1, a kinase that causes a hereditary form of hypertension. Structure *12*, 1303-1311.

Mucignat-Caretta, C., and Caretta, A. (2002). Clustered distribution of cAMP-dependent protein kinase regulatory isoform RI alpha during the development of the rat brain. J Comp Neurol *451*, 324-333.

Mukherjee, K., Sharma, M., Urlaub, H., Bourenkov, G.P., Jahn, R., Sudhof, T.C., and Wahl, M.C. (2008). CASK Functions as a Mg2+-independent neurexin kinase. Cell *133*, 328-339.

Nagar, B., Hantschel, O., Young, M.A., Scheffzek, K., Veach, D., Bornmann, W., Clarkson, B., Superti-Furga, G., and Kuriyan, J. (2003). Structural basis for the autoinhibition of c-Abl tyrosine kinase. Cell *112*, 859-871.

Narayana, N., Cox, S., Nguyen-huu, X., Ten Eyck, L.F., and Taylor, S.S. (1997). A binary complex of the catalytic subunit of cAMP-dependent protein kinase and adenosine further defines conformational flexibility. Structure *5*, 921-935.

Nelson, N.C., and Taylor, S.S. (1981). Differential labeling and identification of the cysteine-containing tryptic peptides of catalytic subunit from porcine heart cAMP-dependent protein kinase. J Biol Chem *256*, 3743-3750.

Olsen, S.R., and Uhler, M.D. (1991). Inhibition of protein kinase-A by overexpression of the cloned human protein kinase inhibitor. Mol Endocrinol *5*, 1246-1256.

Patwardhan, P., and Resh, M.D. (2010). Myristoylation and membrane binding regulate c-Src stability and kinase activity. Mol Cell Biol *30*, 4094-4107.

Pearce, L.R., Komander, D., and Alessi, D.R. (2010). The nuts and bolts of AGC protein kinases. Nature reviews Molecular cell biology *11*, 9-22.

Pepperkok, R., Hotz-Wagenblatt, A., Konig, N., Girod, A., Bossemeyer, D., and Kinzel, V. (2000). Intracellular distribution of mammalian protein kinase A catalytic subunit altered by conserved Asn2 deamidation. J Cell Biol *148*, 715-726.

Ptacek, J., Devgan, G., Michaud, G., Zhu, H., Zhu, X., Fasolo, J., Guo, H., Jona, G., Breitkreutz, A., Sopko, R., McCartney, R.R., Schmidt, M.C., Rachidi, N., Lee, S.J., Mah, A.S., Meng, L., Stark, M.J., Stern, D.F., De Virgilio, C., Tyers, M., Andrews, B., Gerstein, M., Schweitzer, B., Predki, P.F., and Snyder, M. (2005). Global analysis of protein phosphorylation in yeast. Nature *438*, 679-684.

Resh, M.D. (1999). Fatty acylation of proteins: new insights into membrane targeting of myristoylated and palmitoylated proteins. Biochim Biophys Acta *1451*, 1-16.

Richards, M.W., O'Regan, L., Mas-Droux, C., Blot, J.M., Cheung, J., Hoelder, S., Fry, A.M., and Bayliss, R. (2009). An autoinhibitory tyrosine motif in the cell-cycle-regulated Nek7 kinase is released through binding of Nek9. Mol Cell *36*, 560-570.

Romano, R.A., Kannan, N., Kornev, A.P., Allison, C.J., and Taylor, S.S. (2009). A chimeric mechanism for polyvalent trans-phosphorylation of PKA by PDK1. Protein Sci *18*, 1486-1497.

Ryckaert, J.P., Ciccotti, G., and Berendsen, H.J.C. (1977). Numerical integration of the cartesian equations of motion of a system with constraints: molecular dynamics of n-alkanes. J Comp Phys 327–341.

Salomon-Ferrer, R., Case, D.A., and Walker, R.C. (2013a). An overview of the Amber biomolecular simulation package. WIREs Comput Mol Sci *3*, 198-210.

Salomon-Ferrer, R., Goetz, A.W., Poole, D., Le Grand, S., and Walker, R.C. (2013b). Routine microsecond molecular dynamics simulations with AMBER - Part II: Particle Mesh Ewald. J Chem Theory Comput, No 101021/ct400314y.

Sarma, G.N., Kinderman, F.S., Kim, C., von Daake, S., Chen, L., Wang, B.C., and Taylor, S.S. (2010). Structure of D-AKAP2:PKA RI complex: insights into AKAP specificity and selectivity. Structure *18*, 155-166.

Sastri, M., Barraclough, D.M., Carmichael, P.T., and Taylor, S.S. (2005). A-kinase-interacting protein localizes protein kinase A in the nucleus. Proc Natl Acad Sci U S A *102*, 349-354.

Schindler, T., Bornmann, W., Pellicena, P., Miller, W.T., Clarkson, B., and Kuriyan, J. (2000). Structural mechanism for STI-571 inhibition of abelson tyrosine kinase. Science *289*, 1938-1942.

Schroder, T., Lilie, H., and Lange, C. (2011). The myristoylation of guanylate cyclase-activating protein-2 causes an increase in thermodynamic stability in the presence but not in the absence of Ca(2+). Protein Sci *20*, 1155-1165.

Shabb, J.B. (2001). Physiological substrates of cAMP-dependent protein kinase. Chem Rev *101*, 2381-2411.

Shaffer, J., and Adams, J.A. (1999a). An ATP-linked structural change in protein kinase A precedes phosphoryl transfer under physiological magnesium concentrations. Biochemistry *38*, 5572-5581.

Shaffer, J., and Adams, J.A. (1999b). Detection of conformational changes along the kinetic pathway of protein kinase A using a catalytic trapping technique. Biochemistry *38*, 12072-12079.

Shaltiel, S., Cox, S., and Taylor, S.S. (1998). Conserved water molecules contribute to the extensive network of interactions at the active site of protein kinase A. Proc Natl Acad Sci U S A *95*, 484-491.

Shental-Bechor, D., Smith, M.T., Mackenzie, D., Broom, A., Marcovitz, A., Ghashut, F., Go, C., Bralha, F., Meiering, E.M., and Levy, Y. (2012). Nonnative interactions regulate folding and switching of myristoylated protein. Proc Natl Acad Sci U S A *109*, 17839-17844.

Shimizu, T., Matsuoka, Y., and Shirasawa, T. (2005). Biological significance of isoaspartate and its repair system. Biol Pharm Bull *28*, 1590-1596.

Singh, P., Wang, B., Maeda, T., Palczewski, K., and Tesmer, J.J. (2008). Structures of rhodopsin kinase in different ligand states reveal key elements involved in G protein-coupled receptor kinase activation. J Biol Chem *283*, 14053-14062.

Song, K.S., Sargiacomo, M., Galbiati, F., Parenti, M., and Lisanti, M.P. (1997). Targeting of a G alpha subunit (Gi1 alpha) and c-Src tyrosine kinase to caveolae membranes: clarifying the role of N-myristoylation. Cell Mol Biol (Noisy-le-grand) *43*, 293-303.

Steichen, J.M., Iyer, G.H., Li, S., Saldanha, S.A., Deal, M.S., Woods, V.L., Jr., and Taylor, S.S. (2010). Global consequences of activation loop phosphorylation on protein kinase A. J Biol Chem *285*, 3825-3832.

Steichen, J.M., Kuchinskas, M., Keshwani, M.M., Yang, J., Adams, J.A., and Taylor, S.S. (2012). Structural basis for the regulation of protein kinase A by activation loop phosphorylation. J Biol Chem *287*, 14672-14680.

Stephen, R., Bereta, G., Golczak, M., Palczewski, K., and Sousa, M.C. (2007). Stabilizing function for myristoyl group revealed by the crystal structure of a neuronal calcium sensor, guanylate cyclase-activating protein 1. Structure *15*, 1392-1402.

Su, Y., Dostmann, W.R., Herberg, F.W., Durick, K., Xuong, N.H., Ten Eyck, L., Taylor, S.S., and Varughese, K.I. (1995). Regulatory subunit of protein kinase A: structure of deletion mutant with cAMP binding domains. Science *269*, 807-813.

Suzuki, Y., Shimizu, T., Morii, H., and Tanokura, M. (1997). Hydrolysis of AMPPNP by the motor domain of ncd, a kinesin-related protein. FEBS Lett *409*, 29-32.

Szarek, P., Dyguda-Kazimierowicz, E., Tachibana, A., and Sokalski, W.A. (2008). Physical nature of intermolecular interactions within cAMP-dependent protein kinase active site: differential transition state stabilization in phosphoryl transfer reaction. J Phys Chem B *112*, 11819-11826.

Tanaka, T., Ames, J.B., Harvey, T.S., Stryer, L., and Ikura, M. (1995). Sequestration of the membrane-targeting myristoyl group of recoverin in the calcium-free state. Nature *376*, 444-447.

Tasken, K., Skalhegg, B.S., Tasken, K.A., Solberg, R., Knutsen, H.K., Levy, F.O., Sandberg, M., Orstavik, S., Larsen, T., Johansen, A.K., Vang, T., Schrader, H.P., Reinton, N.T., Torgersen, K.M., Hansson, V., and Jahnsen, T. (1997). Structure, function, and regulation of human cAMP-dependent protein kinases. Adv Second Messenger Phosphoprotein Res *31*, 191-204.

Taylor, J.S. (1981). Sarcoplasmic reticulum ATPase catalyzes hydrolysis of adenyl-5'-yl imidodiphosphate. J Biol Chem *256*, 9793-9795.

Taylor, S.S., Ilouz, R., Zhang, P., and Kornev, A.P. (2012a). Assembly of allosteric macromolecular switches: lessons from PKA. Nature reviews Molecular cell biology *13*, 646-658.

Taylor, S.S., Keshwani, M.M., Steichen, J.M., and Kornev, A.P. (2012b). Evolution of the eukaryotic protein kinases as dynamic molecular switches. Philos Trans R Soc Lond B Biol Sci *367*, 2517-2528.

Taylor, S.S., Kim, C., Cheng, C.Y., Brown, S.H., Wu, J., and Kannan, N. (2008). Signaling through cAMP and cAMP-dependent protein kinase: diverse strategies for drug design. Biochim Biophys Acta *1784*, 16-26.

Taylor, S.S., and Kornev, A.P. (2011). Protein kinases: evolution of dynamic regulatory proteins. Trends Biochem Sci *36*, 65-77.

Tereshko, V., Teplova, M., Brunzelle, J., Watterson, D.M., and Egli, M. (2001). Crystal structures of the catalytic domain of human protein kinase associated with apoptosis and tumor suppression. Nat Struct Biol *8*, 899-907.

Thelen, M., Rosen, A., Nairn, A.C., and Aderem, A. (1991). Regulation by phosphorylation of reversible association of a myristoylated protein kinase C substrate with the plasma membrane. Nature *351*, 320-322.

Tholey, A., Pipkorn, R., Bossemeyer, D., Kinzel, V., and Reed, J. (2001). Influence of myristoylation, phosphorylation, and deamidation on the structural behavior of the N-terminus of the catalytic subunit of cAMP-dependent protein kinase. Biochemistry *40*, 225-231.

Thompson, E.E., Kornev, A.P., Kannan, N., Kim, C., Ten Eyck, L.F., and Taylor, S.S. (2009). Comparative surface geometry of the protein kinase family. Protein Sci *18*, 2016-2026.

Tomaszek, T.A., Jr., and Schuster, S.M. (1986). Hydrolysis of adenyl-5-yl imidodiphosphate by beef heart mitochondrial ATPase. J Biol Chem *261*, 2264-2269.

Toner-Webb, J., van Patten, S.M., Walsh, D.A., and Taylor, S.S. (1992). Autophosphorylation of the catalytic subunit of cAMP-dependent protein kinase. J Biol Chem *267*, 25174-25180.

Tsigelny, I., Greenberg, J.P., Cox, S., Nichols, W.L., Taylor, S.S., and Ten Eyck, L.F. (1999). 600 ps molecular dynamics reveals stable substructures and flexible hinge points in cAMP dependent protein kinase. Biopolymers *50*, 513-524.

Valiev, M., Kawai, R., Adams, J.A., and Weare, J.H. (2003). The role of the putative catalytic base in the phosphoryl transfer reaction in a protein kinase: first-principles calculations. J Am Chem Soc *125*, 9926-9927.

Valiev, M., Yang, J., Adams, J.A., Taylor, S.S., and Weare, J.H. (2007). Phosphorylation reaction in cAPK protein kinase-free energy quantum mechanical/molecular mechanics simulations. J Phys Chem B *111*, 13455-13464.

Vultur, A., Villanueva, J., and Herlyn, M. (2010). BRAF inhibitor unveils its potential against advanced melanoma. Cancer cell *18*, 301-302.

Weiergraber, O.H., Senin, II, Philippov, P.P., Granzin, J., and Koch, K.W. (2003). Impact of N-terminal myristoylation on the Ca2+-dependent conformational transition in recoverin. J Biol Chem *278*, 22972-22979.

Welch, E.J., Jones, B.W., and Scott, J.D. (2010). Networking with AKAPs: context-dependent regulation of anchored enzymes. Molecular interventions *10*, 86-97.

Wen, W., Harootunian, A.T., Adams, S.R., Feramisco, J., Tsien, R.Y., Meinkoth, J.L., and Taylor, S.S. (1994). Heat-stable inhibitors of cAMP-dependent protein kinase carry a nuclear export signal. J Biol Chem *269*, 32214-32220.

Westwood, I., Cheary, D.M., Baxter, J.E., Richards, M.W., van Montfort, R.L., Fry, A.M., and Bayliss, R. (2009). Insights into the conformational variability and regulation of human Nek2 kinase. J Mol Biol *386*, 476-485.

Wu, J., Tseng, Y.D., Xu, C.F., Neubert, T.A., White, M.F., and Hubbard, S.R. (2008). Structural and biochemical characterization of the KRLB region in insulin receptor substrate-2. Nat Struct Mol Biol *15*, 251-258.

Wu, J., Yang, J., Kannan, N., Madhusudan, Xuong, N.H., Ten Eyck, L.F., and Taylor, S.S. (2005). Crystal structure of the E230Q mutant of cAMP-dependent protein kinase reveals an unexpected apoenzyme conformation and an extended N-terminal A helix. Protein Sci *14*, 2871-2879.

Xiao, B., Sanders, M.J., Underwood, E., Heath, R., Mayer, F.V., Carmena, D., Jing, C., Walker, P.A., Eccleston, J.F., Haire, L.F., Saiu, P., Howell, S.A., Aasland, R., Martin, S.R., Carling, D., and Gamblin, S.J. (2011). Structure of mammalian AMPK and its regulation by ADP. Nature *472*, 230-233.

Xu, W., Doshi, A., Lei, M., Eck, M.J., and Harrison, S.C. (1999). Crystal structures of c-Src reveal features of its autoinhibitory mechanism. Mol Cell *3*, 629-638.

Yang, J., Campobasso, N., Biju, M.P., Fisher, K., Pan, X.Q., Cottom, J., Galbraith, S., Ho, T., Zhang, H., Hong, X., Ward, P., Hofmann, G., Siegfried, B., Zappacosta, F., Washio, Y., Cao, P., Qu, J., Bertrand, S., Wang, D.Y., Head, M.S., Li, H., Moores, S., Lai, Z., Johanson, K., Burton, G., Erickson-Miller, C., Simpson, G., Tummino, P., Copeland, R.A., and Oliff, A. (2011). Discovery and characterization of a cell-permeable, small-molecule c-Abl kinase activator that binds to the myristoyl binding site. Chem Biol *18*, 177-186.

Yang, J., Cron, P., Good, V.M., Thompson, V., Hemmings, B.A., and Barford, D. (2002). Crystal structure of an activated Akt/protein kinase B ternary complex with GSK3-peptide and AMP-PNP. Nat Struct Biol *9*, 940-944.

Yang, J., Kennedy, E.J., Wu, J., Deal, M.S., Pennypacker, J., Ghosh, G., and Taylor, S.S. (2009). Contribution of non-catalytic core residues to activity and regulation in protein kinase A. J Biol Chem *284*, 6241-6248.

Yang, J., Ten Eyck, L.F., Xuong, N.H., and Taylor, S.S. (2004). Crystal structure of a cAMP-dependent protein kinase mutant at 1.26A: new insights into the catalytic mechanism. J Mol Biol *336*, 473-487.

Yang, J., Wu, J., Steichen, J.M., Kornev, A.P., Deal, M.S., Li, S., Sankaran, B., Woods, V.L., Jr., and Taylor, S.S. (2012). A conserved glu-arg salt bridge connects coevolved motifs that define the eukaryotic protein kinase fold. J Mol Biol *415*, 666-679.

Yonemoto, W., Garrod, S.M., Bell, S.M., and Taylor, S.S. (1993a). Identification of phosphorylation sites in the recombinant catalytic subunit of cAMP-dependent protein kinase. J Biol Chem *268*, 18626-18632.

Yonemoto, W., McGlone, M.L., and Taylor, S.S. (1993b). N-myristylation of the catalytic subunit of cAMP-dependent protein kinase conveys structural stability. J Biol Chem *268*, 2348-2352.

Yount, R.G., Babcock, D., Ballantyne, W., and Ojala, D. (1971). Adenylyl imidodiphosphate, an adenosine triphosphate analog containing a P--N--P linkage. Biochemistry *10*, 2484-2489.

Zeqiraj, E., Filippi, B.M., Deak, M., Alessi, D.R., and van Aalten, D.M. (2009). Structure of the LKB1-STRAD-MO25 complex reveals an allosteric mechanism of kinase activation. Science *326*, 1707-1711.

Zhang, P., Smith-Nguyen, E.V., Keshwani, M.M., Deal, M.S., Kornev, A.P., and Taylor, S.S. (2012). Structure and allostery of the PKA RIIbeta tetrameric holoenzyme. Science *335*, 712-716.

Zheng, J., Knighton, D.R., ten Eyck, L.F., Karlsson, R., Xuong, N., Taylor, S.S., and Sowadski, J.M. (1993a). Crystal structure of the catalytic subunit of cAMP-dependent protein kinase complexed with MgATP and peptide inhibitor. Biochemistry *32*, 2154-2161.

Zheng, J., Knighton, D.R., Xuong, N.H., Taylor, S.S., Sowadski, J.M., and Ten Eyck, L.F. (1993b). Crystal structures of the myristylated catalytic subunit of cAMP-dependent protein kinase reveal open and closed conformations. Protein Sci *2*, 1559-1573.

Zheng, J., Trafny, E.A., Knighton, D.R., Xuong, N.H., Taylor, S.S., Ten Eyck, L.F., and Sowadski, J.M. (1993c). 2.2 A refined crystal structure of the catalytic subunit of cAMP-dependent protein kinase complexed with MnATP and a peptide inhibitor. Acta Crystallogr D Biol Crystallogr *49*, 362-365.

Zoller, M.J., Nelson, N.C., and Taylor, S.S. (1981). Affinity labeling of cAMP-dependent protein kinase with p-fluorosulfonylbenzoyl adenosine. Covalent modification of lysine 71. J Biol Chem *256*, 10837-10842.